



WICHITA STATE  
UNIVERSITY

UNIVERSITY LIBRARIES

**Multi-functional protective nanocomposite  
coatings of modified graphene and hexagonal  
boron nitride nanoparticles on transparent plastics**

Item Type	Thesis
Authors	Tran, Thu Van
Publisher	Wichita State University
Rights	Thu Van Tran; Copyright 2015 Thu Van Tran
Download date	2026-05-20 03:47:05
Link to Item	<a href="http://hdl.handle.net/10057/12118">http://hdl.handle.net/10057/12118</a>

MULTI-FUNCTIONAL PROTECTIVE NANOCOMPOSITE COATINGS OF MODIFIED  
GRAPHENE AND HEXAGONAL BORON NITRIDE NANOPARTICLES ON  
TRANSPARENT PLASTICS

A Thesis by

Thu Van Tran

Bachelor of Science, Wichita State University, 2010

Submitted to the Department of Mechanical Engineering  
and the faculty of the Graduate School of  
Wichita State University  
in partial fulfillment of  
the requirements for the degree of  
Master of Science

December 2015

© Copyright 2015 by Thu Van Tran

All Rights Reserved

MULTI-FUNCTIONAL PROTECTIVE NANOCOMPOSITE COATINGS OF MODIFIED  
GRAPHENE AND HEXAGONAL BORON NITRIDE NANOPARTICLES ON  
TRANSPARENT PLASTICS

The following faculty members have examined the final copy of this thesis for form and content, and recommend that it be accepted in partial fulfillment of the requirement for the degree of Master of Science with a major in Mechanical Engineering.

---

Ramazan Asmatulu, Committee Chair

---

Bin Li, Committee Member

---

Zheng Chen, Committee Member

## DEDICATION

To my family, my husband, my teachers, and my dear friends

## ACKNOWLEDGEMENTS

I would like to thank my direct advisor, Dr. Ramazan Asmatulu, for his many years of thoughtful, patient guidance and strongly supports my study and the work presented in this thesis. Many thanks are also due to my dear friends Aybala Usta for all her helps with lab instruction, equipment, and accesses such as Water Contact Angle, FTIR, UV- Vis, and DSC tests; Sifath M. R. Shagor for all his instructions of silanization process, Max Hinman for his help on SEM images of my samples, Leyla Saeednia for the UV chamber operation instruction and additional lab equipment.

## ABSTRACT

Nanocoating is the result of a coating application of nanomaterials to build a consistent network of molecules in a coating or paint to protect a surface. Graphene is an allotrope of carbon in the two dimensional form, that is on an atomic scale, has a hexagonal lattice with extraordinary physical and chemical properties. Application of graphene in the coating show excellent performances. By adding functionalized graphene into paints or coatings, they will absorb the harmful UV part of sunlight; prevent coating degradation, and the impact of the environmental factors on the coatings to enhance longevity and durability. Boron Nitride (BN) has a similar structure of carbon lattice and excellent thermal and chemical stability. Boron nitride nanocoating is a thermally insulating material for heat dissipation.

In this study, graphene and hexagonal BN (h-BN) were modified with [3- (2-Aminoethylamino) propyl] trimethoxysilane and uniformly added into the polyurethane paint with different amounts, such as 0.1wt %, 0.2wt%, 0.4wt%, and 0.8wt% to increase hardness, and water resistance, and decrease UV degradation. The samples were characterized by using Fourier Transform Infrared Spectroscopy (FTIR), UV Vis, Scanning Electron Microscope (SEM), Water contact angle, and Differential Scanning Calorimetry (DSC). Nanocoatings with h-BN showed very good water contact angle and only a small decrease after the UV chamber with an average amount of 1.30 degree average. The thickness of the coatings was degraded with a small amount of .0007” average, but the surface coating didn’t change color after 20 days in UV chamber. Unlike h-BN coating, the coating with graphene was affected by the UV light with a color change from clear to yellowish, coating thicknesses degraded after 20 days UV chamber with the rate of 0.0038” average. The water contact angle also changed with a larger amount of 1.33 degree compared to the nanocomposite coatings of h-BN inclusions.

## TABLE OF CONTENTS

Chapter	Page
1. INTRODUCTION .....	1
1.1 Introduction.....	1
1.2 Background & History .....	2
1.3 Objectives of Study.....	4
2. LITERATURE REVIEW .....	6
2.1 UV Degradation on Plastics.....	6
2.2 Degradation of Polymer Coatings under UV Lights.....	8
2.3 The Mechanism of Polymer Coating Degradation by Ultraviolet Light.....	12
2.4 Inclusion of Silanized Graphene Nano Sheets and h-BN into Polymer Coatings .....	14
2.4.1 Graphene.....	14
2.4.2 Boron Nitride .....	18
3. MATERIALS AND EQUIPMENT.....	21
3.1 Plexiglas [Poly (methyl methacrylate)].....	21
3.2 Coating/Paint.....	22
3.2.1 Miniwax Fast Drying Polyurethane Clear Gloss Paint .....	22
3.3 Graphene .....	23
3.4 Boron Nitride .....	23
3.5 Graphene-Boron Nitride .....	24
3.6 Preval Spray System .....	25
3.7 Weighing Scale .....	25
3.8 Hot Plate/Magnetic Stirrer .....	26
3.9 Sonicator .....	27
3.10 Mitutoyo 293-725 Digimatic Micrometer.....	27
3.11 UV Chamber .....	28
3.12 Fourier Transform Infrared (FTIR) Spectrometer.....	29
3.13 Optical Contact Angle Goniometer.....	29
3.14 UV Visible Spectroscopy.....	30
3.15 Scanning Electron Microscopy .....	31

## TABLE OF CONTENTS (continued)

Chapter	Page
3.16 DSC.....	32
4. METHODS .....	34
4.1 Silanization Process of Graphene .....	34
4.2 Silanization Process of h-BN .....	36
4.3 Stability of Graphene and h-BN in Acetone Suspension to Prove Successful Silanization.....	37
4.4 Preparation for Plexiglas Surface.....	41
4.5 Preparation for Based Coat .....	41
4.6 Preparation for Top Coat.....	43
4.7 Top Coat Painting .....	43
4.8 UV Exposure Test.....	45
4.9 Surface Characterization .....	46
4.9.1 Water Contact Angle Measurements .....	46
4.9.2 ATR-FTIR Analysis.....	47
4.9.3 UV Vis Spectroscopy.....	47
4.9.4 DSC Test.....	48
5. RESULTS AND DISCUSSION.....	50
5.1 UV Chamber Studies .....	50
5.2 FTIR Studies .....	53
5.3 UV-Vis Studies .....	61
5.4 Water Contact Angle Measurements .....	65
5.5 Differential Scanning Calorimeter Test .....	69
5.5.1 DSC Analysis.....	69
5.5.2 Glass Transition Temperature Comparisons.....	76
5.5.3 Crystallinity of Silanized & Unsilanized Nanocomposite Coatings .....	79
CONCLUSIONS.....	82
FUTURE DEVELOPMENT .....	85
REFERENCES.....	87

## LIST OF TABLES

Table	Page
1. The Thickness of PU Coating with Different Percentages of Silanized Graphene.....	51
2. The Thickness of PU Coating with different Percentages of Silanized h-BN.....	52
3. The Light Absorbing Group, Excitation, Max Wavelength, and Solvents.....	62
4. Contact Angle Measurement of 1 mm Thick Coating with Various Percentages of Silanized Graphene, h-BN, and G & h-BN under Different Exposed Times.....	65
5. The Glass Transition temperature of Coatings with Different Percentages of Silanized Graphene & BN.....	75
6. The Glass Transition temperature of Coatings with Different Percentages of Unsilanized Graphene & BN.....	75

## LIST OF FIGURES

Figure	Page
1. Modern Automotive Equipped with Polymeric Glasses for Roof, Windows, and Cover Light.....	3
2. Photo Degradation in many Polymers .....	7
3. Biodegradation of PLA (Polylactic Acid).....	7
4. IR Spectrum shows Carbonyl Absorption due to UV Degradation of Polyethylene [21] .....	8
5. The Electromagnetic Spectrum.....	9
6. The Wavelength in micrometers.....	9
7. Diagram shows the Various Kinds of Electronic Excitation that may occur in organic Molecules .....	10
8. The Effect of the Atmosphere on the Intensity of Solar Radiation at Sea Level in the UV & Visible Light Bands.....	11
9. Process of UV light Degradation such as Photolysis, Autoxidation, and Embrittlement of Paint Film .	13
10. Scanning Probe Microscopy Image of Graphene.....	15
11. Graphene honeycomb lattice with Bond Strength Shows.....	16
12. Electron Shell Hybridization in Graphene .....	16
13. Photograph of Graphene in Transmitted light.....	17
14. Boron Nitride Layer and Structural Arrangement of Boron and Nitride .....	18
15. Magnified Sample of Crystalline hexagonal boron nitride .....	20
16. Plexiglas 0.093” x 36” x 48” Clear Acrylic Sheet .....	21
17. Polyurethane Synthesis, the Urethane Group –NH-(C=O) – links the Molecular units .....	22
18. Unmodified Graphene Nano flakes Obtained from Graphene Supermarket .....	23
19. Hex Boron Nitride (h-BN) Powder and its SEM images.....	24
20. Preval Spray System used to Spray Paint Test Samples .....	25
21. Mettler Toledo Weighing Scale used to Weight Nanomaterials.....	26

LIST OF FIGURES (continued)

Figure	Page
22. Hot Plate from Fisher Scientific used to mix the Coating System.....	26
23. Fisher Scientific FS 200 Sonicator used to Mix the Nanoparticles inside the Coating System.....	27
24. Mitutoyo 293-725 Digimatic Micrometer used to Control the Coating thickness.....	28
25. QUV Accelerated Weathering Cabinet used to Simulate the Weathering of anocomposite Coatings .	28
26. Thermal Nicolet Magna 850 IR Spectrometer used to Perform FTIR Studies .....	29
27. Optical Water Contact Angle Goniometer.....	30
28. UV-Vis Spectrometers U-2900 Hitachi .....	31
29. SIGMA Series of Field Emission Scanning Electron Microscope .....	32
30. Different Scanning Calorimetry Q-2800.....	33
31. Silanized Graphene Preparation (Part 1); a) measure 2g of graphene; b-c) Pour graphene in a beaker d) Mix 2g of graphene with 200 ml ethanol f) Cover mixture of graphene and ethanol g) Mix graphene and ethanol suspension by high power sonification for 1 hour.....	34
32. Silanized Graphene Preparation (part 2); h) pour mixture into Erlenmeyer flask i) Add magnetic stirrer to the flask and turn the hot plate on j) Add 12 ml of Silane Surfactant into the mixture k) Seal the flask completely and let the graphene .....	35
33. Silanized Graphene Preparation (part 3); n) Rinse the graphene with 500 ml DI water o) Let all the water seep through the filter p-q) Collect the graphene in a small container and add more DI water r) Place the container in the oven at 70°C (overnight) s) Collect the silanized graphene.....	36
34. SEM Image of Unsilanized Graphene (left) and Silanized Graphene (right).....	37
35. SEM Image of Unsilanized h-BN (left) and Silanized h-BN (right).....	38
36. SEM Image of Silanized Graphene & h-BN.....	39
37. Sample of Graphene, h-BN, and Graphene & h-BN dissolving Acetone a) Pristine Graphene, b) Silanized Graphene, c) Pristine h-BN, d) Silanized h-BN, e) Pristine Graphene & h-BN, f) Silanized Graphene & h-BN.....	40
38. Test Samples for Coating before (left) and after peeled off the masking Plastic and Cleaning.....	41
39. Based Coat of Pure PU on the Substrate.....	42
40. Mixture of PU & Silanized h-BN (left), PU & Silanized graphene (center), PU and Graphene & h-BN .....	43

## LISTS OF FIGURES (continued)

Figure	Page
41. Clear Top Coat with a) 0.1% S-G with PU, b) with 0.1% h-BN with PU .....	44
42. Coating with 0.1 wt% h-BN (a), 0.2wt % h-BN (b), 0.4wt% h-BN (c), and .....	44
43. Coatings with 0.1wt.% S-G (a), 0.2wt.% S-G (b), 0.4wt.% S-G (c), 0.8wt.% S-G (d) .....	45
44. UV Degradation Test Using the QUV Weathering Tester.....	45
45. Theoretical Interpretation of Water Contact Angle [56].....	47
46. Test Samples after UV Chamber, color change to yellow of graphene and PU coating (a) more than h-BN and PU coating (b) and graphene & h-BN coating (c).....	50
47. Coating thickness Graph of Silanized Graphene after 20 days in the UV Chamber.....	52
48. Coating Thickness after UV Chamber after 20 days of h-BN Nanocomposite Coating.....	53
49. The General Regions of Infrared Spectrum .....	55
50. ATR-FTIR Spectrum of Coated Test Sample Coating 0% Silanized material after 20 days in UV Chamber.....	56
51. ATR-FTIR Spectrum of Coated Test Samples Containing 0.1% Silanized and unsilanized h-BN.....	57
52. ATR-FTIR Spectrum of Coated Test Samples Coating Containing 0.1wt% Silanized & Unsilanized Graphene after UV Chamber.....	58
53. Silanized and Unsilanized h-BN after UV Chamber 20 days .....	59
54. Combination of Pure PU (top), Coating with Silanized Graphene (second), with Silanized h-BN (third), Coating with Graphene & h-BN (bottom) before UV Chamber.....	60
55. Combination of Pure PU (top), Coating with Silanized Graphene (second), with Silanized h-BN (third), Coating with Graphene & h-BN (bottom) after UV Chamber.....	61
56. UV –Vis Graphs of 0.4wt%Unsilanized and Silanized Graphene Coatings.....	63
57. UV-Vis Graphs of 0.4wt. % Silanized and Unsilanized h-BN Coatings .....	64
58. UV-Vis Graphs of 0.4wt% Silanized Graphene, h-BN, and Graphene & h-BN Coatings .....	65
59. Contact Angle Measurement of various UV Exposed Coatings Different percentages of pure PU, Silanized Graphene, Silanized h-BN, and Silanized Graphene & h-BN.....	66
60. Water Contact Angle pure PU (left), Silanized Graphene (right), and Silanized & h-BN (bottom)....	67

LIST OF FIGURES (continued)

Figure	Page
61. Water Contact Angle of Pure PU (left), Silanized Graphene (right), and Silanized Graphene & h-BN (Bottom).....	68
62. DSC of Polyurethane Floor finish Dried after Application for 48 hours.....	70
63. DSC of Polyurethane and 0.1wt% Silanized h-BN with Tg = 35.53°C.....	71
64. DSC of Polyurethane with 0.1wt % Unsilanized h-BN with Tg =32.63°C.....	72
65. DSC of Polyurethane with 0.4wt% Silanized h-BN with Tg =33.99°C.....	72
66. DSC of Polyurethane and 0.4wt% Unsilanized h-BN with Tg =33.09°C.....	73
67. DSC of Polyurethane and 0.1wt% Silanized Graphene with Tg =35.14°C.....	73
68. DSC of Polyurethane and 0.1wt% Unsilanized Graphene with Tg =38.34°C.....	74
69. DSC of Polyurethane and 0.4wt% Silanized Graphene and Tg = 34.37°C.....	74
70. DSC of Polyurethane and 0.4wt% Unsilanized Graphene with Tg =17.22°C.....	75
71. DSC of Polyurethane and 0.4 % of Silanized Graphene & h-BN with Tg =31.03°C.....	75
72. Glass Transition Temperature of PU and Functionalized Nanocomposites Coatings.....	77
73. Tg of PU and Unfunctionalized Nanocomposite Coatings.....	77
74. Enthalpy of Nanocomposite Coatings with Silanized Graphene and h-BN.....	78
75. Enthalpy of Nanocomposite Coatings with Unsilanized Graphene and h-BN.....	78
76. Crystallinity (%) of the Nanocomposite Coatings with PU Silanized Graphene & h-BN.....	79
77. Crystallinity (%) of the Nanocoatings of PU and Unfunctionalized Graphene & h-BN.....	79

## LIST OF ABBREVIATIONS

H-BN	Hexagonal Boron Nitride
BN	Boron Nitride
ATR	Attenuated Total Reflectance
SEM	Scanning Electron Microscope
S-GNF	Silanized Graphene Nano Flakes
PU	Polyurethane
UV	Ultra Violet
WCA	Water Contact Angle
DSC	Differential Scanning Calorimeter
FTIR	Fourier Transform Infrared Spectroscopy
UV-Vis	Ultraviolet Visible Spectroscopy

## LIST OF SYMBOLS

$\mu$	Micron
$^{\circ}$	Degree
nm	Nanometer
mm	Millimeter
$\mu\text{m}$	Micrometer (micron)
$\Omega$	Ohm
Y	Interfacial surface
S	Solid
G	Gas
L	Liquid
S-G	Silanized Graphene
S-BN	Silanized Boron Nitride

# CHAPTER 1

## INTRODUCTION

### 1.1 Introduction

Nanotechnology has been involved in many industrial applications from automobiles, airplanes, sporting goods, health care, and uses in households [1]. Therefore, nanotechnology promises breakthroughs in areas such as materials, structures, coatings, corrosion protection, and manufacturing. Nanoparticles take advantage of their nanosize, large surface area to volume ratio, so this means their optical properties become a function of the particle diameter. The increased surface area of nanomaterials makes them ideal for use in composites, coatings, reacting system, and energy storage [2]. By increasing the surface area, the number of surface atoms increases dramatically, meaning the surface plays a vital role in material performance because a larger amount of a substance comes into contact with the surrounding material.

At nanoscale, surface and interface forces become dominant. When the size of the materials are comparatively smaller than the wavelength of visible light, they do not scatter light and can be used in applications where transparency is of great importance [3]. Coatings have been used to improve the surface properties of substrates such as corrosion resistance, durability, wetting ability, and adhesion. Paints are a special category of coating and are used to protect, beautify, and reduce maintenance requirements. By applying nanomaterials in coatings, we can have the ability to improve the performance of the substrate in several functions such as UV absorption, corrosion resistance, wetting ability, and high wear & scratch resistance.

## 1.2 Background & History

Plastics and epoxy are finding and increasing use in manufactured goods. For example, automobiles have plastic body panels and aircraft have plastic interior paneling, exterior skin panels formed of plastics, and plastic composites. Plastics offer several excellent properties some of which are light weight, formability, low cost, and transparency. Compared with plastics, glass is a brittle material, much heavier and more expensive. Glass also thought has excellent strength, scratch resistance and remains the material of choice in applications such as safety glass in automobiles and in larger aircraft windshields [4]. By substituting glass with polymeric materials such as stretched acrylic or polycarbonate, it would lead to lighter transparencies. Most polymers are adversely affected by ultraviolet radiation (sunlight) and oxygen which will weaken and break the primary bonds (covalent) resulting in scission (splitting) of long chain polymer molecules. The polymers then become brittle, degraded, and stiff.

Fuel consumption of a transportation vehicle is an important factor for both manufacturers and consumers. For today's economy, there is a desire to produce a vehicle with lighter weight and thus lower fuel consumption. This has been vigorously developed in recent years. Reducing the weight of the vehicle by replacing the heavy glass parts with light polymeric glass-like sheets can lead to significant weight reduction. For example, some parts that have been replaced are a laminated glass windshield of some airplanes, headlights, windows, and windshields of cars [5]. Polymeric materials such as stretched acrylic or polycarbonate would lead to lighter transparencies, but would also pave the way for re-designing the overall shape of vehicles [6]. Figure 1 shows a modern automobile equipped with transparent nanostructure polymers for roof, windows and cover light.

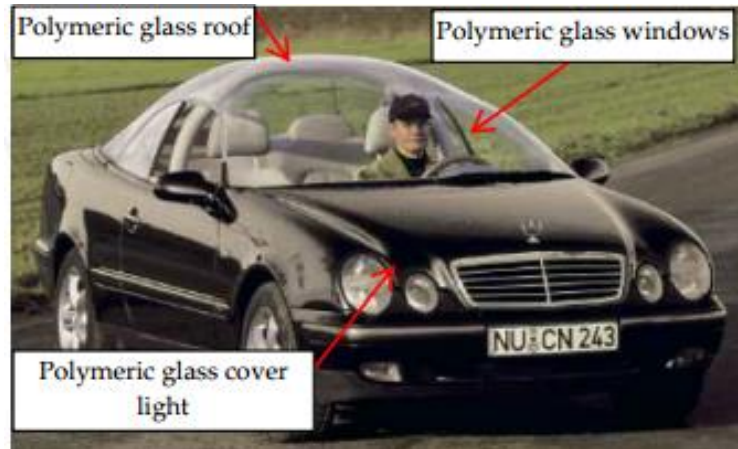


Figure 1: Modern Automotive Equipped with Polymeric Glasses for Roof, Windows, and Cover Light

Currently, stretched acrylic materials are used to fabricate aircraft passenger windows. Acrylic is used because of its flexibility, light weight, easy formability, versatility, and low cost. However, acrylics are soft materials and hence can be easily scratched. Water absorption, chemical and UV attack, and mechanically induced scratches can lead to crazing when stress is applied to acrylic materials such as in a passenger window application [7]. Polymeric materials are susceptible to particle (e.g. sand/water) induced erosion and chemical crazing, protective hard coatings are needed to maintain the optical quality of the windows in use. In general, plastic surfaces are not as hard or abrasion resistant as glass surfaces.

There is a need for a durable, transparent, hard coating that improves the plastic component's lifetime by providing UV protection, improving resistance against chemicals commonly encountered in product maintenance, and weather ability characteristics. The coating should be both hard and flexible, so that it tolerates the flexing of the polymeric material due to operational and thermal stresses with simple processes. These coatings are hydrophobic (or super-hydrophobic) surfaces, on which the water contact angle (WCA) is  $150^\circ$  and higher (Wang and Jiang) [8]. For example, we would like to attain the attributes of a lotus leaf which is a

classic sample of a natural hydrophobic surface with a WCA of larger than  $150^\circ$  [9]. The super-hydrophobic effect is due to both the low surface energy materials and hierarchical (nano/micro) structures.

Previous research has shown that water droplets on the textured surfaces of the lotus leaves readily sit on the apexes of the nanostructures due to the air bubbles that fill the valleys of the structures under the droplets. Water drops on such surfaces can't penetrate the micro- or nanostructures and wet the surface, resulting in extremely high contact angles; thus, these naturally occurring leaves exhibit considerable super-hydrophobicity. Numerous methods, including photolithography [10], plasma treatment [11], template [12], chemical vapor deposition (CVD) [13], sol-gel processes [14], chemical vapor deposition [15], casting [16], and chemical etching [17] have been utilized to fabricate super-hydrophobic surfaces.

### **1.3 Objectives of Study**

The development of hydrophobic/super-hydrophobic polymers and nanocomposites has become an interesting subject in materials science. This study is a development of transparent coating techniques by adding nanoadditives in the coatings to create super-hydrophobic surfaces. This along with UV-curing techniques is designed to directly duplicate lotus leaf surface properties for substrates such as Plexiglas and polycarbonate plastics. The nanomaterials that were used in this study are graphene nanosheets and hexagonal boron nitride (h-BN) nanoparticles. These materials will be modified through silanization processes to provide mechanical strength to the resulting film and show high stability in organic paints before application on the substrate. In this experiment, the fabrication coatings of the graphene nanosheets and hexagonal boron nitride nanoparticles on transparent plastic substrate are reported. A Preval spray gun was used to generate thin films of silanized graphene nanosheets,

silanized h-BN nanoparticles, and a mixture silanized of graphene & h-BN dispersions into polyurethane clear gloss paint, and then apply these thin coatings on Plexiglas substrates. All the characteristics of the nanocomposite coatings such as UV absorption, UV degradation, corrosion resistance and photo responsiveness will be tested by using Water Contact Angle, Fourier Transform Infrared Spectroscopy (FTIR), UV Vis, Scanning Electron Microscope (SEM), and Differential Scanning Calorimetry (DSC).

## CHAPTER 2

### LITERATURE REVIEW

#### 2.1 UV Degradation of Plastics

Plastic has become an essential material in every aspect of modern day life replacing other materials such as glass, metal, and wood. There are many advantages in using plastic, but a disadvantage of using this material is that it is subject to a natural aging. Some examples are polymerization, polyaddition or polycondensation reactions. The composition and molecular weight start changing when the polymer is subjected to further shear stress, heat, light, air, water, radiation, or mechanical loading. Exposure to such conditions starts chemical reactions (degradation) in the polymer leading to a modification of its physical and optical properties [18].

Photo degradation (Figure 2) is a process that takes place when the products are exposed to sunlight. Common synthesis polymers such as polypropylene and Low Density Polyethylene (LDPE) can be attacked with the tertiary carbon bond  $(\text{H}_3\text{C})_2\text{C}=(\text{CH}_3)_2$  in their chain structures being the center of the attack. Ultraviolet rays interact with these bonds to form free radicals (an atom, molecule, or ion that has unpaired valence electrons and is usually reactive), which react further with oxygen in the atmosphere, producing carbonyl groups in the main chain [19]. The exposed surfaces of products may crack, chalk, or have color changes and the loss of physical properties or disintegration can occur.

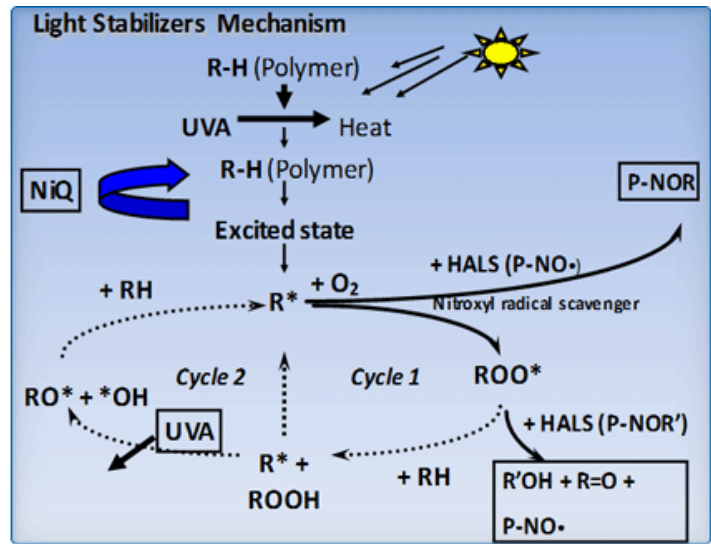


Figure 2: Photo Degradation in many Polymers

Since photo degradation [20] generally involves sunlight, thermal oxidation takes place in parallel to photo oxidation. Photo oxidation differs from thermal oxidation in that it can be started by absorption of UV light. Most pure polymers are theoretically incapable of absorbing UV light directly but trace amounts of other compounds within the polymer, such as degradation products or catalyst residues, can absorb UV light. In practice, high concentrations of UV absorbers and sufficient thickness of the polymer are required before enough absorption takes place to effectively retard photo degradation (Figure 3 & 4).

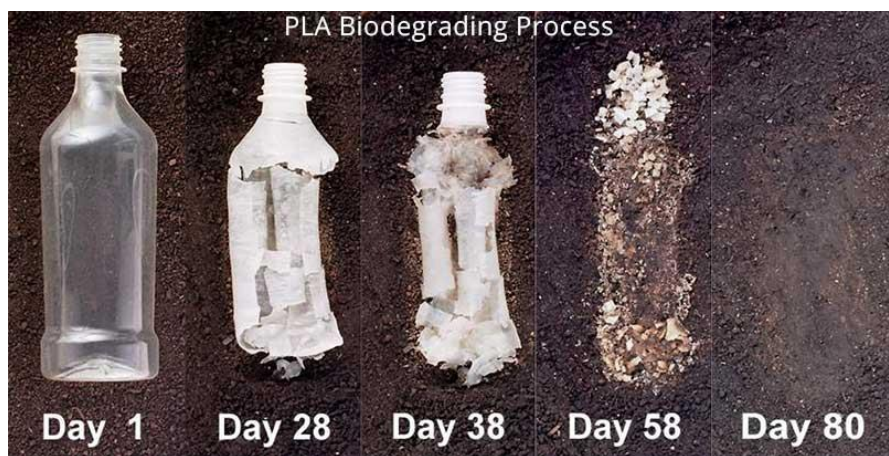


Figure 3: Biodegradation of PLA (Polylactic Acid)

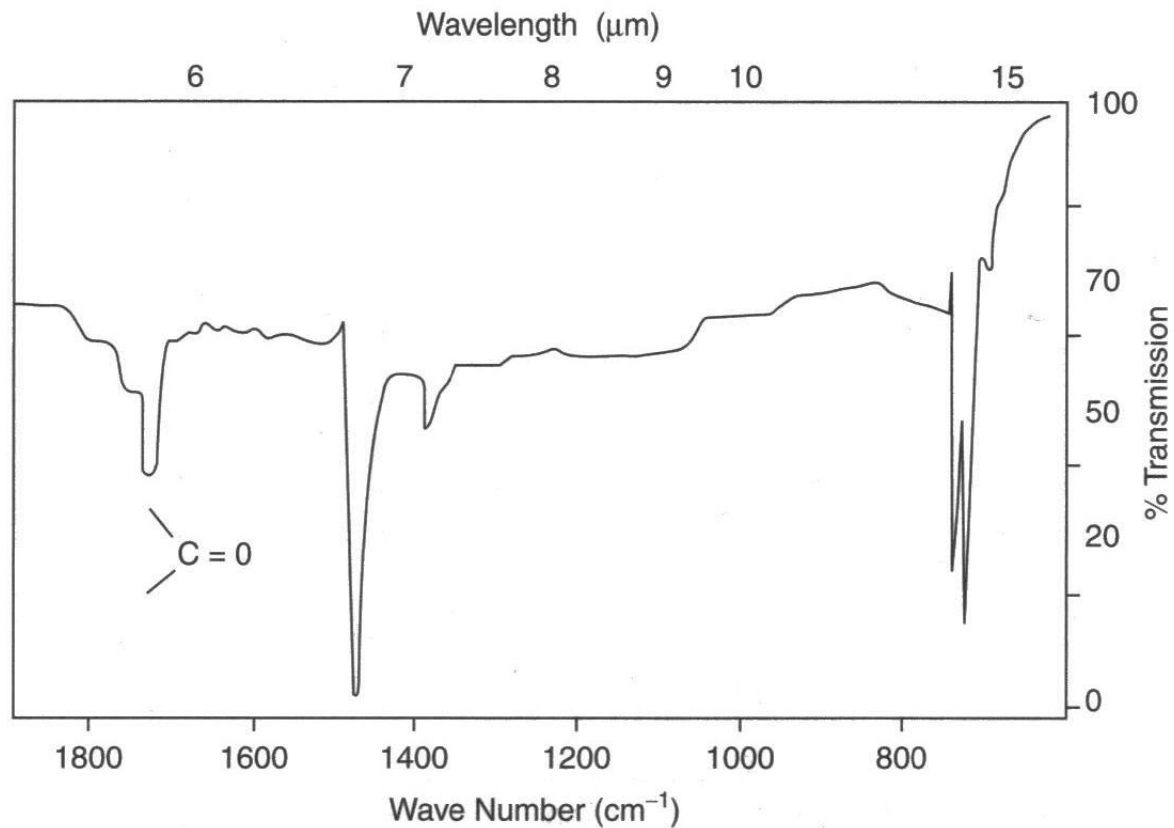


Figure 4: IR Spectrum shows Carbonyl Absorption due to UV Degradation of Polyethylene [21]

## 2.2 Degradation of Polymer Coatings under UV Lights

The major source of radiation on earth is the sun. It supplies warmth (heat or infrared radiation), light radiation (both visible and ultraviolet light), and a wide range of energy of other types (e.g., X-rays, gamma rays, and cosmic rays) in the electromagnetic spectrum [22] (Figure 5 & 6). The visible light that human eyes can see is usually defined as having wavelengths in range of 400-700 nanometer (nm) (Textbook of Practical Physiology) [22]. The electromagnetic spectrum ranges from very short wavelengths (including gamma and x-ray) to very long wavelengths (including microwaves and broadcast radio waves). The following chart displays many of the important regions of this spectrum, and demonstrates the inverse relationship between wavelength and frequency.

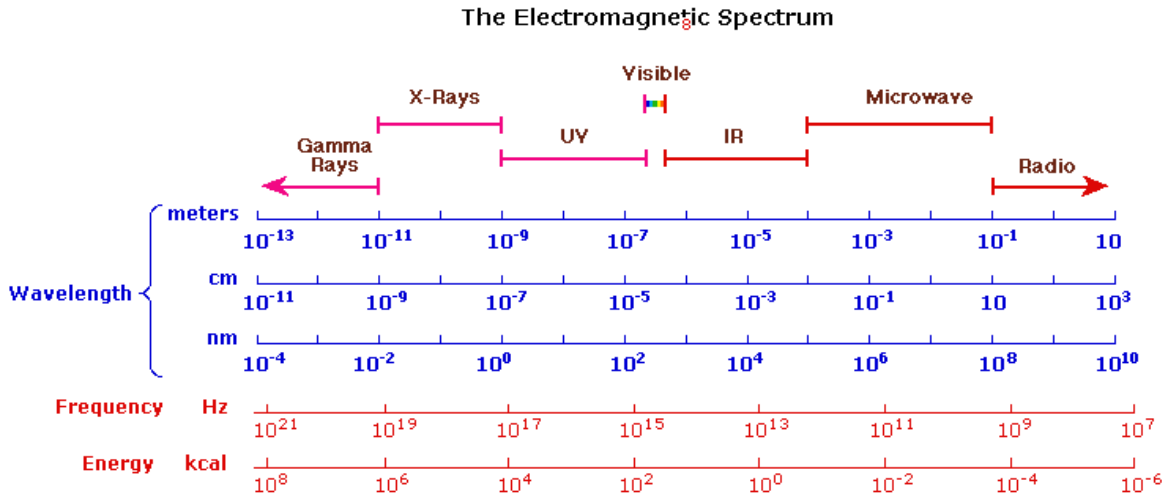


Figure 5: The Electromagnetic Spectrum

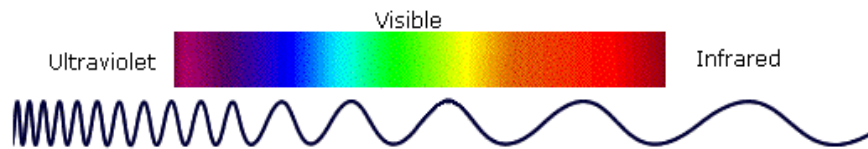


Figure 6: The Wavelength in micrometers

The energy associated with a given segment of the spectrum is proportional to its frequency. The bottom equation describes this relationship, which provides the energy carried by a photon of a given wavelength of radiation. The diverse forms of electromagnetic radiation related in the formula below with the wavelength  $\lambda$  (lamda), their frequency  $\nu$  (nu), and  $c$  is the speed of light ( $c = 3 \times 10^{10}$  cm/sec) (Anatomy of Paint) [23].

$$\nu = \frac{\lambda}{c}$$

$\nu$  frequency of wave cycles/second  
 $\lambda$  wavelength (nanometers to kilometers)  
 $c$  speed of light ( $3 \times 10^8$  meters/second)

$$\Delta E = h \cdot \nu$$

(1)

$E$  = Energy,  $\nu$  = Frequency,  $h$  = Planck's constant ( $h = 6.6 \times 10^{-27}$  erg/sec)

The energies mentioned above are sufficient to promote or excite a molecular electron to a higher energy orbital. Consequently, absorption spectroscopy carried out in this region is sometimes called "electronic spectroscopy" [24]. The diagram (Figure 7) shows the various kinds of electronic excitation that may occur in organic molecules. Of the six transitions outlined, only the two with the lowest energy (left-most, colored blue) are achieved by the energies available in the 200 to 800 nm spectrum. As a rule, energetically favored electron promotion will be from the highest occupied molecular orbital (HOMO) to the lowest unoccupied molecular orbital (LUMO), and the resulting species is in an excited state [25].

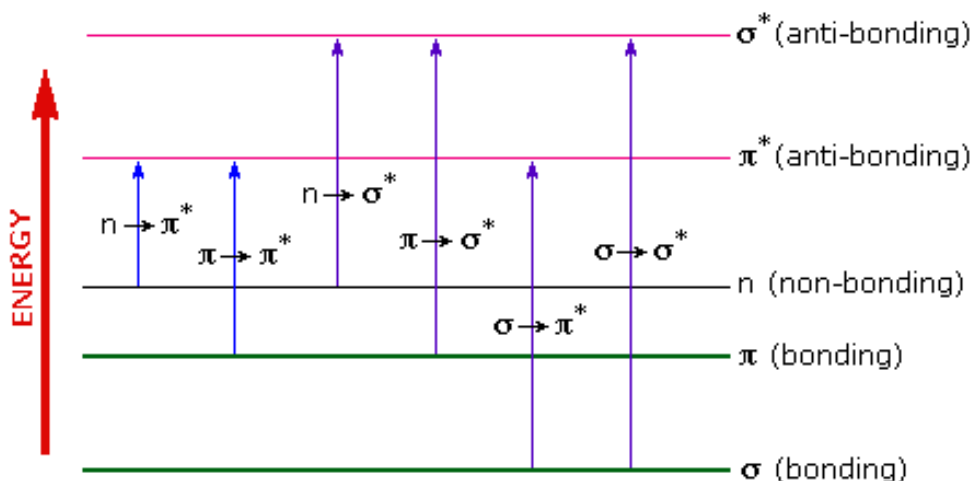


Figure 7: Diagram shows the Various Kinds of Electronic Excitation that may occur in organic Molecules

Molecules of all types are excited by a selectively absorbing radiant energy from radiation at specific wavelengths across the electromagnetic spectrum. Glass, which allows visible light to pass through it without absorption, is not as transparent to ultraviolet light and is virtually opaque to ultraviolet light of the shorter wavelengths (Hare) [26]. This is one reason why coating films last far longer indoors than outside. Ultraviolet light has sufficient energy to disrupt and break

the covalent bonds of organic molecules. Along with oxygen and water which are two of the three primary agencies that induce degradation (aging) of many organic polymers which includes those that bind in paint film (htt) [26].

The effects of ultraviolet light increase directly with the intensity of the radiation and inversely with the wavelength of the radiation (Figure 8). The atmosphere around us acts like a huge filter which absorbs the larger part of the powerful shorter wavelength radiations, including short wave ultraviolet light before they reach ground level. Radiation of wavelengths below 300 nm (UV-B & UV-C) is almost completely absorbed by the atmosphere, and only a relatively small amount of long wave ultraviolet light remains (UV-A between 300 nm - 380 nm). Nevertheless, the harmful effects of even small amount of radiation on the molecular structure paint films are now well recognized (Hare) [26]. However, UV light has major benefits, such as it induces production of vitamin D in the skin which helps to regulate calcium metabolism (vital to the nervous system and bone health) immunity, and cell issues such as insulin secretion and blood pressure [26].

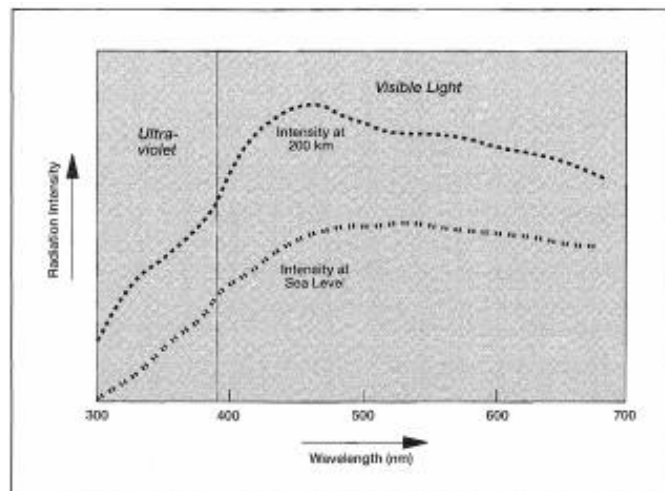


Figure 8: The Effect of the Atmosphere on the Intensity of Solar Radiation at Sea level in the Ultraviolet and Visible Light bands

On the right side of the electromagnetic spectrum is the long wavelength and low energy infrared light. This is a useful region to analyze the organic compounds and has the wavelength range from 2,500 to 16,000 nm, with a corresponding frequency range from  $1.9 \times 10^{13}$  to  $1.2 \times 10^{14}$  Hz [27]. Photon energies associated with the infrared region (from 1-15 Kcal/mole) are not large enough to excite electrons, but may induce vibration excitation of covalent bonded atoms and groups [27]. Due to the mobile nature of organic molecules, the covalent bonds of molecules are not rigid but are more like springs that can be stretched and bent. Consequently, all organic compounds will absorb infrared radiance that corresponds in energy to their bond natural frequency vibrations. There are six vibration modes with descriptive names such as symmetric stretching, asymmetric stretching, scissoring, rocking, wagging, and twisting [27].

### **2.3 Mechanism of Polymer Coating Degradation by Ultraviolet Light**

As noted earlier, there are three types of UV lights such as UV-A, UV-B, and UV-C. The UV-A, with the wavelengths 400 nm – 315 nm, are long wave UV or black light and not absorbed by the ozone layer. This is a major issue for both skin aging and degradation on polymers. The second UV type is UV-B, with the wavelengths 280 nm-315 nm, it is the medium UV light and is mostly absorbed by the ozone layer. The third UV light band is UV-C, with the wavelengths of 100 nm-280 nm, it is the shortest UV length. This is completely absorbed by the ozone layer and the atmosphere around us. Sunburn, freckling, and skin cancer are familiar effects of over exposure. Living things, materials, and products would be severely damaged by ultraviolet radiation from the sun if most of it wasn't filtered out by the earth's atmosphere or the ozone layer.

According to Larche, et al. [28], to understand the process of ultraviolet light degradation, we must understand the photo-degradation mechanism (Figure 9). On the un-pigmented films,

the first phase is known as photolysis, where the polymer absorbing ultraviolet radiation becomes excited, and is raised to the higher energy state than normal. This excess energy needs to be eliminated. The elimination is accomplished by the cleavage of the primary bonded structure of the polymer to form highly reactive free radicals. The primary bonded structures are dependent upon the strength of the covalent bonds. For example, C-C bonds have greater bond strength than C=C bonds. Polymers made up entirely of the stronger bonds are more resistance to ultraviolet. However, these polymers become more susceptible to damage as the wavelength of the radiation gets shorter.

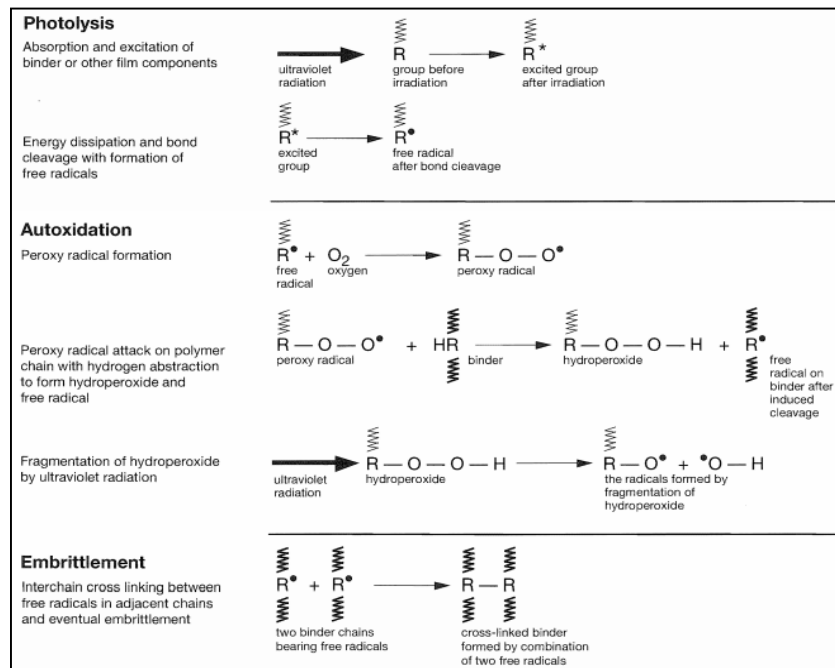


Figure 9: Process of UV light Degradation such as Photolysis, Autoxidation, and Embrittlement of Paint Film

The second phase of this mechanism is the photo oxidation. This is the reaction of the free radical of the photolysis phase with oxygen to form peroxide radicals (The degradation of Coatings by Ultraviolet Light and Electromagnetic Radiation) [29]. These peroxide radicals react with the polymer backbone by abstracting (removing) a hydrogen atom to form

hydroperoxide and other free radicals. Because hydroperoxide is extremely vulnerable to photolysis, it will readily fragment to provide more free radicals which will attack other sites on the polymeric backbone. Photolysis of other atoms in the coating is also possible, again producing excited, high energy moieties and then free radicals. All of these reactions produce more, equally harmful free radicals, which may attack and cause cleavage of the binder molecules [30].

Geuskens G. and David C. (1979) [31] said that the increase in production of highly reactive free radicals within the film can result in the occurrence of many complex intra-polymeric reactions. These reactions may include chain scission (splitting), depolymerization, and even the volatilization (evaporation) of smaller polymeric fragments. In addition, interchain cross linking can lead to excessive cross link density and embrittlement. While the exact nature of the changes will depend upon the polymer structure, the net effect is a marked change (deterioration) in physical, chemical, and performance properties which will be affected by hydrogen chloride and may produce corrosion of the substrate that the film originally intended to protect [32].

## **2.4 Inclusion of Silanized Graphene Nanosheets and h-BN into Polymer Coatings**

### **2.4.1 Graphene**

In the field of material design, the nanocomposites often show outstanding performances. Polymer nanocomposites compared with pure-polymer matrix, possess better mechanical properties and thermal dynamic performances [33]. In the past few years, carbon materials, including zero-dimension fullerene [34], one-dimensional carbon nanotubes [35], and three-dimensional diamond [36] have been widely applied in polymer composites. Graphene is a new

type of carbon material which was discovered by Konstantin Novoselov and Andre Geim in recent years [37]. It is a two-dimension, atomic scale, hexagonal carbon lattice in which one atom forms each hexagon vertex (Figure 10).

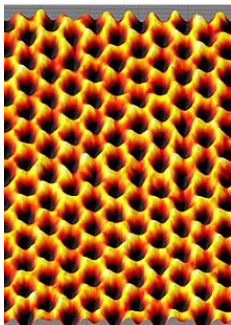


Figure 10: Scanning Probe Microscopy Image of Graphene

Graphene is composed of a two-dimensional lattice of covalently bonded carbon atoms arranged in a honeycomb structure (Figure 11). This structure can be described as a two dimensional hexagonal lattice offset from one another. Graphene has a lattice constant is  $2.46 \text{ \AA}$ . Each carbon atom is covalently bound to its three nearest neighbors. The two possible graphene edges are the “armchair” edge and the “zigzag” edge. Zigzag edges are known to have a metallic state whereas armchair edges do not.

Carbon, group IV in the Periodic table, has six total electrons, with four of them in a valence shell, and they are normally arranged in the  $1s^2 2s^2 2p_x^1 2p_y^1$  configuration. In graphene, the carbon atoms become  $sp^2$  hybridized, meaning that instead of occupying either the 2s or 2p shells, the electrons end up in a hybridized sp shell (see Figure 12) and are arranged in the  $1s^2 sp^1 sp^1 sp^1 2p_z^1$  configuration [38]. In this hybridized configuration, each carbon atom can covalently bond to its three nearest neighbors with an  $\sigma$  bond, the one remaining  $\pi$  bond shared between the atom and its nearest neighbors. Theory predicts that these weakly shared  $\pi$  bonds

are the sole source of graphene's extraordinary electronic properties, though both the  $\sigma$  and  $\pi$  bonds contribute to its physical strength and elasticity [39-41]. In graphene the s-shell has a spherical electron distribution, while the p-shell has a symmetric lobe-shaped distribution. The hybridized sp shell only has a one-sided lobed distribution. In the hybridized structure, the carbon atom shares two electrons in each of its sp shells and two electrons in its  $p_z$  shell with its three nearest neighbors.

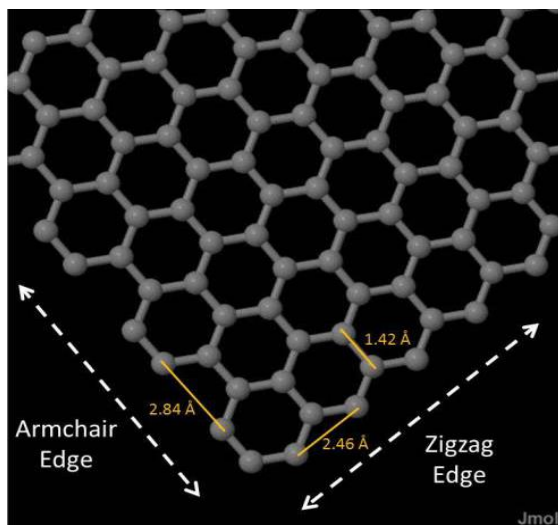


Figure 11: Graphene honeycomb lattice with Bond Strength Shows.

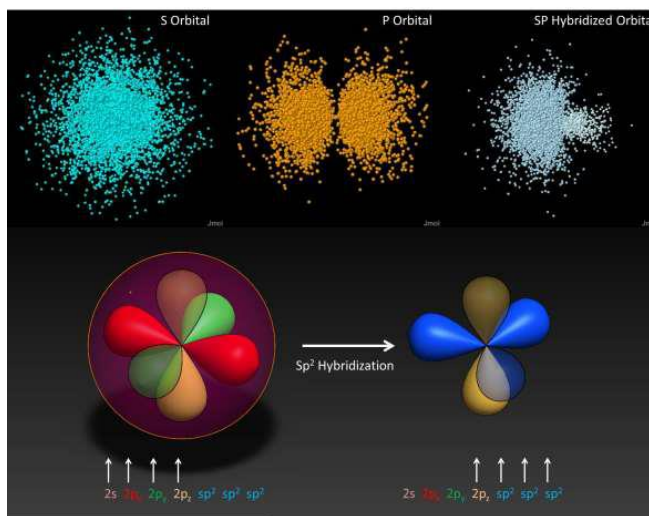


Figure 12: Electron Shell Hybridization in Graphene

Graphene's unique optical properties produce an unexpectedly high opacity for an atomic monolayer in vacuum, absorbing  $\pi\alpha \approx 2.3\%$  of red light, where  $\alpha$  is the fine-structure constant [42]. Graphene's band gap can be tuned from 0 to 0.25 eV (about 5 micrometer wavelength) by applying voltage to a dual-gate bilayer graphene field-effect transistor (FET) at room temperature [47]. The carbon-carbon bond length in graphene is about .142 nm and graphene sheets stack to form graphite with an interplanar spacing of 0.335 nm (Figure 13) [43]. This one atom thick crystal can be seen with the naked eye because it absorbs approximately 2.6% of green light and 2.3% of red light.

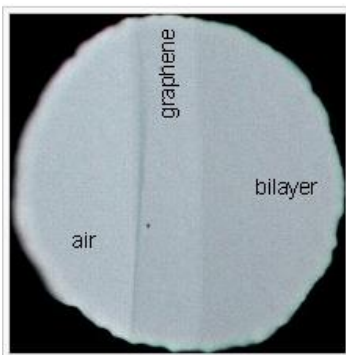


Figure 13: Photograph of Graphene in Transmitted light

The liquid phase production of graphene-based materials is very unstable and severely hampered by the poor solubility of graphene in common organic solvents, which is mainly due to the strong van der Waals force (or dispersion force) attraction between graphene sheets. In order to solve the problem, the most common method is to modify or silanized graphene with other molecules or substances to achieve a uniform dispersion of graphene. Then the nanocoating with the modified graphene and polymer matrix was prepared by a solution method and revealed a better performance.

## 2.4.2 Boron Nitride

Boron Nitride (BN) is binary compound that is made of group III and V elements, with its characteristics mentioned on section 2.4, has a band gap of 6.0 eV and possesses a high intrinsic in-plane thermal conductivity of 30-300 W/mK [44]. Two dimensional boron nitride nanoparticles (BN) [45] consist of equal numbers of boron and nitrogen atoms. BN is an isoelectronic (Boron and Nitrogen have the same number of electrons or a similar electron configuration), are similarly structured such as a carbon lattice and exists in various crystalline forms. Hexagonal boron nitride (h-BN) corresponding to graphite is the most stable and softest among BN polymorphs. It is also called  $\alpha$ -BN or g-BN (graphitic BN) and has a layered structure similar to graphite (Figure 14). Within each layer, boron and nitrogen are bound by strong covalent bonds, whereas the layers are held together by the weak van der Waals forces.

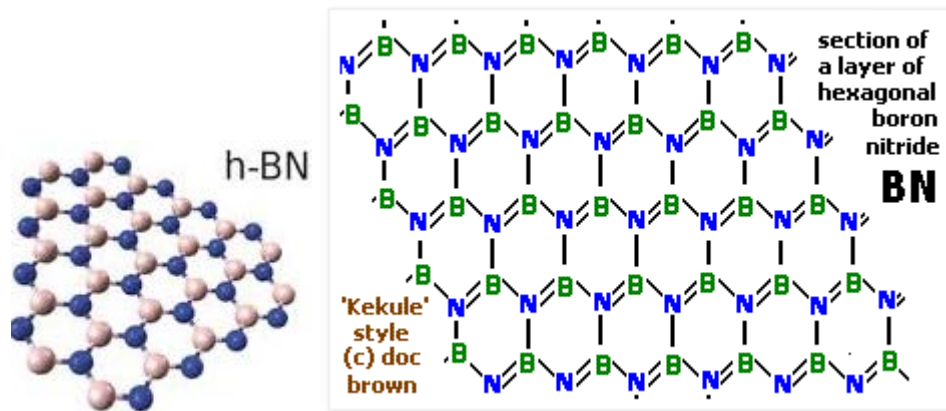


Figure 14: Boron Nitride Layer and Structural Arrangement of Boron and Nitride

Boron Nitride is a white and slippery solid with a layered structure, physically similar to graphite in this respect [46]. Like layers of graphite or graphene, it has a 2D planar regular covalent network. Due to its color, it can be confused with “white graphite” even though they have the same structure (Figure 18). The BN bond possesses a local dipole moment that is due

to the difference in electro negativity between boron (B) and nitrogen (N) atoms. This gives the covalent bond between B and N a significant polar nature [47].

BN is very stable and chemically, it is very inert. This compound has a great chemical stability but it is very unreactive to oxidizing gas and liquid solution. It melts under pressure at around 3000°C which is a great testament to its thermal stability. In the hexagonal form of boron nitride, alternate boron and nitrogen atoms are linked to form interlocking hexagonal rings, just like the carbon atoms in graphite do. Therefore in each hexagonal ring, there are 3 boron atoms and 3 nitrogen atoms and with each bond length being .145nm. This isn't an alternative single-double bond system but the above diagram (Figure 15) shows it's just a single valence-bond representative.

The B-N-B or N-B-N bond angle is 120° as expected for a perfect hexagonal ring bond network. It also found in graphite and  $sp^2$  hybridization for the boron atom bonds. The B-N bonding in the 2D layers is very strong which gives boron nitride great thermal stability with a great melting point. However, the layers are held together by weak intermolecular forces (Van der Waal forces, instantaneous dipole-induced dipole forces) and the layers are .334 nm apart; this distance is similar to the interlayer gap in graphite. H-BN particles can be incorporated in ceramics, alloys, resins, and plastics, rubbers to give them self-lubricating properties and form composite coatings shown to improve resistance to electrochemical corrosion [48].



Figure 15: Magnified Sample of Crystalline hexagonal boron nitride

Like graphene, BN shows impermeability to standard gas [49], excellent thermal stability, and remarkable inertness to oxidizing gas and liquid solutions [50]. In addition, BN nanoparticles were directly incorporated into polymers, metal, and composites to form composite coatings which show improved resistance to electrochemical corrosion [51]. Hexagonal boron nitride is obtained by the reacting boron trioxide ( $B_2O_3$ ) or boric acid ( $B(OH)_3$ ) with ammonia ( $NH_3$ ) or urea ( $CO(NH_2)_2$ ) in a nitrogen atmosphere [52]. An additional advantage of h-BN is that it is very good lubricant at both low and high temperature, and that its viscosity doesn't require water or gas strapped between the layers [51].

## CHAPTER 3

### MATERIALS AND EQUIPMENT

#### 3.1 Plexiglas [Poly (Methyl Methacrylate)]

The substrate used for the experiment is Poly (methyl methacrylate) – (PMMA), also known as acrylic or acrylic glass as well as by the trade names Plexiglas, Acrylite, Lucite, and Perspex among several others, is a transparent thermoplastic often used in sheet forms as a lightweight or shatter resistant alternative to glass [52]. It is not the type of silica-based glass, the substance, like many thermoplastics, is often technically classified as a type of glass (Figure 16). The Plexiglas with the thickness of 0.093” x 36” x 48” was purchased from Lowes’. It is many times stronger (fracture resistance) than glass, well-known for maximum energy saving, blocks harmful UV rays, and shatter resistant. Its chemical formula is  $(C_5O_2H_8)_n$ , density is  $1.18 \text{ g/cm}^3$ , melting temperature is  $160^\circ\text{C}$  ( $320^\circ\text{F}$ ,  $433\text{K}$ ), and its refractive index of 1.4905 at the wavelength of 589 nm [52]. Plexiglas is used in many applications such as building windows, skylights, bullet proof security barriers, sign & displays, sanitary wares, LCD screens, and many other applications.

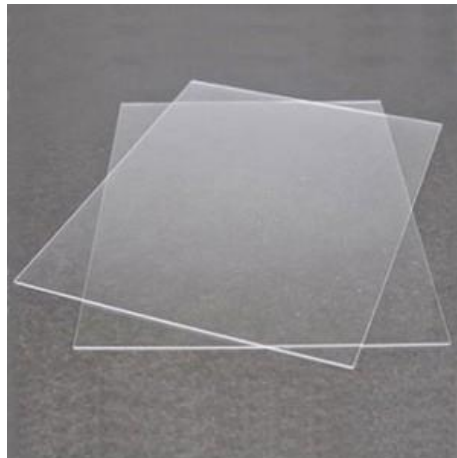


Figure 16: Plexiglas 0.093” x 36” x 48” Clear Acrylic Sheet

## 3.2 Coating/Paint

### 3.2.1 Miniwax Fast Drying Polyurethane Clear Gloss Paint

The coating used for the paper was Polyurethane clear gloss paint (PUR or PU).

Polyurethane is a polymer composed of a chain of organic units joined by carbonate (urethane) links. Polyurethane polymers are traditionally and most commonly formed by reacting a di- or polyisocyanate with a polyols. Both the isocyanates and polyols used to make polyurethanes contain on average two or more functional groups per molecule (Figure 17). Some noteworthy recent efforts have been dedicated to minimizing the use of isocyanates to synthesize polyurethanes, because the isocyanate raises severe toxicity issues. Non-isocyanate based polyurethanes (NIPUs) have recently been developed as a new class of polyurethane polymers to mitigate health and environmental concerns [53].

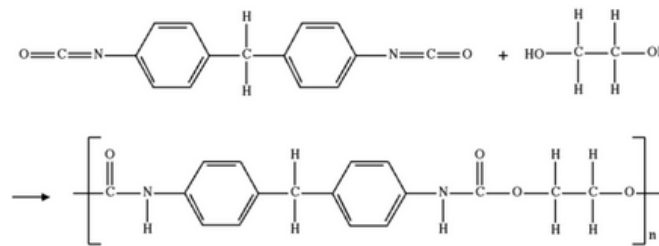


Figure 17: Polyurethane Synthesis, the Urethane Group  $-\text{NH}-(\text{C}=\text{O})-$  links the Molecular units

Polyurethanes are in the class of compounds called reaction polymers, which includes epoxies, unsaturated polyester and phenol [54]. Polyurethanes are produced by reacting an isocyanate containing two or more isocyanate groups per molecule ( $\text{R}-(\text{N}=\text{C}=\text{O})_{n \geq 2}$ ) with a polyol containing on average two or more hydroxyl groups per molecule ( $\text{R}'-(\text{OH})_{n \geq 2}$ ) in the presence of a catalyst or by activation with ultraviolet light [54]. Polyurethane paint doesn't soften or melt when heated because they are thermosetting polymers. In addition, it contains aromatic isocyanates, contains chromophores that interact with light. This is a particular

characteristic of polyurethane coatings, with light stability as a critical factor. When aromatic isocyanates in polyurethanes is exposed to visible light; it discolors and turns from off white to yellow or reddish brown [55].

### 3.3 Graphene

The graphene used in this experiment is graphene nanopowder with 12 nm flakes which was bought from Graphene Supermarket. The product number for the purchased graphene is SKU-NP-FLAO-5G1, its specific surface area is  $80 \text{ m}^2/\text{g}$ , purity 99.2 %, average flake thickness is 12 nm (30-50 monolayer), and average particle (lateral) size is around 4500 nm (1500-10000 nm). The pictures below show the purchased graphene container and a picture from scanning electron microscopes (Figure 18).



Figure 18: Unmodified Graphene Nanoflakes Obtained from Graphene Supermarket

### 3.4 Hexagonal Boron Nitride

The h-BN was used in this paper is bullet coating reloading hexagonal boron nitride powder dry lube-nano with an Atomic Particle Size (APS) of 70 nm and is 99% pure from Amazon (Figure 19). Because h-BN has the higher thermal conductivity when compared with

graphene, it has the best potential as a filler material in nanocomposite coatings. The main challenge with BN is that the surface is very inert. This leads to poor interfacial adhesion between BN and epoxy resin [55]. One way to counter this effect is to coat the surface of the BN nanoparticles with an ultrathin layer of a material that adheres well to the polymer. Any film grown on a BN particle must be extremely thin because the thermal conductivity ( $T_c$ ) through the BN particle/film composite will be reduced with the added thermal resistance of the film material.

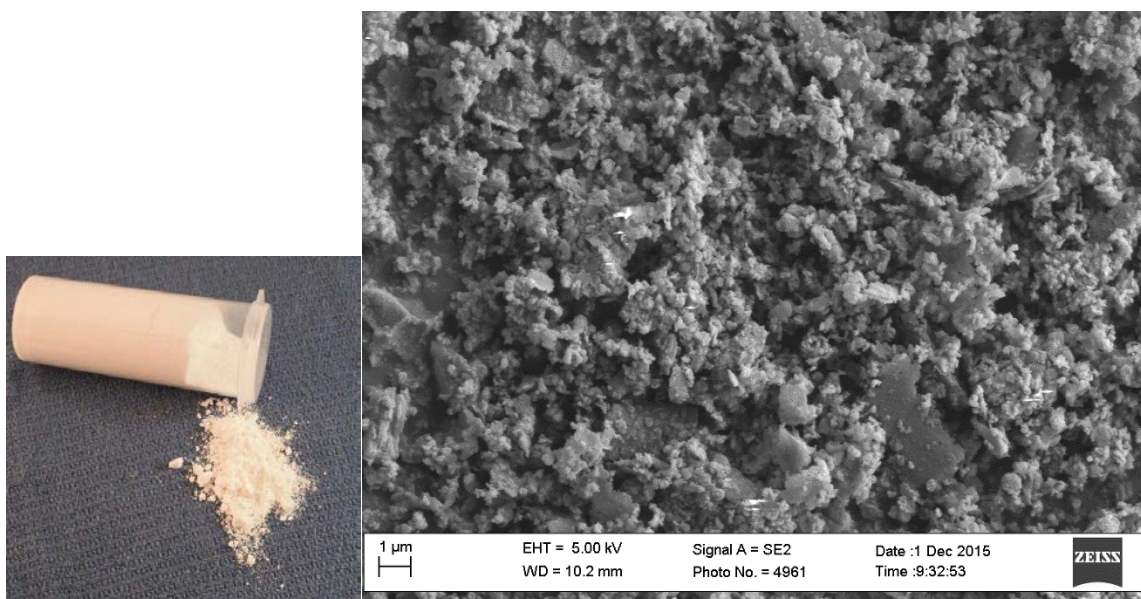


Figure 19: Hex Boron Nitride (h-BN) Powder and its SEM images

### 3.5 Graphene & h-Boron Nitride Mixture

With the similar characteristics of graphene and h-BN such as almost identical lattice parameters, bond angles, and bond spacing. Given the fact that graphene is black and h-BN is white so when we combine two nanomaterials together they become graphene and BN heterostructure. By using this approach, Chenxi Zhang, Jun Lou, and Jizhou Song developed a cohesive law for interfaces in graphene and h-BN heterostructure that was

based on the van der Waals force. In this structure h-BN serves as a dielectric layer between graphene and substrate to reduce the substrate influences on graphene. The h-BN is strong in plane bonds, large band gap, and planar structure provides an ideal flat, insulating, and inert surface which isolates the graphene from the substrate [56].

### 3.6 Preval Spray System

Preval spray system (Figure 20) is removable, refillable, and replaceable container which offers a professional-grade spray stream for virtually any surface. It is designed with a patented venture vacuum process (50 psi) that pulls liquid from the container then delivers a professional-grade stream that also can be used for a variety of paints or liquid products.



Figure 20: Preval Spray System used to Spray Paint Test Samples

### 3.7 Weighing Scale

A high-precision weighing scale used was a Mettler Toledo XS 64. The accuracy of the scale is  $1/1000^{\text{th}}$  gram ensuring accurate measurements. The Mettler Toledo XS 64 uses a smart grid weighing pan which reduces the effect of turbulences inside the weighing chamber; this smart grid also allows the reduction of stabilization times and permits accurate measurements.

The Mettler Toledo XS 64 also comes with a grid weighing pan that enhances secure placement of tare vessels. The Mettler Toledo XS 64 is shown in Figure 21.

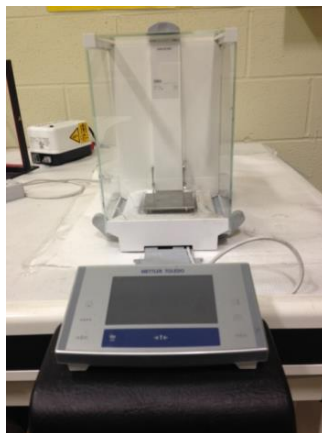


Figure 21: Mettler Toledo Weighing Scale used to Weight Nanomaterials

### 3.8 Hot Plate/Magnetic Stirrer

A hot plate used in conjunction with a magnetic stirrer was employed to guarantee a uniform dispersion of the nanoadditives in the coating. The magnetic stirrer used was from Fisher Scientific, and the stirring process was done using a magnetic stirring bar rotating at 100 rpm. The timeframe to carry out the mixing process is 4 hours. The magnetic stirrer used in this research is shown in Figure 22.



Figure 22: Hot Plate from Fisher Scientific used to mix the Coating System

### 3.9 Sonicator

A sonicator which produces ultrasonic waves was used as a secondary mixing process. The sonicator is used to help in breaking up the agglomeration of the nanoparticles as a way to ensure a uniform distribution of the nanoadditives. The breaking of agglomerates is possible due to the flow of the dispersion medium (paint) between the nanoparticles. The sonicator applies a mechanical stress on the nanoparticles through a pressure gradient resulting from the ultrasonic waves; this mechanical stress weakens the attraction forces between the nanoparticles, hence breaking up the agglomeration. Figure 23 shows the sonicator used in this research; inside of it is a water bath in which to place the beaker containing the paint.



Figure 23: Fisher Scientific FS 200 Sonicator used to Mix the Nanoparticles inside the Coating System

### 3.10 Mitutoyo 293-725 Digimatic Micrometer

A Mitutoyo 293-725 Digimatic Micrometer was used to measure the thickness of the coating. The objective of using a micrometer was to be able to measure the coating thickness on each specimen that was sprayed, and hence assure a uniform coating on all specimens. The

coating thickness maintained was 1 mil ( $\approx 25.4$  microns). This was subsequently repeated to the four to six coats that I used. The micrometer used in this research is shown in Figure 24.



Figure 24: Mitutoyo 293-725 Digimatic Micrometer used to Control the Coating thickness

### 3.11 UV Chamber

Light exposure and weathering are major causes of damage to plastics, coatings, and other organic materials. The QUV accelerated weathering cabinet was used to reproduce the UV light necessary to simulate the damaging effect of sunlight. It simulates solar radiation by using UVA-340 lamps which only produce the ultraviolet part of the light spectrum. The QUV chamber used in this research causes photo degradation in a very short amount of time (twenty days) when compared to outdoor testing that could take months or even years. The QUV accelerated weathering tester is shown in Figure 25.



Figure 25: QUV Accelerated Weathering Cabinet used to simulate the Weathering of nanocomposite Coatings

### 3.12 Fourier Transform Infrared (FTIR) Spectrometer

An FTIR analysis was carried out after UV exposure to examine the mechanism of degradation of the polyurethane coating. The FTIR instrument employed was the thermal Nicolet magna 850 R spectrometer. To study the degradation mechanism, a modified method of standard FTIR was exercised; this method is called the attenuated total reflectance (ATR) FTIR. The reason why ATR-FTIR was applied is because the test specimens were opaque and hence the infrared beam could not penetrate them. In order to perform the ATR-FTIR, a modular attachment known as the Nicolet NIC-plan was used in conjunction with the thermal Nicolet magna 850 IR spectrometer, as shown in Figure 26.



Figure 26: Thermal Nicolet magna 850 IR Spectrometer used to Perform FTIR Studies

### 3.13 Optical Contact Angle Goniometer

In this research, an optical water contact angle goniometer was used to study the surface integrity of the coating. The goniometer measures high and low water contact angles; a high contact angle indicates a hydrophobic surface, and a low contact angle indicates a porous or wettable surface. The model used was the Model CAM 100 from KSV Instruments Limited. The

CAM 100 consists of a compact CCD camera used to measure the contact angles of liquids on solids; it comes with shape-analysis software that ensures the measurements are error-free and user-independent. The Cam 100 contact angle goniometer is designed for education, industrial, and R&D applications. As seen in Figure 27, the CAM 100 contact angle meters can display the profile of the liquid on the surface through its integrated built-in camera and software interface.



Figure 27: Optical Water Contact Angle Goniometer

### **3.14 UV Visible Spectroscopy**

Ultraviolet-visible spectroscopy or ultraviolet-visible spectrophotometer (UV-Vis) refers to absorption spectroscopy the ultraviolet-visible spectra region. This means it uses light in the visible and adjacent (near- UV and infrared (NIR)) range. In this paper, the UV-Visible Spectrophotometers U-2900 double beam spectroscopy system for biotechnical applications measuring small sample volumes. It offers high performance, ease to use, and reliability. This system can be used in many applications from routine to research (Figure 28)



Figure 28: UV-Vis Spectrometers U-2900 Hitachi

### 3.15 Scanning Electron Microscopy

Scanning electron microscope (SEM) was used for the surface imaging of silanized and non-silanized graphene nanoflakes and BN nanoparticles. SEM is an approved imaging technique, and was also used to look at the dispersion of the nanoadditives inside the coating. The scanning electron microscope used was the SIGMA series of Field Emission Scanning Electron Microscopes (FE-SEM); it is manufactured by the Carl Zeiss Group, a leading international company in the fields of optoelectronics and optics. The SIGMA FE-SEM from Zeiss has a GEMINI design which provides stability and low voltage imaging; it is able to image structures as tiny as 1.5 nm, and it delivers a very high resolution of up to 1.0 nm. It has fully integrated image navigation software, which makes it easy to orient and position specimens inside the chamber with the aid of a digital overview image. The SIGMA FE-SEM is available at the WSU engineering labs; it is shown in Figure 29.



Figure 29: SIGMA Series of Field Emission Scanning Electron Microscope

### 3.16 Different Scanning Calorimeter

Differential Scanning Calorimeter (DSC) uses to measure a number of characteristic properties of a sample such as fusion, crystallization, oxidation as well as glass transition temperature ( $T_g$ ). It is a thermal analytical technique in which the difference in the amount of heat required to increase the temperature of a sample and reference (Figure 30). The DSC analysis was used in this paper is Q 2800 which performed under a  $N_2$  atmosphere and using approximately 10 mg of each sample. Samples were initially heated from ambient temperature to  $250^\circ\text{C}$  at a heating rate of  $10^\circ\text{C}$  per minute, cooling down until  $-50^\circ\text{C}$  and then heat again at a rate of  $10^\circ\text{C}$  per minute to  $250^\circ\text{C}$ .



Figure 30: Different Scanning Calorimetry Q-2800

## CHAPTER 4

### METHODS

#### 4.1 Silanization Process of Graphene

The organosilane used in this study to 34 sonicator pristine graphene was the technique grade [3- (2-Aminoethylamino) propyl] trimethoxysilane, purchased from Sigma-Aldrich, Inc. First, 2 grams of pristine graphene was weighted as shown in Figure 31 (a); the graphene was then put inside a beaker, Figure 31 (b-c), and then was dispersed in 200 ml ethanol (95%) by high powered ultra-sonication for 1 hour, Figure 31 (d-g).

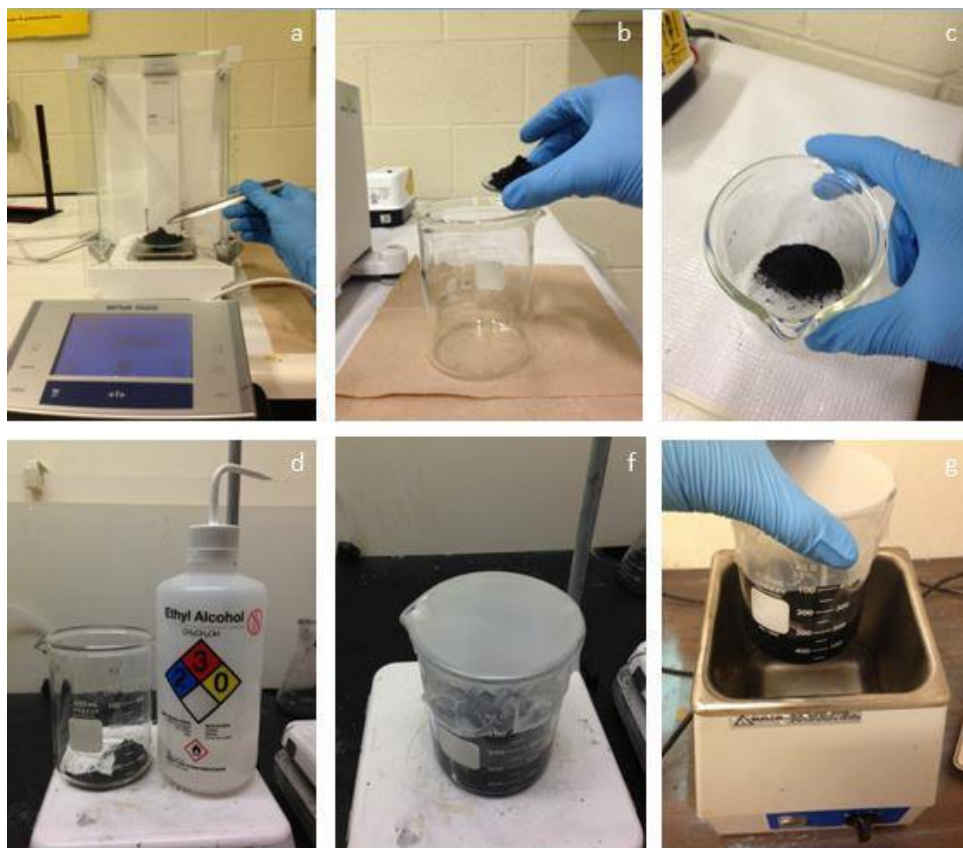


Figure 31: Silanized Graphene Preparation (Part 1); a) measure 2g of graphene b-c) Pour graphene in a beaker d) Mix 2g of Graphene with 200 ml ethanol f) Cover mixture of graphene and ethanol g) Mix graphene and ethanol suspension by high power sonification for 1 hour

The resultant homogeneous graphene/ethanol suspension was removed to an Erlenmeyer flask as shown in Figure 32 (h). The flask was then heated up to approximately 120°C in order to boil the ethanol, and a magnetic stirrer was added inside of it, Figure 32 (i). Next were the drop-wise injection of the silane surfactant (12 ml) into the sealed Erlenmeyer flask and the sealing of the flask as seen in Figure 32 (j-k). After 5 hours of reaction, the graphene/ethanol mixture was cooled down to room temperature, and the resulting silanized graphene suspension was rinsed with 500 ml DI water through a filtration process as shown in Figure 32 (l-m) and Figure 33 (n-o).

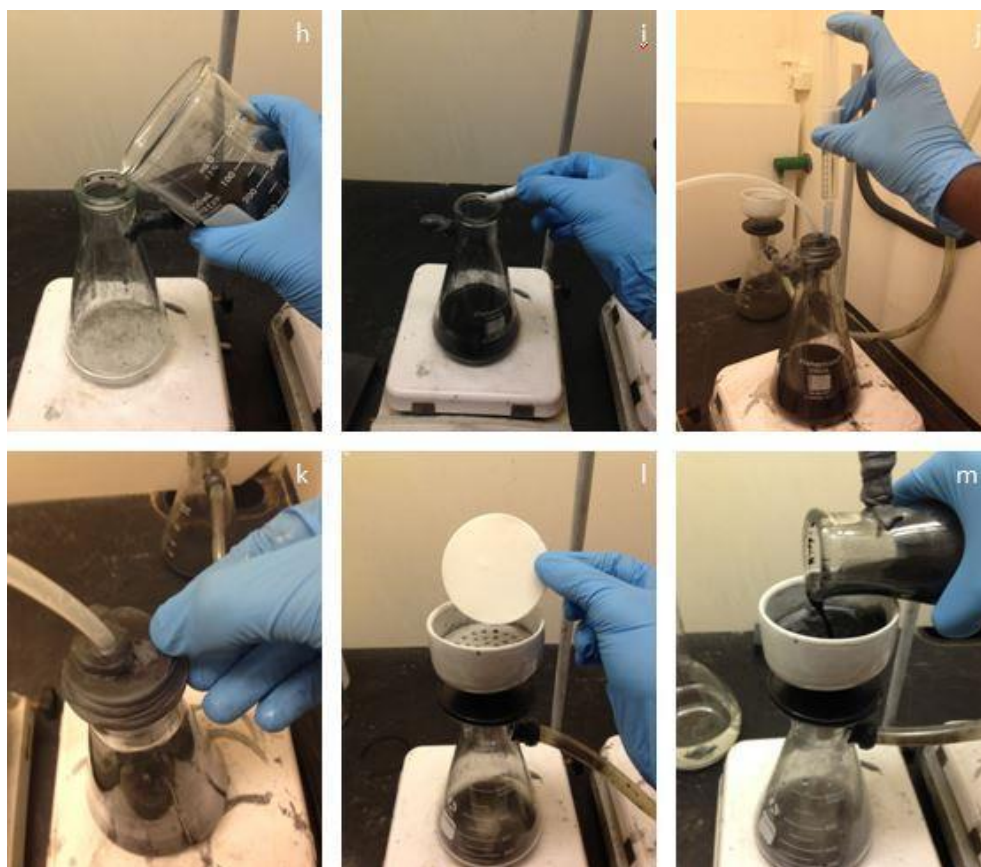


Figure 32: Silanized Graphene Preparation (Part 2); h) Pour mixture into Erlenmeyer flask i) Add magnetic stirrer to the flask and turn the hot plate on j) Add 12 ml of Silane Surfactant to the mixture k) Seal the flask completely and let the graphene ethanol suspension react for 5 hrs. l-m) After 5 hrs. reaction, collect the graphene through the filtration process

In order to collect the silanized graphene, it was mixed with DI water first, Figure 33 (p-q), and then dried overnight in the oven at 70°C for further use as shown in Figure 33 I; the collected silanized graphene is shown in Figure 33 (s).

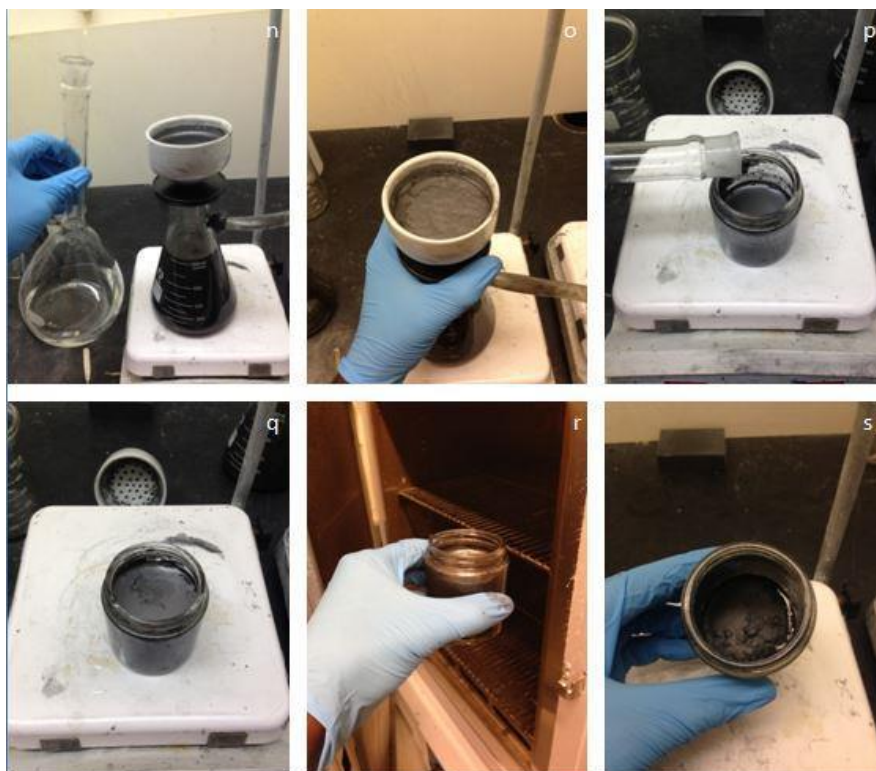


Figure 33: Silanized Graphene preparation (Part 3); n) Rinse the graphene with 500 ml DI water o) let all the water seep through the filter p-q) Collect the graphene in a small container and add more DI water r) Place the container in the oven at 70°C (overnight) s) Collect the Silanized graphene

#### 4.2 Silanization Process of h-BN

The silanization process of h-BN is similar with graphene, by using the same organosilane [3- (2-Aminoethylamino) propyl] trimethoxysilane, purchased from Sigma-Aldrich, Inc. The same procedure and method that had been done with graphene to silanized h-BN was used. The collection of silanized h-BN was placed in the oven at 70°C overnight.

### 4.3 Stability of Graphene and h-BN in Acetone Suspension to Prove Successful Silanization

Surface morphology of the graphene nanoflakes and BN nanoparticles were characterized using SEM (Figure 34 & 35 & 36). After silanization, the appearance of the graphene nanoflakes do not change much; this suggests that the silanization process is non-destructive, and mild to the graphene structure. The apparition of a bright substance is seen on the surface of the silanized graphene and not on the unmodified graphene; this substance could be the silane particles attached to the graphene surface. In order to truly confirm the silanization process of graphene particles, there are other methods that can be used as well.

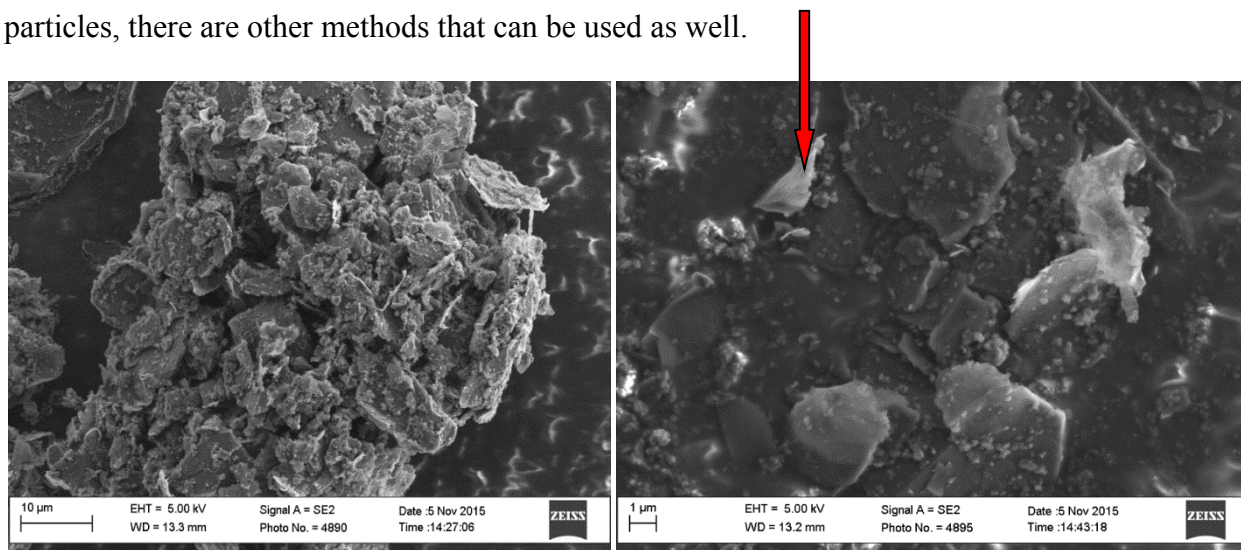


Figure 34: SEM Image of Unsilanized Graphene (left) and Silanized Graphene (right)

Opposite with graphene, after the silanization process, the h-BN nanoparticles were still clumped together and had some long strings. Its particles appeared to form boron nitride nanotubes or strings see SEM pictures (see Figure 35). Because h-BN doesn't conduct electricity, it was difficult to get detail pictures of silanized h-BN at nanoscale level to see if possibly they form nanotubes or nanostrings. The questions that remain are how did BN particles react with organosilane and why did they form like string? When pressing silanized

BN, it had the texture of rubber, was clustered together, and needed a little bit of force to break apart.

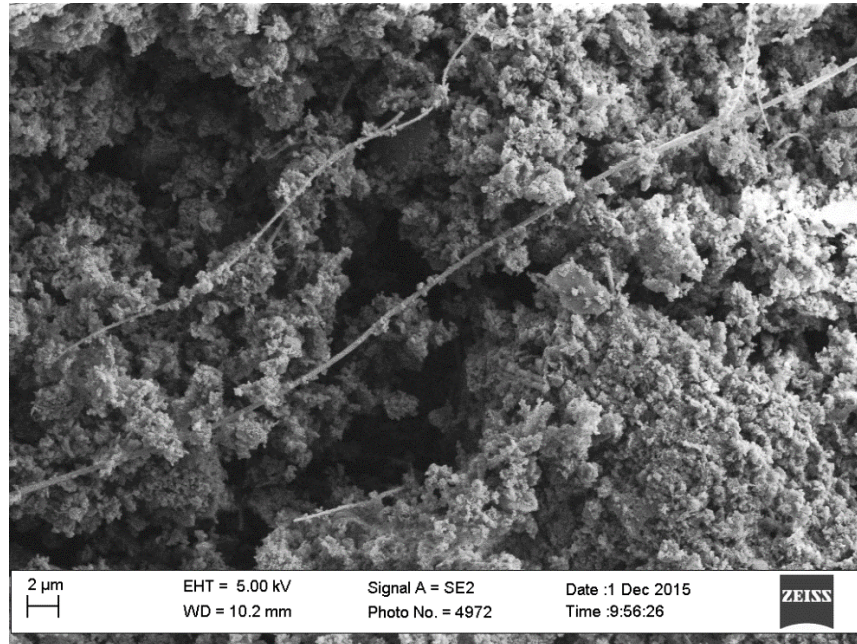
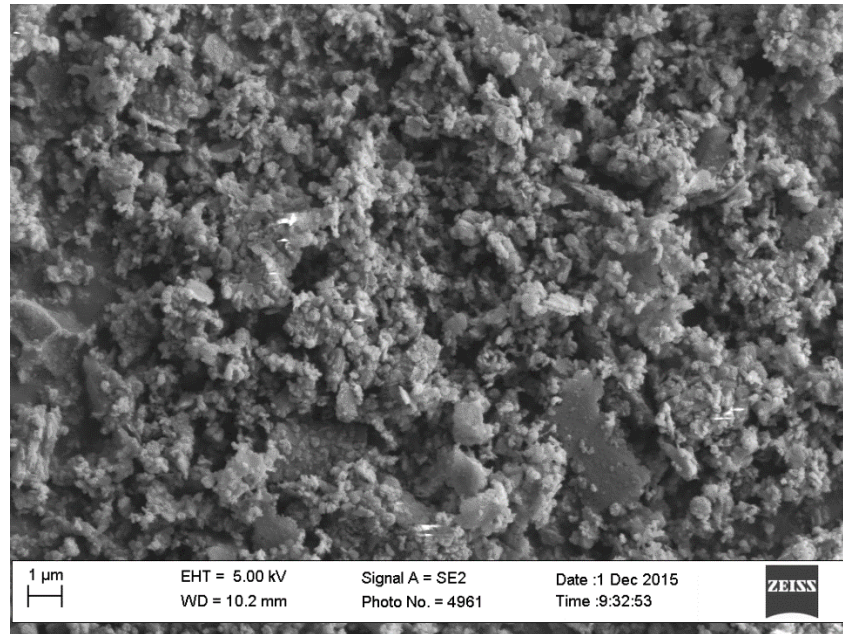


Figure 35: SEM Image of Unsilanized h-BN (top) and Silanized h-BN (bottom)

The mixture of Graphene and h-BN after silanization showed the success of exfoliating the graphene sheets and h-BN nanoparticles. Figure 36 shows the dark color of graphene sheets and the lighter color of h-BN particles are separated and mixed together at 10  $\mu\text{m}$  scale.

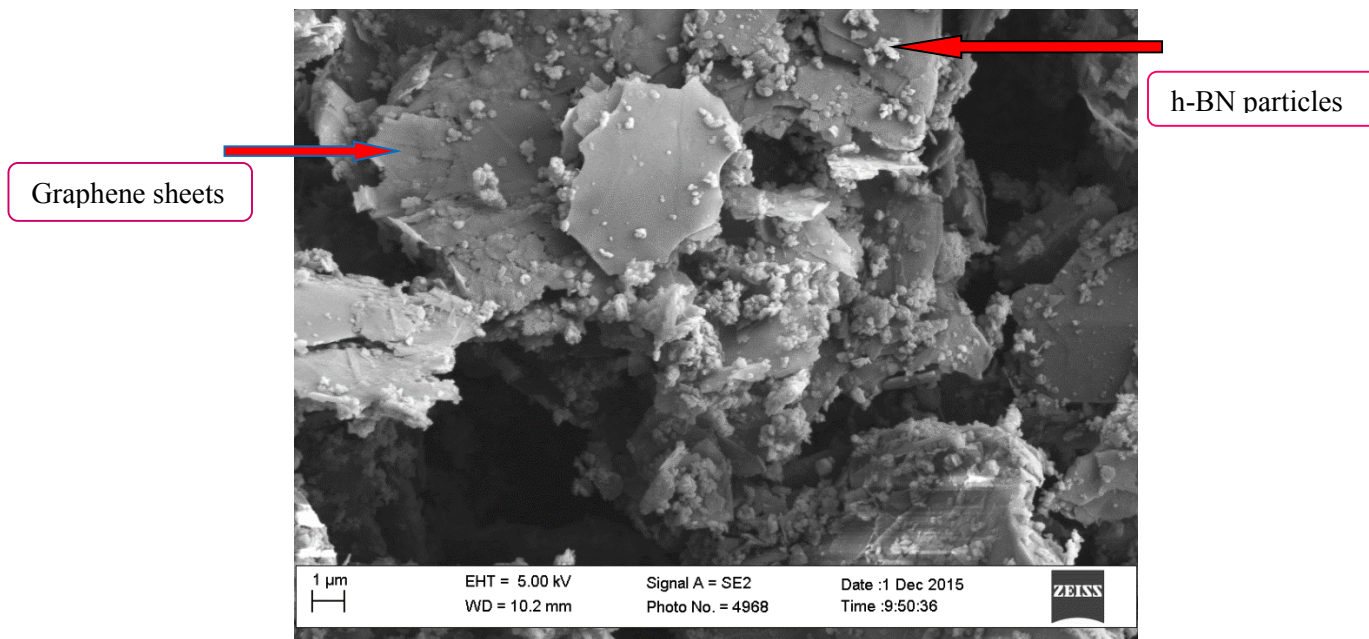


Figure 36: SEM Image of Silanized graphene & h-BN

The most efficient method to prove the successful surface modification of graphene through silanization is the investigation of its stability in acetone [57]. Samples of pristine graphene and silanized graphene were each dissolved in acetone for 5 minutes through an ultrasonic bath, and then each of the samples was put in repose for 5 hours. Even though the pristine graphene and the silanized graphene dispersed homogeneously in the acetone solution after the ultra-sonication treatment, a major difference is seen between the two after 5 hours. As shown in Figure 37, sample (b) which corresponds to the silanized graphene solution stays dispersed much longer than sample (a) corresponding to the pristine graphene solution. This observation clearly

indicates that the silanization was successful, and that the silane molecules chemically bonded to the graphene surface.

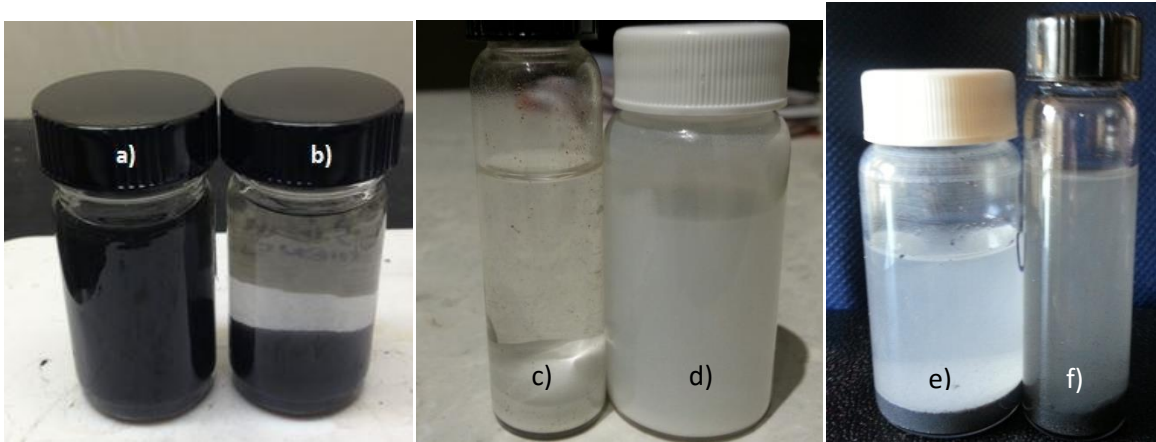


Figure 37: Samples of Graphene, h-BN, and graphene & h-BN Dissolving Acetone a) Pristine Graphene, b) Silanized Graphene, c) Pristine h-BN, d) Silanized h-BN, e) Pristine Graphene & h-BN, f) Silanized graphene & h-BN

On the other hand, silanized h-BN didn't show the success of surface modification. Pristine h-BN and silanized h-BN were distributed into acetone for 5 minutes through an ultra-sonification bath, and then the mixtures were sustained for 5 hours. Figure 37 (c) shows pristine h-BN bonded to the surface longer and figure 37 (d) shows silanized h-BN didn't bond to the surface, they were still distributed everywhere in the acetone liquid. The mixture of pristine graphene in acetone (Figure 37 e) shows the h-BN dispersed into acetone liquid, but the graphene precipitated at the bottom of the substrate. They will make good bond to the surface; however the mixture with pristine graphene & h-BN let the material's residues on the surface substrate. Figure 37 (f) the silanized graphene & h-BN bonded to the surface better than the pristine graphene & h-BN. After silanization using the same amount of graphene and h-BN, graphene's color is almost always the dominant color (dark) in contrast with h-BN in Figure 37 (e)

#### 4.4 Preparation for Plexiglas Surface

Plexiglas was purchased as a sheet .093” x 36” x 48” and covered with film masking to protect the plastic’s surface. The sheet was cut into 3” x 3” pieces and used as substrate. The samples had the film masking peeled off on both sides, and then the surfaces were prepped with the isopropyl alcohol or ethanol or acetone to make a good surface adhesive for coating. Then the substrates were allowed to dry for 1 minute to ensure that all cleaning agents would evaporate completely (figure 38).

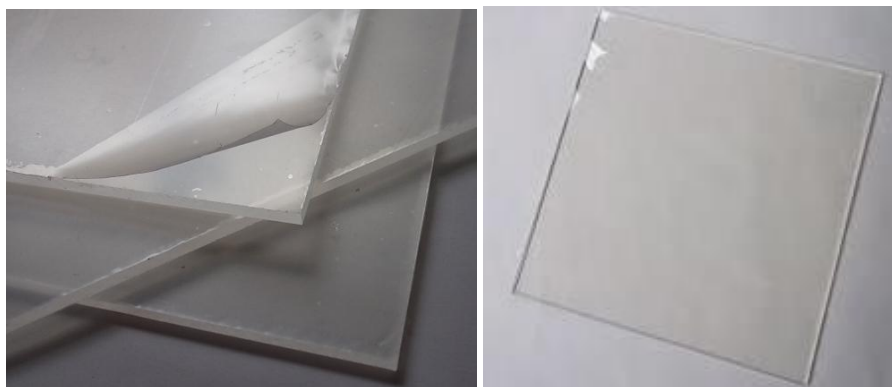


Figure 38: Test samples for Coating before (left) and after peeled off the masking Plastic and cleaning

#### 4.5 Preparation for Based Coat

The polyurethane paint itself was used for the based coat on the plastic substrates. In application of a base coat of PU it was stirred before and during use to eliminate setting in the bottom of the can. Put a portion of pure PU paint, which has been stirred, in the Preval spray gun then applying a thin coat on all test sample surfaces. The polyurethane paint used had the main ingredients of Med. Aliphatic Hydrocarbon Solvent 53.8 % by weight and Methyl Ethyl Ketoxime 0.1% by weight. The PU paint didn’t contain benzene rings. The PU paint contained

mixtures of either saturated, long straight chain (normal- paraffin) or branched chain (isoparaffin) or cyclic-paraffin. Common vehicles used in paints and coatings are mineral spirits, hexanes, heptanes, and VM&P naphtha.

PU paint is considered hazardous by the OSHA Hazard Communication Standard (29 CFR 1910 1200) which is stated in the MSDS. It is a flammable liquid with category #3, skin sensation category #1, specific target organ toxicity category #3, and aspiration hazard category #1. Lab safety should take care careful when working with PU paint by following the material safety data sheet. The fume hood is needed when spraying the paint and care should be taken and minimal people should be in the lab when applying.

After applying a based coat on the surface of all the test samples, then let then dry at room temperature about 6 hrs. Or put then in an oven (to increase the curing process) at 77°C for a couple hours before apply second coat. The dry times of PU paint are based on good ventilation, temperature of 77°F and 50% relative humidity. Lower temperature, higher humidity, lack of air movement or application of thick coats will extend drying times (Figure 39).



Figure 39: Based Coat of Pure PU on the substrate

## 4.6 Preparation for Top Coat

To prepare for the top coat, the first thing is to make sure the based coats were dried completely on the substrate samples. The top coat consists of nanoadditives with varying weight percentages. The silanized graphene, h-BN, and G & h-BN were weight 0.1wt %, 0.2wt%, 0.4wt %, and 0.8wt %, placed into beakers, and then PU paint was added. The mixture of nanomaterial and PU paint was put into a sonicator at room temperature for 30 minutes. After the sonication process, the mixture was stirred by the stirrer for 4 hours at room temperature which allowed good distribution of the nanoadditives in the top coat (Figure 40).



Figure 40: Mixtures of PU & Silanized h-BN (left), PU & Silanized graphene (center), PU and graphene & h-BN (right)

## 4.7 Top Coat Painting

After preparation, the top coat was applied to the test samples by the Preval spray gun. After application, the test specimens were then air-dried for 6 hours at room temperature. The coating method was repeated to reach the thickness of the whole coating system is 1 mm (25.4 micron). Figure 41 (a) shows the plastic test samples

coated with 0.1wt% graphene and PU. It is very clear and has a good transparent coating on the plastic substrate. Figure 41 (b) is the clear top coating of 0.1wt% silanized h-BN in the PU on the plastic substrate; we can see the white residues of silanized h-BN on the substrate.

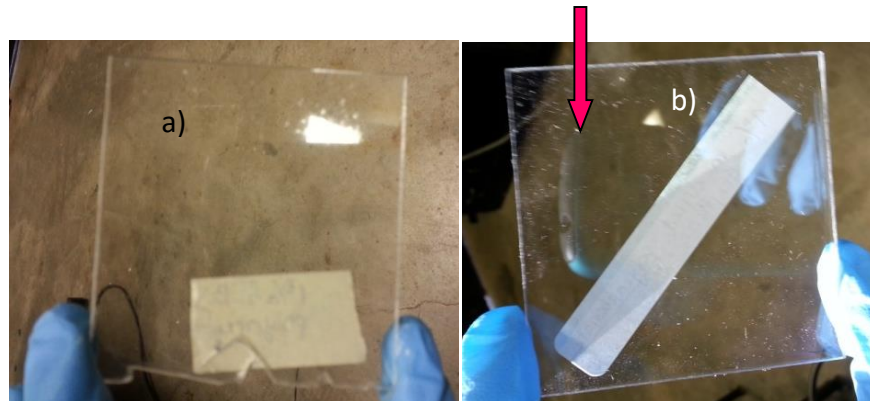


Figure 41: Clear Top Coat with a) 0.1wt% S-G with PU, b) with 0.1% h-BN with PU

Figure 42 shows the coatings of different percentages of silanized h-BN with polyurethane paint on the plastic substrates. The h-BN nanoparticles kept its natural off white color through the silanization and blending process. The more silanized the h-BN is when combined with PU paint, the whiter the coating on the substrate. Figure 43 is the coating of graphene with PU on the substrate with different percentages of graphene.

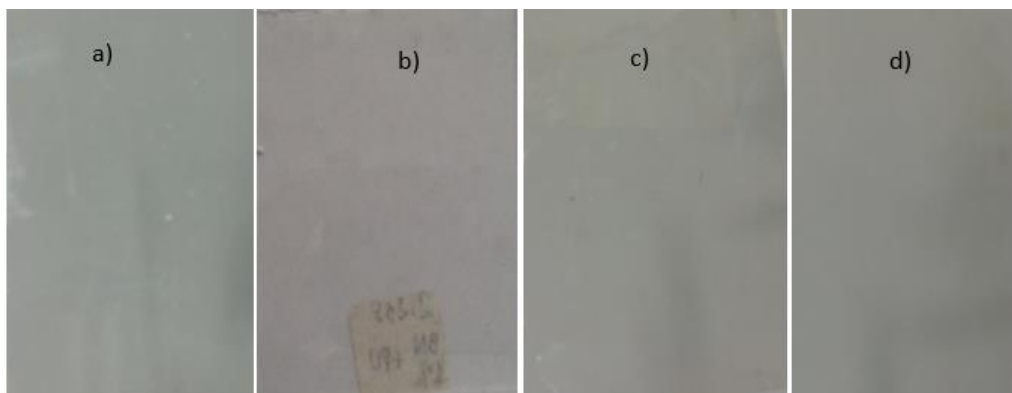


Figure 42: Coatings with 0.1wt% h-BN (a), 0.2wt % h-BN (b), 0.4wt% h-BN (c), and 0.8wt% h-BN (d)

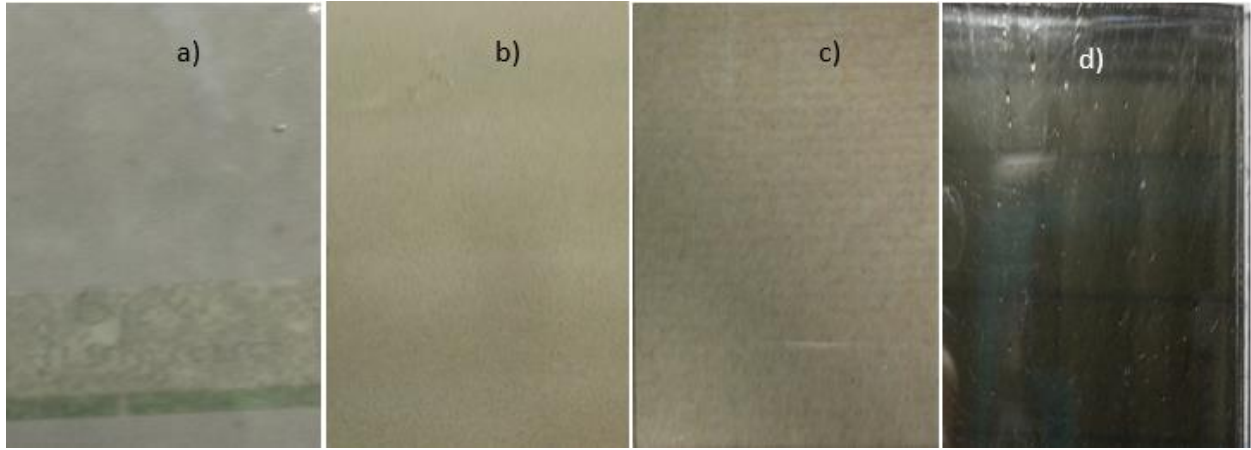


Figure 43: Coatings with 0.1wt% S-G (a), 0.2wt% S-G (b), 0.4wt% S-G (c), 0.8wt% S-G (d)

#### 4.8 UV Exposure Test

The UV degradation test was performed using the QUV accelerated weathering chamber. The testing was performed according to the SAE standard ASTM D 4587-09, which shows the basic process of exposing paint and related coatings to UV light. The specimens were tested for a total of 20 days and characterized for surface morphology, hydrophilic/hydrophobic behavior and also coating thickness in 5-day intervals. Figure 44 shows the specimens placed in the UV tester after the test.



Figure 44: UV Degradation Test Using the QUV Weathering Tester

## 4.9 Surface Characterization

### 4.9.1 Water Contact Angle Measurements

The contact angle can be described as the angle at which the solid interface meets the liquid / vapor interface. The Young-Dupre equation is used to express contact angle when thermodynamic equilibrium is assumed between the three phases [58]. Figure 45 shows the theoretical interpretation of contact angle, with  $\gamma_{SV}$  representing the solid-vapor interfacial energy,  $\gamma_{SL}$  representing the solid-liquid interfacial energy, and  $\gamma_{LV}$  representing the liquid-vapor interfacial energy; the relationship between these interfacial energy is represented in the Young-Dupre equation:

$$\cos \theta = \frac{\gamma_{SV} - \gamma_{SL}}{\gamma_{LV}} \quad (2)$$

where  $\gamma_{SV}$  represents the solid-vapor interfacial energy,  $\gamma_{SL}$  represents the solid-liquid interfacial energy and  $\gamma_{LV}$  represents the liquid-vapor interfacial energy.

Young's equation defines the contact angle as the result of thermodynamic equilibrium between the solid, liquid, and vapor interphase. When measuring contact angle values of polymeric surfaces a measurement of  $90^\circ$  is considered hydrophilic, but a measurement of more than  $90^\circ$  up to  $150^\circ$  is considered hydrophobic. When the polymeric surface contact angle is more than  $150^\circ$ , then the surface is described as a super hydrophobic surface, and when the contact angle values are found to be less than  $5^\circ$ , and then the surface is described as a super hydrophilic surface. However, measured contact angles are very sensitive to the type of the solid's surface. When contact angle measurements methods are used as a high-resolution probe to examine the surfaces of solids, and microscopic roughness can cause considerable changes in the calculated contact angle [59]. The water contact angles were measured during days 0, 5, 10,

15, 16, and 20 to investigate the deterioration of the nanocomposite coating surface properties during testing.

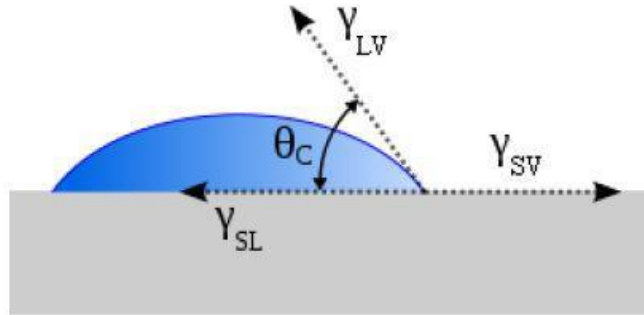


Figure 45: Theoretical Interpretation of Water Contact Angle [56]

#### 4.9.2 ATR-FTIR Analysis

An attenuated total reflectance FTIR analysis was carried out after UV exposure to examine the mechanism of degradation of the polyurethane coating with different percentages of nanoadditives inclusion. An IR spectrum is obtained based on factors of compounds such as photoconductivity, emission, absorption, and scattering. The purpose of this test is to measure how much light is absorbed by the compounds at different wavelengths and what the bond types of the compound at specific wavelength of lights. Infrared light spectrum causes vibrational excitation of bond in the molecules. The % transmittance is the percentage of IR emitted that actually passes through the sample. FTIR images of control specimens (0% S-GNP) and nanocoating specimens containing 0.1wt% and 0.4wt% silanized graphene nanoflakes were taken.

#### 4.9.3 UV Vis Spectroscopy

UV/VIS Spectrophotometer is used to determine the absorption or transmission of UV/VIS light (180 to 820 nm) by a sample. It can also be used to measure concentrations of absorbing

materials based on developed calibration curves of the material. A sample is placed in the UV/VIS beam and a graph of the transmittance or absorbance versus the wavelength is obtained. The absorption or transmission in the visible range will affect the perceived color of the chemical involved. This method is most often used in a quantitative way to determine concentrations of an absorbing species in solution, using the Beer-Lambert law:

$$A = \log_{10}\left(\frac{I_0}{I}\right) = \epsilon cL \quad (3)$$

where A is the measurement absorbance,  $I_0$  is the intensity of the incident light at a given wavelength, (I) is the transmitted intensity, L is the path length through the sample, and c is the concentration of the absorbing species. For each species and wavelength,  $\epsilon$  is a constant known as the molar absorptivity or extinction coefficient. The constant is a fundamental molecular property in a given solvent, at a particular temperature and pressure, and has units of  $1/(\text{M}\cdot\text{cm})$  or often AU/M.cm. The Hitachi U2900 spectrometer was used in this paper to show the light absorbance of variety percentages of silanized and un-silanized nanoadditives in the coatings such as 0.1wt% un-silanized graphene (or unmodified– G), 0.1wt% silanized graphene, 0.1wt% un-silanized BN0, 0.1wt% un-silanized-BN, 0.4wt% un-silanized G, 0.4wt% silanized G, 0.4wt% un-silanized BN, 0.4wt% silanized BN, and 0.4wt% silanized G-BN.

#### **4.9.4 DSC Test**

Differential Scanning Calorimetry (DSC) is a thermal analytical technique for measuring the heat energy necessary to establish a nearly-zero temperature different between a test substance (reaction products) and an inert reference material, while the two samples are subject to an identical (heating, cooling or constant) temperature program. This technique helps to quantitatively determine the various material

transitions that take place in a substance, and hence quantify certain specific physical properties of substance. This is a valuable method for the characterization of thermal plastic materials.

The Q2800 differential Scanning Calorimeter was used in this paper to find the glass transition temperature of the coating samples with 0.1wt % and 0.4wt % of graphene and h-BN in the coating. The DSC plots of each sample will show the T<sub>g</sub> (glass transition temperature), melting (T<sub>m</sub>) & boiling points, crystallization time & temperature, enthalpy ( $\Delta H$ ), and thermal stability.

## CHAPTER 5

### RESULTS AND DISCUSSION

#### 5.1 UV Chamber Studies

Polyurethanes, especially those made using aromatic isocyanates, contain chromophores that interact with light [60]. This is of particular interest in the area of polyurethane coatings, where light stability is a critical factor and is the main reason that aliphatic isocyanates are used in making polyurethane coatings. When PU coating, which is made using aromatic isocyanates, is exposed to visible light, it discolors, turning from off-white to yellow to reddish brown [60]. It has been generally accepted that apart from yellowing, visible light has little effect on PU paint. It has been reported that exposure to visible light can affect the variability of some physical property test results [61]. Figure 46 shows the test specimens after 20 days of UV chamber.

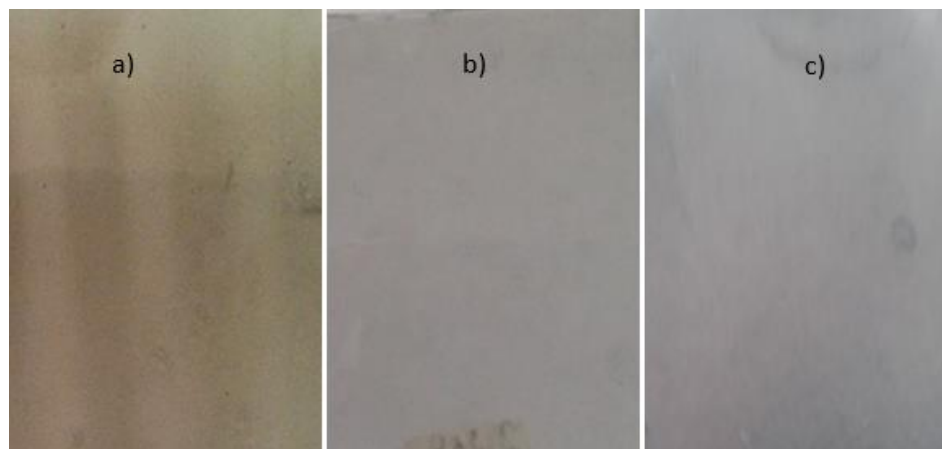


Figure 46: Test Samples after UV Chamber, color change to yellow of the graphene and PU coating (a) more than h-BN and PU coating (b) and graphene & h-BN coating(c)

In addition to the changes of color of coatings after UV chamber, the thickness of coatings degraded as well. The bare plastic substrate is  $0.093'' = 2.3622$  mm and the coating thickness is

1mm for all different percentages of graphene. Table 1 shows the changes of graphene coating thicknesses after 5 days interval. The more graphene added to the coating, the less UV degradation of the coating (see the graph in Figure 47). On the coating with 0.1wt % silanized graphene, there are some bare areas on the coatings surfaces because the coating came off the substrate and stuck into the tape which used to hold the test specimens in the UV chamber. This problem didn't happen with the coatings with 0.4 wt % and 0.8 wt % graphene. In addition, the more graphene added into the coating, the less transparency of the plastic substrates.

In contrast, the coatings with h-BN didn't change much in color. They retain their milky color of h-BN as their appearance and the degradation rate is very small amount of .0009 mm average compare to the coatings with graphene. Table 2 shows the thickness of silanized h-BN coating after 20 days in UV chamber. As with graphene, the more h-BN added to the coatings, the less transparency through the substrates. Additionally, the h-BN coating didn't come off the substrates when the holding tapes were pulled off the coating surface after 20 days in comparison with graphene coatings. Figure 48 is the graph of the coatings with different percentages of silanized h-BN after UV chamber 20 days.

TABLE 1  
THE THICKNESS OF PU COATING WITH DIFFERENT PERCENTAGES OF  
SILANIZED GRAPHENE

<b>Days</b>	<b>0.1wt%G</b>	<b>0.2wt% G</b>	<b>0.4wt% G</b>	<b>0.8wt% G</b>
0	3.3622	3.3622	3.3622	3.3622
5	3.36	3.3612	3.3619	3.362
10	3.3565	3.3593	3.361	3.36175
15	3.3534	3.357	3.36	3.3615
20	3.3482	3.353	3.3585	3.36105

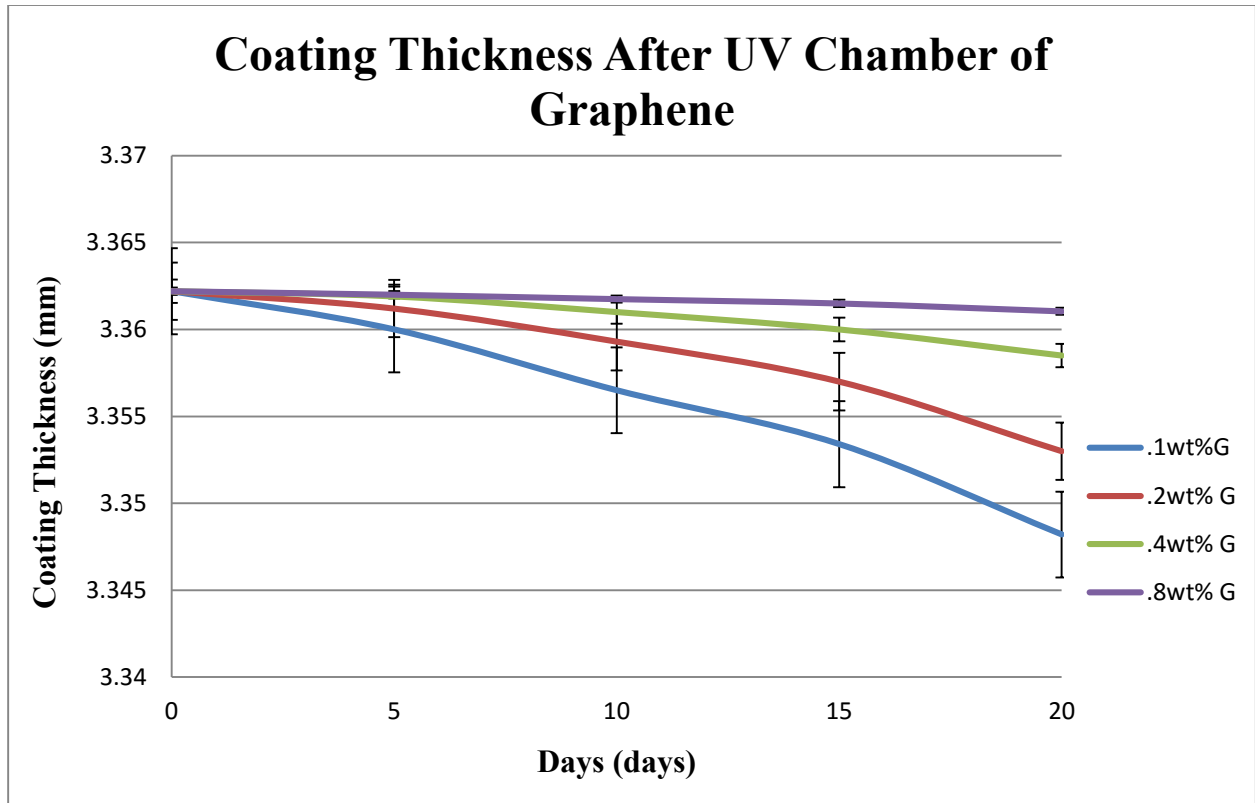


Figure 47: Coating Thickness Graph of Silanized Graphene after 20 days in the UV Chamber

TABLE 2

THE THICKNESS OF THE PU COATING WITH DIFFERENT PERCENTAGES OF SILANIZED h-BN

Days	0.1wt% h-BN	0.2wt% h-BN	0.4wt% h-BN	0.8wt% h-BN
0	3.3622	3.3622	3.3622	3.3622
5	3.36202	3.3621	3.36205	3.36215
10	3.36183	3.362	3.3619	3.3621
15	3.35983	3.3615	3.3617	3.36205
20	3.35753	3.3592	3.361	3.362

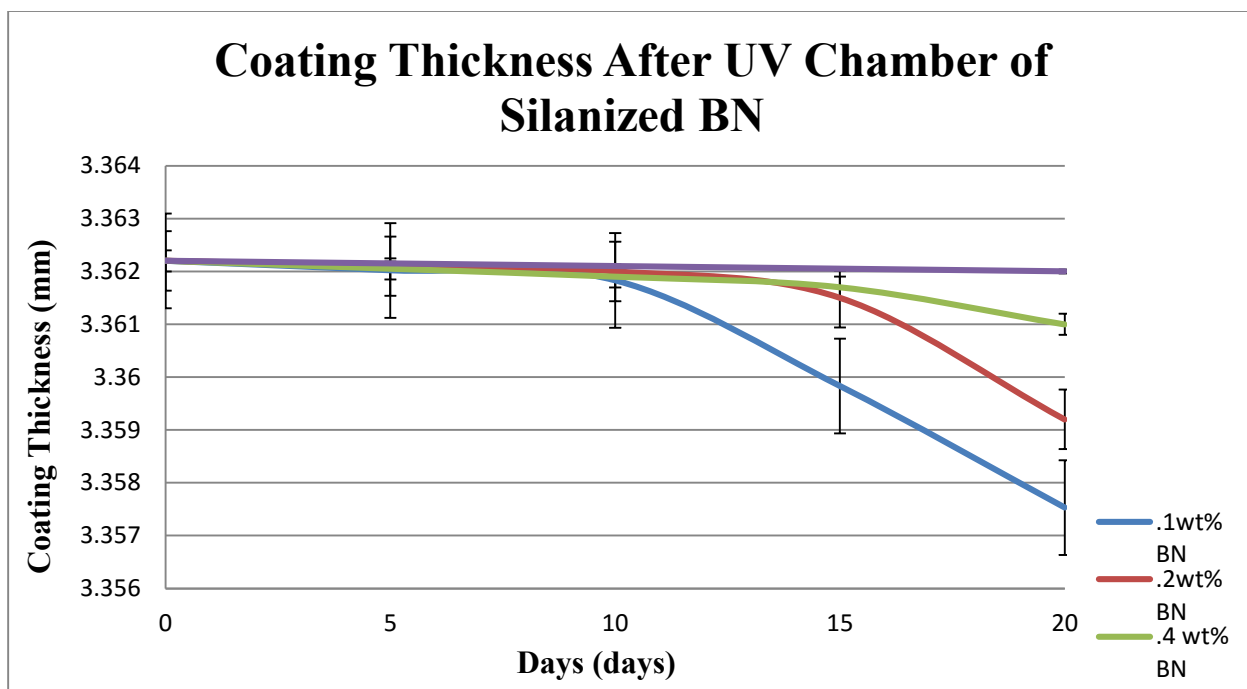


Figure 48: Coating Thickness after UV Chamber after 20 days of h-BN nanocomposite coating

## 5.2 FTIR Studies

Polymer coating degradation has been studied for many years. Under weathering exposure, ultra-violet (UV), Infrared radiation, H<sub>2</sub>O, and O<sub>2</sub> are four critical factors for coating degradation [61]. All organic compounds will absorb infrared radiation which will permit the covalent bonds to absorb a spectrum of the compounds that are unique reflection of their molecular structure and the vibrations in the FTIR spectroscopy. Ranby and Rabek reported that photo-degradation occurred in polyurethane by forming hydro-peroxides in the presence of oxygen to form carbonyl or peroxide group with main chain scission [62]. Thus, photo-initiated oxidation produces peroxides, ketones and aldehydes, and further photo-oxidation of peroxides and ketones yields free radiations, which continue the oxidative degradation as oxidants.

We have noted above that the covalent bonds of organic/polymer molecules are not rigid, but they are more like flexible springs that can stretch and bend. At ordinary temperature

these bonds vibrate in a variety of ways. These vibration modes are often given descriptive names such as stretching, bending, scissoring, rocking, and twisting. The exact frequency at which a given vibration occurs is determined by the strengths of the bonds involved and the mass of the component atom. The equation below describes the major factors that influence the stretching frequency of a covalent bond between two atoms with mass  $m_1$  and  $m_2$  [63].

$$\bar{\nu} = \frac{1}{2\pi c} \sqrt{\frac{f(m_1+m_2)}{m_1 \cdot m_2}} \quad (4)$$

$\bar{\nu}$  = frequency in  $\text{cm}^{-1}$   
 $f$  = the force constant  
 $c$  = the velocity of light

There are general methods that need to be followed when analyzing the FTIR graph such as (i) stretching frequencies are higher than corresponding bending frequencies (it is easier to bend the bond than stretch or compress it). (ii) Bonds to hydrogen have higher stretching frequency than those to heavier atoms. (iii) Triple bonds have higher stretching frequencies than corresponding double bonds, which in turn have higher frequencies than double bonds (except for bonds to hydrogen). The general regions of the infrared spectrum (Figure 49) [64] show various kinds of vibrational bands which are outlined in the following chart. Note that the blue colored sections above the dashed line refer to stretching vibrations, and the green colored band below the line encompasses bending vibrations. The complexity of infrared spectra in the  $1450$  to  $600 \text{ cm}^{-1}$  IR region makes it difficult to assign all the absorption bands, because of the unique patterns found there, it is often called the **fingerprint** region. Absorption bands in the  $4000$  to  $1450 \text{ cm}^{-1}$  IR region are usually due to stretching vibrations of diatomic units, and this is sometimes called the **group Frequency** region [62].

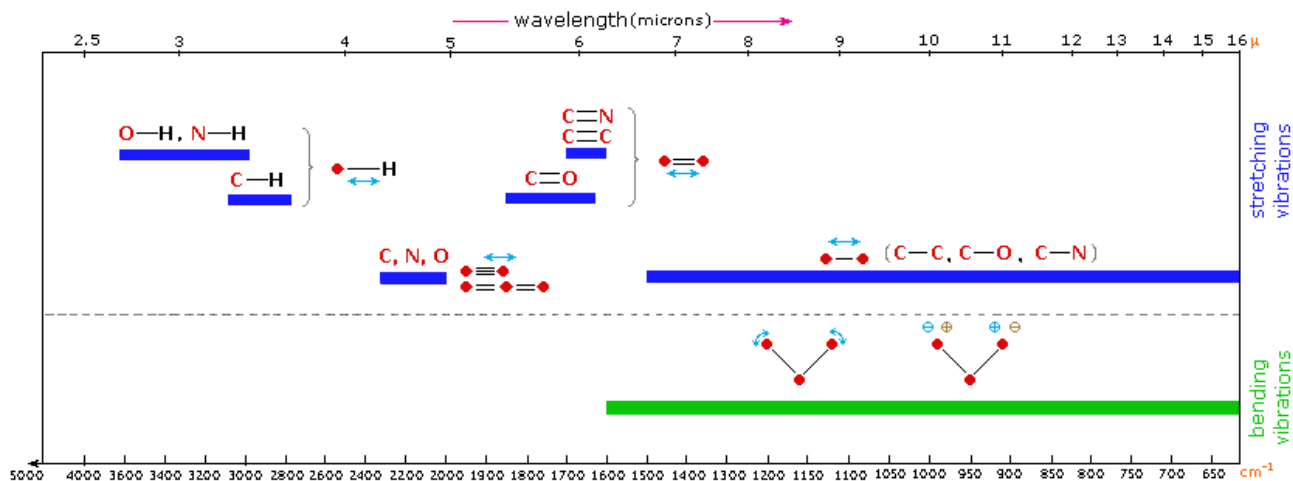


Figure 49: The General Regions of Infrared Spectrum

To verify the scission of polyurethane chains and corresponding chemical groups, The FTIR studies were performed. A usual scale factor was used to obtain the FTIR images, and the transmittance percentage was kept between 0% - 120% for the test specimen with the wavelength range between 4000-500  $\text{cm}^{-1}$ . Figure 50 shows the FTIR spectrum of polyurethane paint only without silanized nanomaterials after UV chamber 20 days and an examination was performed. To begin at the left side of the graph, the spectrum of delaminated coating which obtained from the surface of a sample with coating adhesion problems. Main absorption bands were found in the first peak at 2946.84  $\text{cm}^{-1}$  and this is the single bond stretch of N-H group. This is a urethane group  $[\text{NH}-(\text{C}=\text{O})-\text{O}]$ . The N-H stretches are medium in intensity, but broader in appearance. However, this could be a C-H stretch (an Alkanes group with two bands) because the main ingredient of polyurethane paint which contains 53.8% medium hydrogen carbon. The second peak is 1722.21  $\text{cm}^{-1}$  with a strong and sharp peak, this should be saturated Ketone (C=O) or Aldehyde (C=O) which contains carbonyl bond. The third peak is at 1434.85  $\text{cm}^{-1}$ , it presents the  $\alpha$ -CH<sub>2</sub> bending with a strong intensity. The small peaks are between 1434.85  $\text{cm}^{-1}$  and 1141.71  $\text{cm}^{-1}$  suggest the symmetric and asymmetric stretching of the CH<sub>2</sub> and CH<sub>3</sub> group. The

last peak at  $1141.71\text{ cm}^{-1}$  and numbers of peaks after that shows the single bond stretch C-O group or carbonyl which is main chain scission.

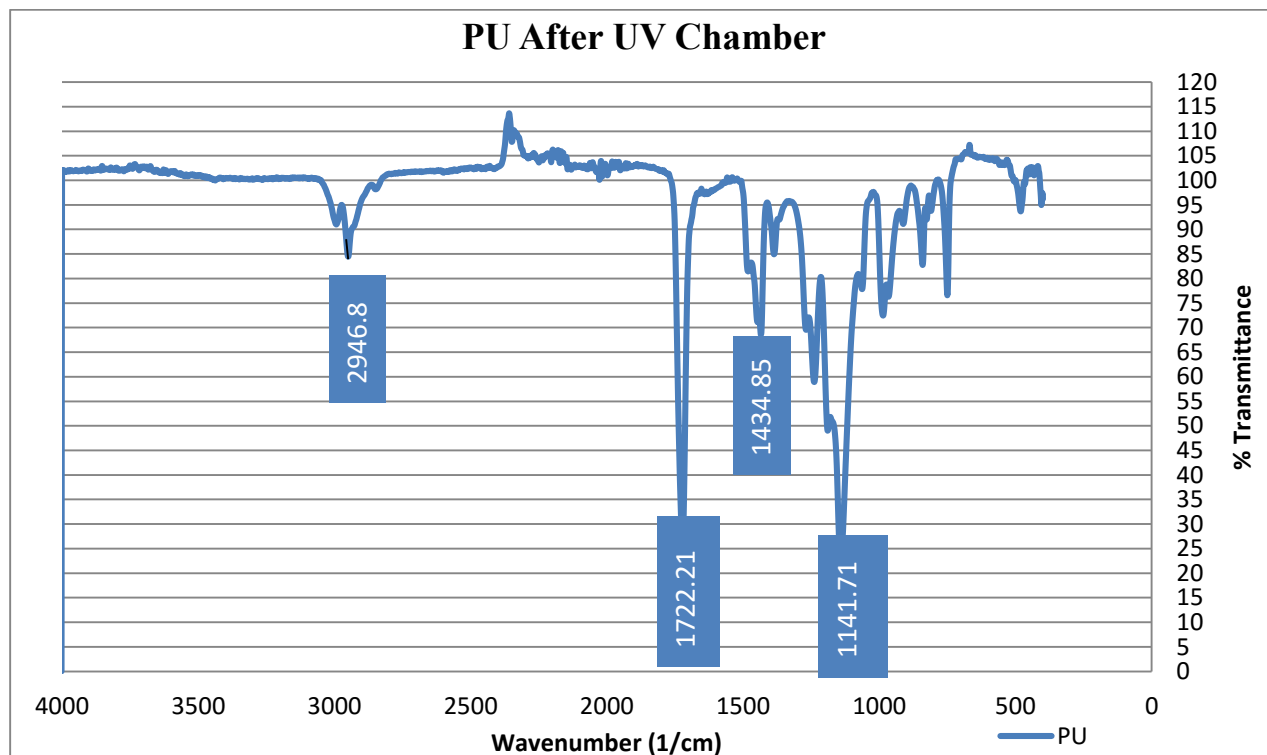


Figure 50: ATR-FTIR Spectrum of Coated Test Sample Contains 0% Silanized Material after 20 days in UV Chamber

Figure 51 shows the ATR-FTIR spectrum of the coating that contains 0.1wt% modified and un-modified BN after 20 days of UV chamber. The silanized BN coating was also extracted with the [3- (2-Aminoethylamino) propyl] trimethoxysilane. The FTIR spectrum of the two coatings is similar and present absorption bands characteristic of polyamide. A decrease in the wavelengths of three vibrational bands of the silanized h-BN coating at  $2964.64\text{ cm}^{-1}$ , they are  $\text{CH}_3$ ,  $\text{CH}_2$ , and  $\text{CH}$  bonds. The vibration at  $1768.73\text{ cm}^{-1}$  is  $\text{C}=\text{O}$  (Esters) bond, with contains a carbonyl center. Esters are structurally flexible functional groups because the rotation of  $\text{C}-\text{O}-\text{C}$  bond. They have a low barrier, polarity, and tend to be less rigid (lower melting point) and more volatile (lower boiling point).

The unmodified h-BN coating has vibration at  $2945.65\text{ cm}^{-1}$  with functional Alkanes stretching and three bands corresponding to  $\text{CH}_3$ ,  $\text{CH}_2$ , and  $\text{CH}$  bonds. The second vibration is at  $1723.23\text{ cm}^{-1}$  which regard the strong intensive saturated Aldehyde ( $\text{C}=\text{O}$ ), as well as the appearance of absorption bands at  $1350\text{ cm}^{-1}$  and  $1470\text{ cm}^{-1}$  which may be assigned to the vibration of  $\text{CH}_2$  &  $\text{CH}_3$  deformation group with medium intensity. In addition, the graph of silanized h-BN coating shows 13 deep peaks after the wavelength of  $1500\text{ cm}^{-1}$  compare with 13 shallow peaks of the un-modified BN coating. This means that the coating contains silicon function groups such as  $\text{Si-O-Si}$  and  $\text{Si-CH}_3$ . Then  $\text{C-O}$  adsorption peak at  $1102.39\text{ cm}^{-1}$ .

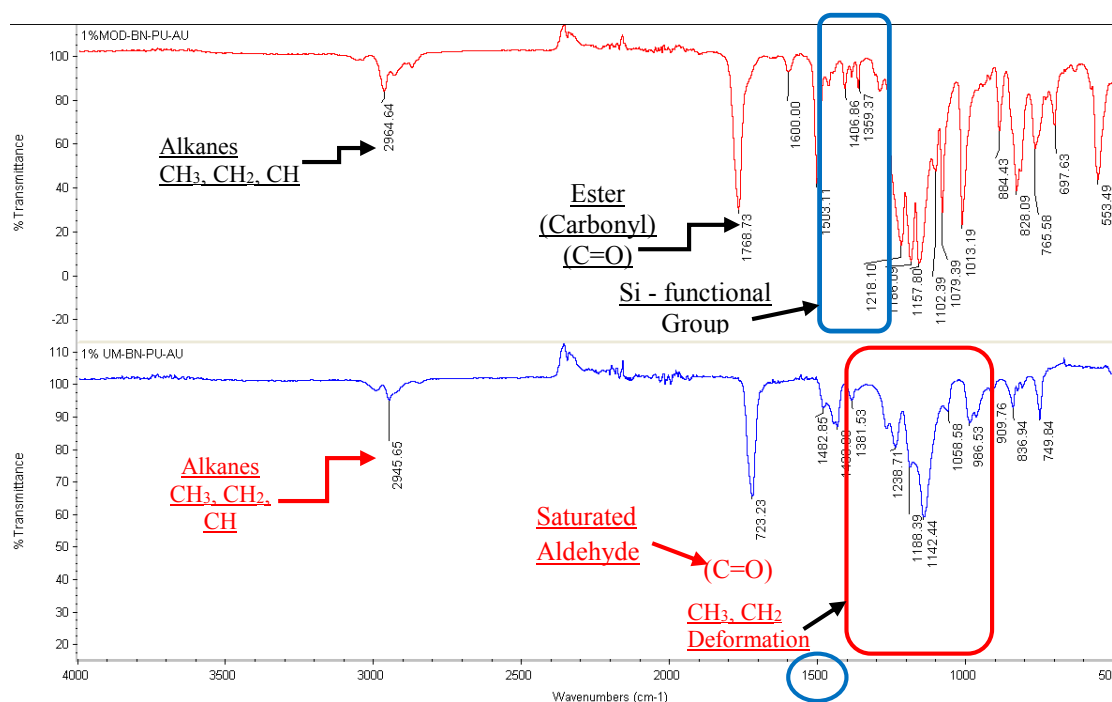


Figure 51: ATR-FTIR Spectrum of Coated Test Samples Containing 0.1% Silanized and Unsilanized h-BN

Figure 52 is the graph of 0.1wt% un-modified and modified graphene after UV chamber for 20 days. This graph was put together for comparison purpose. The 0.1wt% modified graphene graph (red color) goes through the stretching of  $\text{CH}_3$ ,  $\text{CH}_2$ , and  $\text{CH}$  bond of Alkanes

group at the wavelengths  $2993.14\text{ cm}^{-1}$  and  $2949.79\text{ cm}^{-1}$ . Then it begins degradation at the deep carbonyl peak ( $\text{C}=\text{O}$ ) of saturated Ketone at the wavelength  $1722.45\text{ cm}^{-1}$ . The stretching vibration of the benzene ring structure from the silane surfactant at  $1434.54\text{ cm}^{-1}$  is lighter than the unsilanized graphene. The absorption bond of silicone group at  $1142.09\text{ cm}^{-1}$  could represent the stretching vibration of  $\text{Si}-\text{O}-\text{Si}$ . Then it continues with six bending  $\text{CH}_2$  deformation bonds. Compare with the 0.1wt.% un-modified graphene graph (blue color), it also goes through the stretching of  $\text{CH}_3$ ,  $\text{CH}_2$ ,  $\text{CH}$  at the earlier wavelength of  $2964.64\text{ cm}^{-1}$  then stretches again with a strong intensity at the wavelength  $1769.07\text{ cm}^{-1}$  of carbonyl  $\text{C}=\text{O}$  (anhydrides). After that is the bending of  $\text{N}-\text{H}$  at  $1503.30\text{ cm}^{-1}$ ,  $\text{C}-\text{O}$  stretching at  $1219.10\text{ cm}^{-1}$  of the urethanes group, and  $\text{C}-\text{C}$  bending because of unsilanized graphene didn't dissolve in the PU paint.

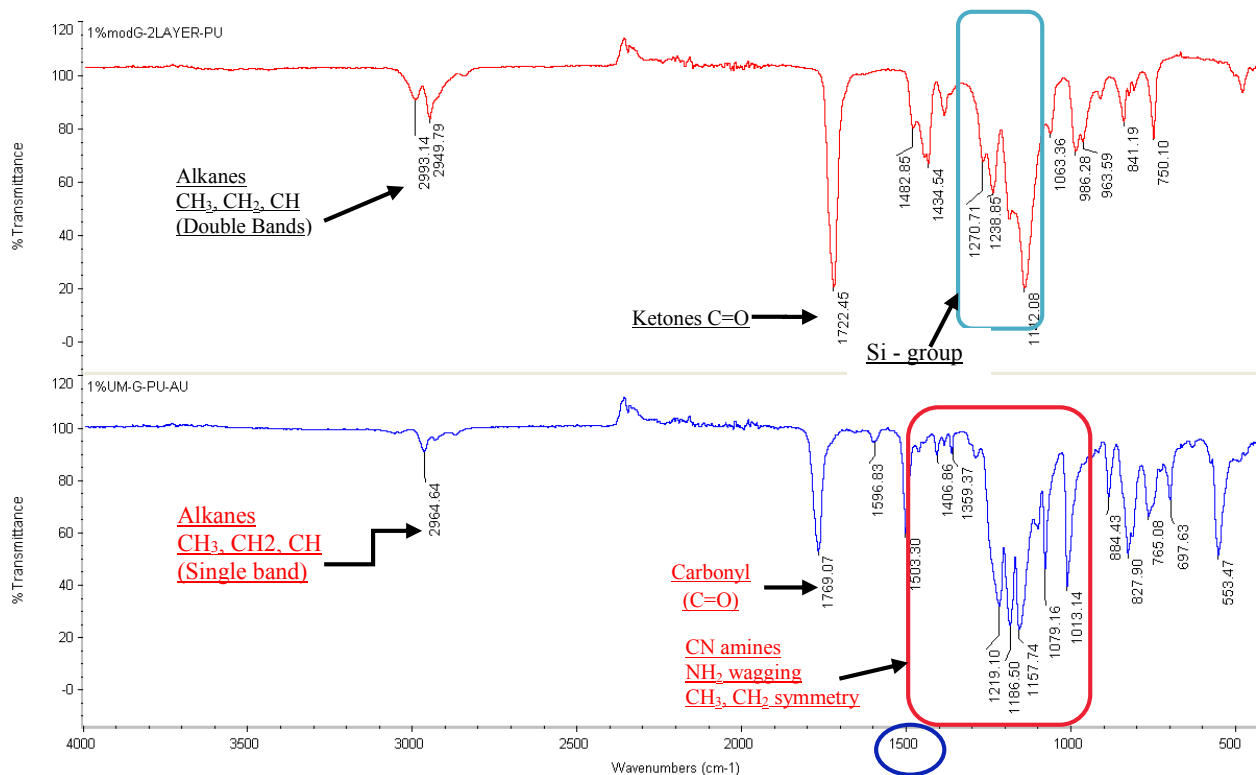


Figure 52: ATR-FTIR Spectrum of Coated Test Samples Containing 0.1wt. % Silanized and Unsilanized Graphene after UV Chamber

Figure 53 is the FTIR graphs of modified and un-modified h-BN after UV chamber. The modified h-BN coating started stretching at the wavelength 2964.64 is CH<sub>3</sub>, CH<sub>2</sub>, and CH of the Alkanes group with three bands. Then the second incident shows a deeper peak stretching at 1768.73 cm<sup>-1</sup> of carbonyl C=O. After that is C=C, C=N in a ring of phenol at 1600 cm<sup>-1</sup> and 1503.11 cm<sup>-1</sup> and ten oscillations of silicone functional group Si-O-Si and CH deformation. The same results are seen with the modified h-BN coating, the un-modified h-BN coating started with a stretching of Alkanes group at the wavelength of 2945.65 cm<sup>-1</sup>, then the second deep stretch at 1723.23 cm<sup>-1</sup> of carbonyl C=O anhydrides. At the end there are eight bending vibrations of CH<sub>3</sub>, CH<sub>2</sub> deformation and CH<sub>2</sub> is rocking.

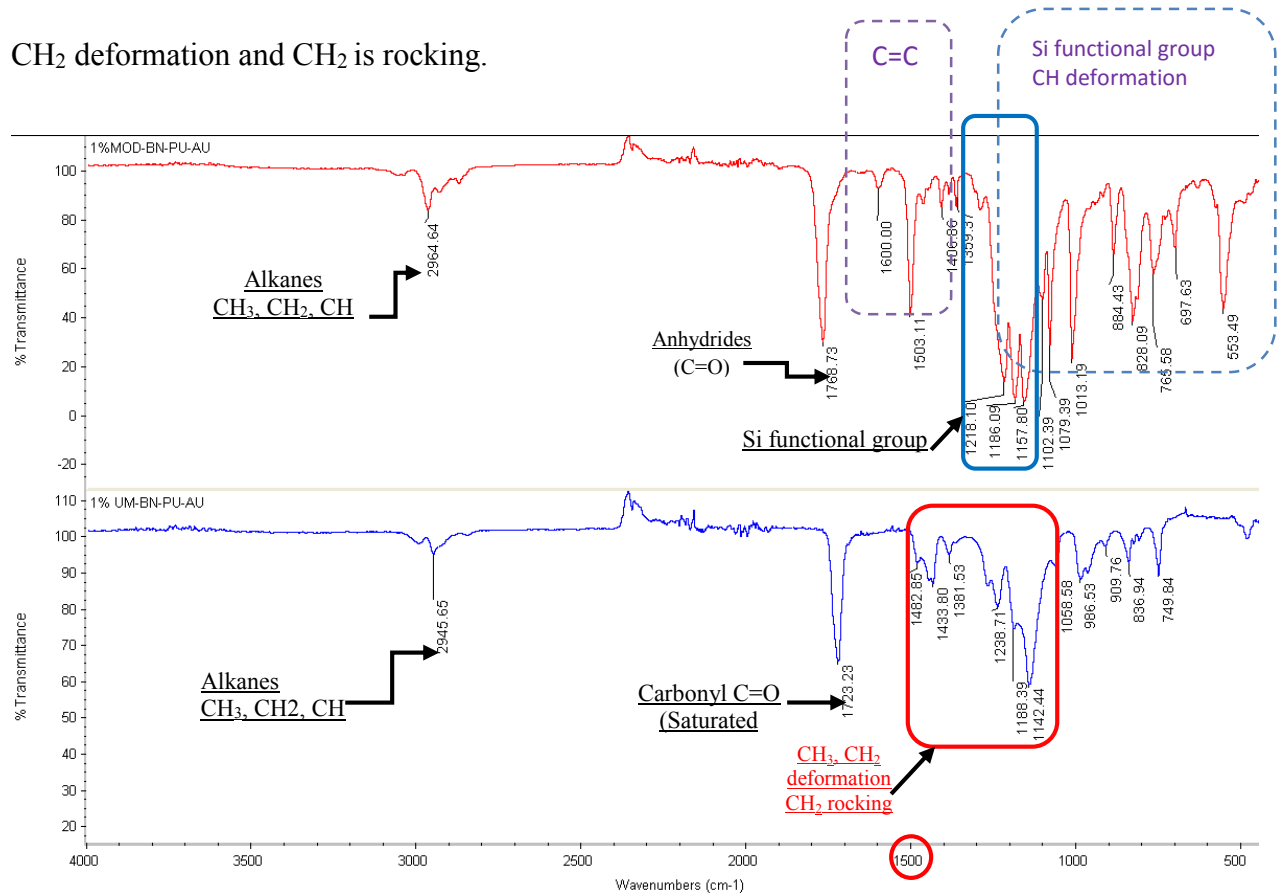


Figure 53: Silanized and Unsilanized h-BN after UV Chamber 20 days

Figure 54 shows four different coating graphs before UV Chamber. All four graphs have the same variety O-H or N-H bonds at the wavelength of 3580-3650 cm<sup>-1</sup> that indicate sharply stretching of alcohol and phenols groups. Then the broad N-H stretching at the wavelength of

3200-3500 $\text{cm}^{-1}$  is due to the urethane and aliphatic isocyanate groups. After that are there are two bands of  $\text{CH}_3$ ,  $\text{CH}_2$ , and  $\text{CH}$  bonds vibrations at the wavelength of 3000 – 2800  $\text{cm}^{-1}$ . These are the hydrocarbon solvent in the PU paint. These started degrading at the wavelength of 1500-1700  $\text{cm}^{-1}$  with carbonyl bonds  $\text{C}=\text{O}$  (aldehyde & Ketones) of urethane linkage, amide II (NH bending and CN stretching). Finally, they go to the  $\text{C}-\text{O}$ , NH bending, and  $\text{CH}$  stretching.

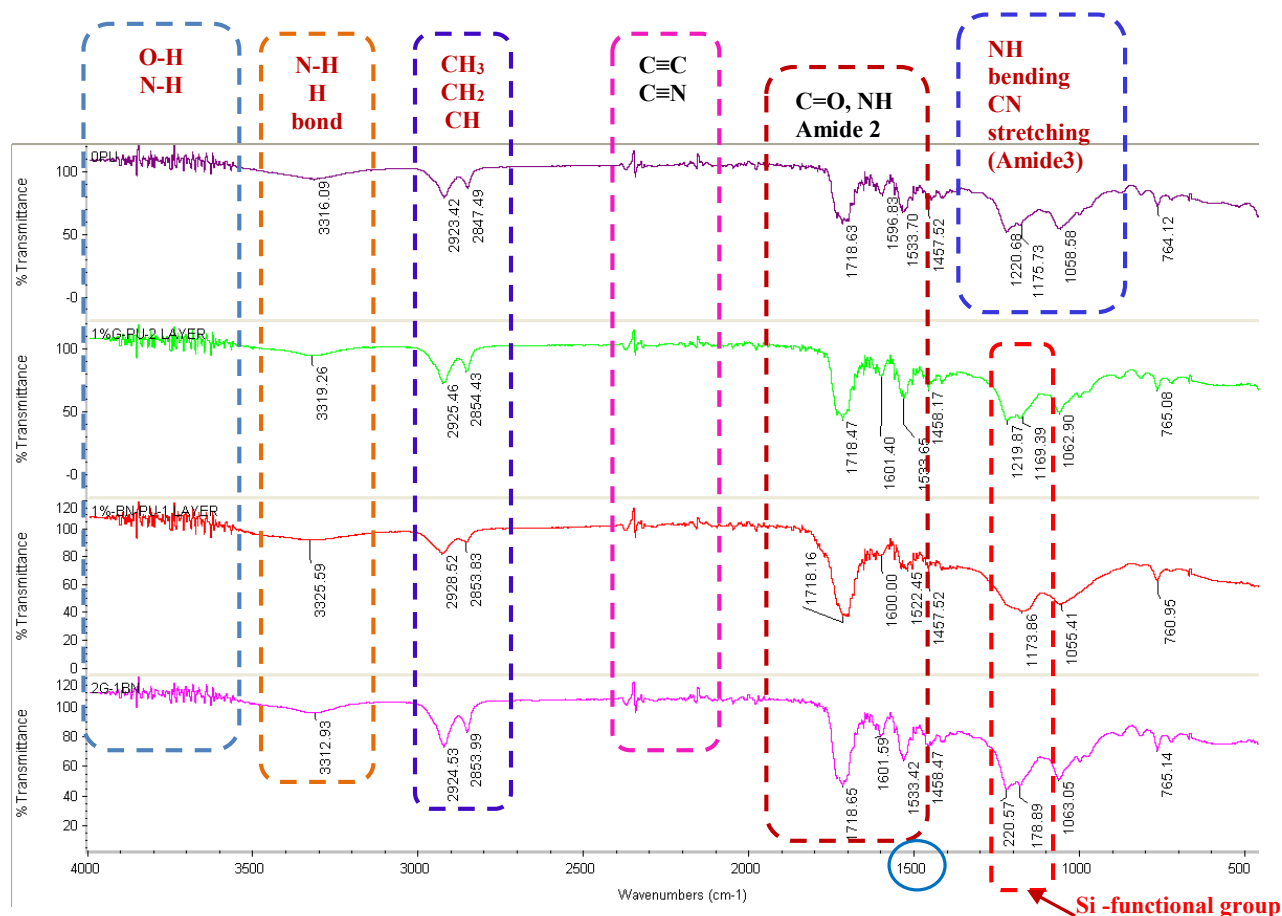


Figure 54: Combination of Pure PU (top), Coating with Silanized Graphene (second), Coating with Silanized h-BN (third), Coating with Silanized Graphene & h-BN (bottom) before UV Chamber

Figure 55 is the FTIR image of the four graphs after UV chamber. Compare with the Figure 54 above (the same coating before the UV chamber). After the UV chamber, the graphs don't have the erratic sharp vibration of O-H and N-H bonds, but they show the smooth transition during the silanization process. They start stretching at the wavelength of 2950 – 3000  $\text{cm}^{-1}$  with

CH<sub>3</sub>, CH<sub>2</sub>, and CH of Alkanes group but are lighter in comparison to the Figure 54. The graph on Figure 55 continues to stretch with the C=O bond at the wavelength of 1720 cm<sup>-1</sup>. They go through the Si functional group such as Si-O-Si, and Si-CH<sub>3</sub> at the wavelength of 1250 -1000 cm<sup>-1</sup>. They degrade at the wavelength of 1400 cm<sup>-1</sup> with CH<sub>3</sub>, CH<sub>2</sub>, and CH deformation, C-H bending, finally is NH wagging.

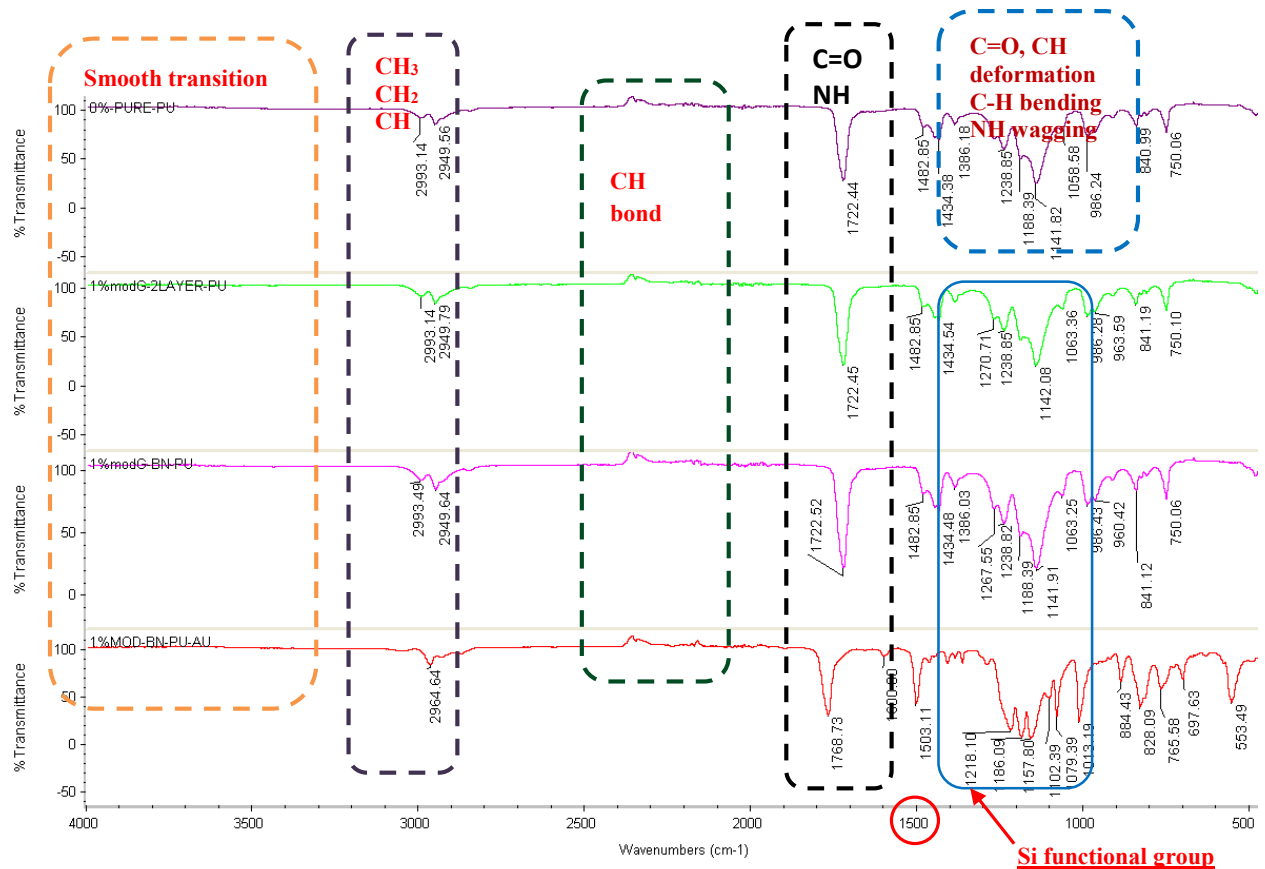


Figure 55: Combination of PU Coating (top), Coating with S- Graphene (second), Coating with S h-BN (third) and Coating with S – Graphene & h-BN (bottom) after UV Chamber

### 5.3 UV-Vis Studies

Visible light absorption is known to all of us, because this is what causes objects to be seen and showed color, When light is absorbed by a material, valence (outer) electrons are promoted from their normal (ground) states to higher energy (excited) states. Figure 56 show the UV-Vis chart of unsilanized and silanized graphene, the silanized graphene coating absorbed more

visible light and UV light than the unsilanized graphene coating. The max wavelength absorbance of visible light ( $\lambda_{\max}$ ) is 487 nm and  $\lambda_{\max} = 344$  nm of UV region, which conjugated to the C=O chromophore hydrocarbon solvent in PU paint, of the silanized graphene coating, and the  $\lambda_{\max} = 433$  nm of visible light and  $\lambda_{\max} = 375$  nm of UV light of the unsilanized graphene coating. In the UV spectrum, it is important to understand about how conjugation of double and triple bonds also shifts the absorption maximum about 30 nm in the same direction. Table 3 shows the lights absorbing groups (chromophores), excitation states, maximum wavelength, and solvent [63].

TABLE 3

THE LIGHT ABSORBING GROUP, EXCITATION, MAX WAVELENGTH, AND SOLVENTS

Chromophore	Example	Excitation	$\lambda_{\max}$ , nm	$\epsilon$	Solvent
C=C	Ethene	$\pi \rightarrow \pi^*$	171	15,000	hexane
C $\equiv$ C	1-Hexyne	$\pi \rightarrow \pi^*$	180	10,000	hexane
C=O	Ethanal	$n \rightarrow \pi^*$	290	15	hexane
		$\pi \rightarrow \pi^*$	180	10,000	hexane
N=O	Nitromethane	$n \rightarrow \pi^*$	275	17	ethanol
		$\pi \rightarrow \pi^*$	200	5,000	ethanol
C-X X=Br X=I	Methyl bromide	$n \rightarrow \sigma^*$	205	200	hexane
	Methyl iodide	$n \rightarrow \sigma^*$	255	360	hexane

The difference with graphene coatings, which is shown by Figure 56, the UV-Vis graphs of unsilanized and silanized h-BN coatings. The unsilanized h-BN coatings absorbed more visible light with  $\lambda_{\max} = 484$  nm than the silanized h-BN coating ( $\lambda_{\max} = 448$  nm), but the

silanized h-BN coating absorbed more UV light than the unsilanized h-BN coating with  $\lambda_{\max} = 360$  nm which conjugated with N=O bonds of ethanol solvent during the silanization process.

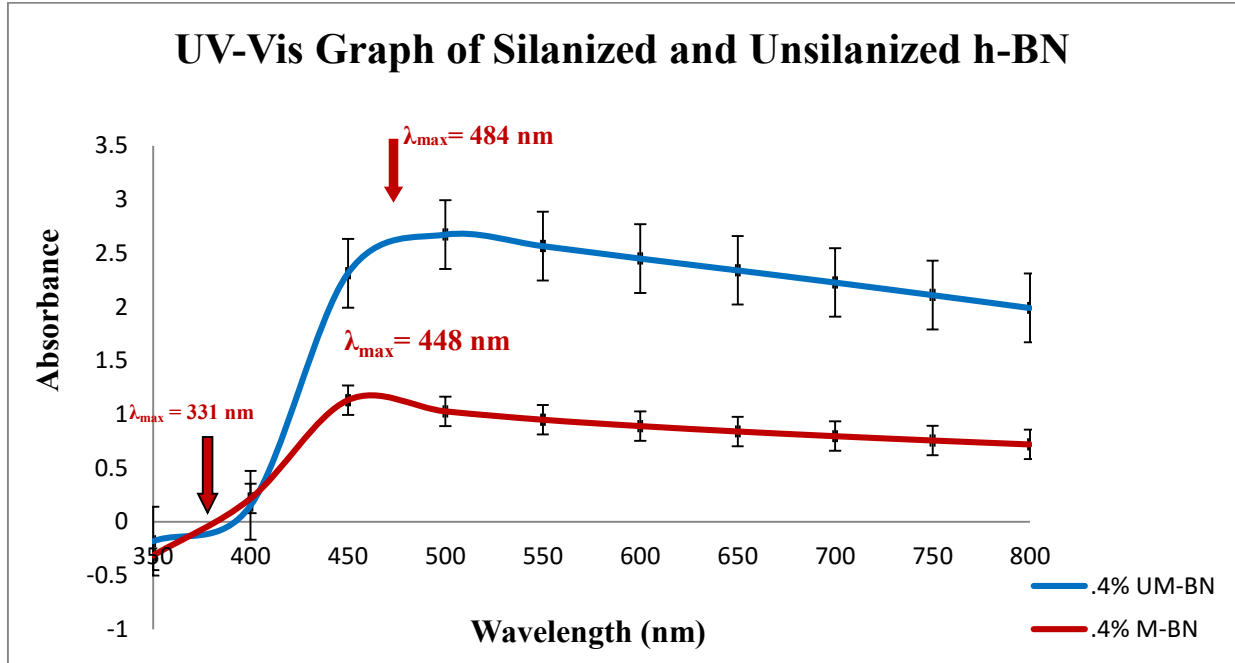


Figure 56: UV–Vis Graphs of 0.4wt% Unsilanized and Silanized Graphene Coatings

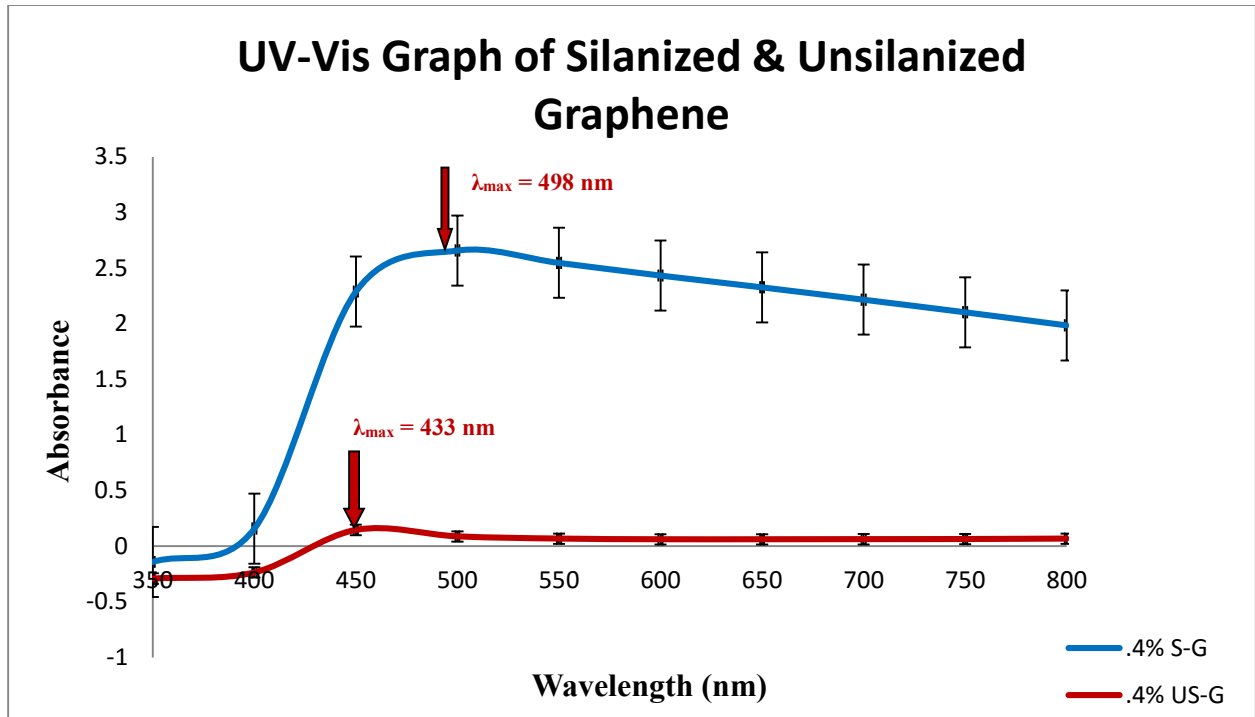


Figure 57: UV-Vis Graphs of 0.4wt % Silanized and Unsilanized h-BN Coatings

At Figure 57, the silanized graphene coating absorbed more visible light with the  $\lambda_{\max} = 498$  nm and the UV light at  $\lambda_{\max} = 360$  nm than the unsilanized graphene coating ( $\lambda_{\max} = 433$  nm). On figure 58, the silanized graphene and h-BN coating has  $\lambda_{\max}=450$  nm in the visible region and  $\lambda_{\max}=345$  nm of the UV region. The third graph is the silanized h-BN coating with  $\lambda_{\max}=448$  nm in the visible region and  $\lambda_{\max}=389$  nm in the UV region. In comparison, the silanized graphene coating absorbed more visible light than the other two, but the silanized graphene & h-BN coating absorbed the most UV light with the absorbance at 0.422 (0.375 of silanized graphene and 0.216 of silanized h-BN).

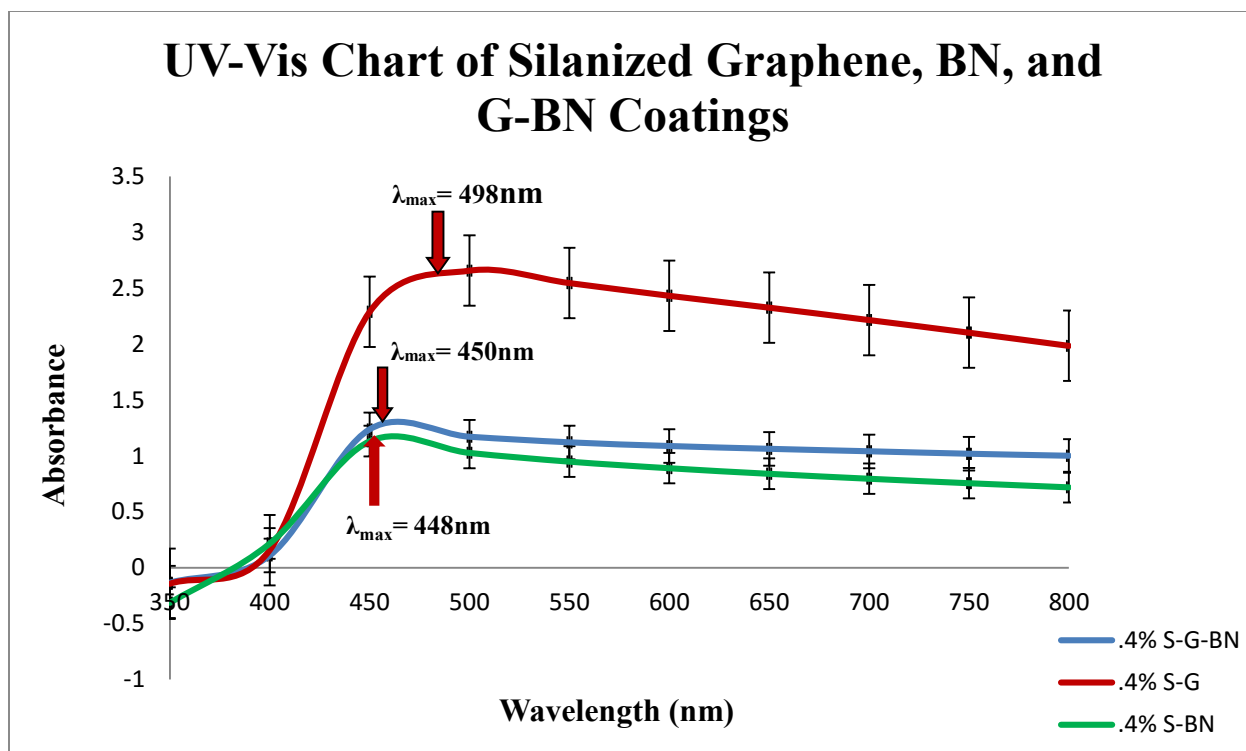


Figure 58: UV-Vis graphs of 0.4wt% Silanized graphene, h-BN, and Graphene & h-BN Coatings

#### 5.4 Water Contact Angle Measurements

The different contact angle values of coated test samples containing various percentages of silanized graphene and h-BN is shown in Table 4. The contact angle measurements were taken during the UV exposure in 5-day intervals for 20 days. Hence, these measurements were taken at days 0, 5, 10, 15, and 20. On day 0 the contact angle of the samples was high, but as time progressed, exposure increased as the contact angle diminished progressively. Contact angle measurements being an indication of hydrophobicity, it can be observed that the longer the samples were exposed to UV slightly the less hydrophobic they became.

TABLE 4

CONTACT ANGLE MEASUREMENTS OF 1 MIL THICK COATING WITH VARIOUS PERCENTAGE OF SILANIZED GRAPHENE, h-BN, AND G & h-BN UNDER DIFFERENT EXPOSED TIMES

Days	PU	0.1wt% h-BN	0.1wt% G	0.4wt% H-BN	0.4wt% G	0.4wt% G & h-BN
0	78.62	89.56	87.12	90.37	85.78	81.56
5	77.21	87.05	84.25	88.65	84.23	81.00
10	70.58	86.55	83.10	87.23	84.12	79.88
15	68.90	85.10	82.45	86.45	83.56	77.55
20	65.84	84.27	80.12	85.32	82.15	76.98

The results shown in Table 4 are graphically represented in Figure 59. It can be observed that coated test samples with the highest percentages of silanized h-BN had their contact angles decrease at a lower rate than samples with certain amount percentages of silanized graphene and silanized G & h-BN. Compared with the pure PU coating after the UV chamber, the coatings with silanized nanomaterials had the lowest decreasing rate of water contact angles. These results suggest that samples with silanized h-BN are less prone to losing their hydrophobicity than samples with silanized graphene, silanized G & h-BN, and with no inclusion of silanized nanomaterials (or pure PU coating). It can be observed from Figure 59 that the plastic specimen without any protective coating suffers the biggest decrease in contact angle: Before exposure, the plastic specimen has a contact angle of 78.62°, but at the end of the 20-day test cycle, the contact angle decreased to 65.84°. Nevertheless, the addition of silanized h-BN in various percentages does enhance the resistance against degradation; this is depicted by the smaller decrease in contact angle of coated specimens containing silanized h-BN. For the plastic specimen containing 0.8wt% silanized graphene, the contact angle decreased from 87.64° to 83.44°, but for

the coated specimens containing various percentages of silanized graphene and silanized h-BN, the nanocomposite coating with 0.8wt% silanized h-BN gave the best results as shown in Figure 45. The coated specimen with 0.4wt% silanized graphene & h-BN inclusion had an original contact angle of 81.56°; after 20 days of exposure, the contact angle diminished to 76.98°. It was noted that a higher increase in the percentage of silanized h-BN by weight significantly improved the water resistance.

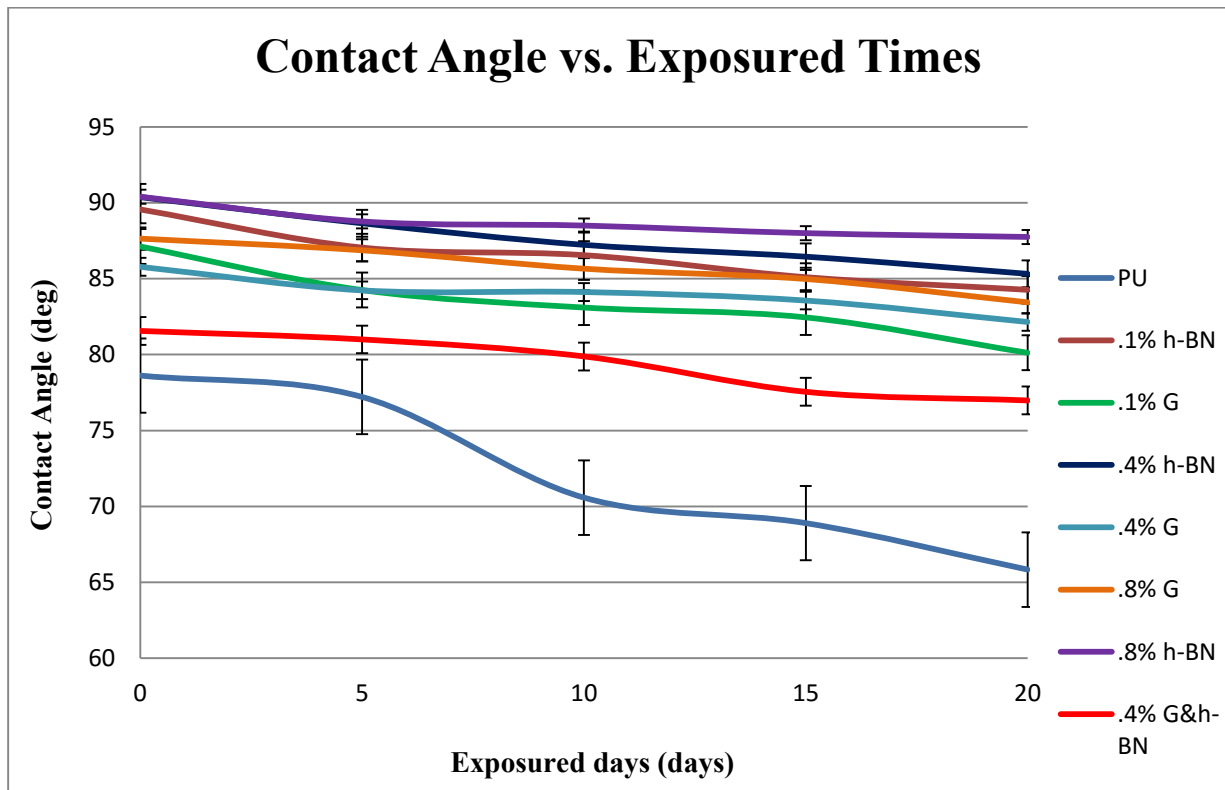


Figure 59: Contact Angle Measurement of various UV Exposed Coatings Containing Different percentages of PU, Silanized Graphene, Silanized h-BN, and Silanized graphene & h-BN

Figure 60 shows the water contact angle of the coating without silanized nanomaterials (pure PU), the coating with silanized graphene, and the coating with silanized h-BN before UV

chamber. The water contact angle of silanized h-BN coating is shown to have less contact with the surface than with the pure PU coating only and the coating with silanized graphene.

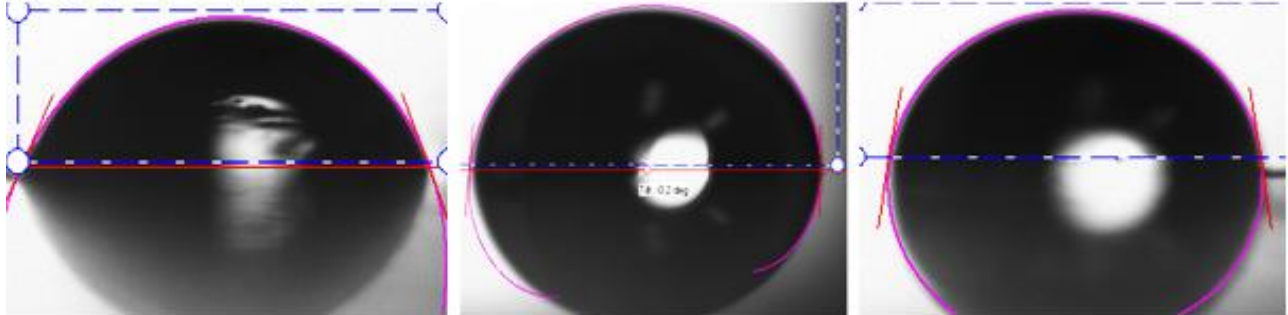


Figure 60: Water Contact Angle of pure PU (left), Silanized Graphene (right), and Silanized graphene & h-BN (bottom)

Figure 61 shows the three examples of water contact angle of the coatings without nanomaterials (left), with silanized graphene (center), and silanized h-BN (right) after the UV chamber. The contact angle of the coating with silanized h-BN didn't change much after the UV chamber compares the coating with silanized graphene. As seen with the coating without nanomaterials (PU coating only), the water contact angle changed dramatically. It was observed that the most important factors governing the degradation are the chemical structure at the surface, adhesion between coating surface, humidity, and biological materials. According to this new finding, a coating with silanized nanomaterials would improve the failure of coatings caused by weathering such as moisture and atmosphere.

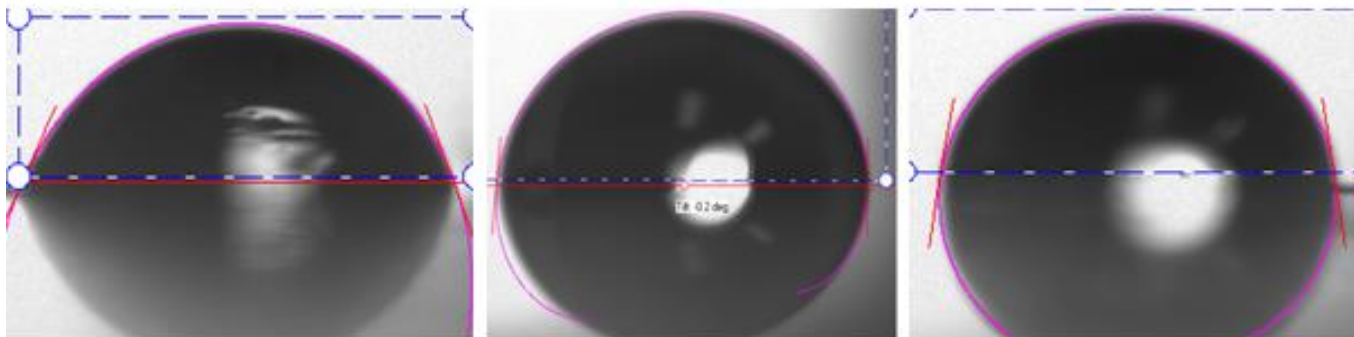


Figure 61: Water Contact Angle of pure PU (left), Silanized graphene (right), and Silanized graphene & h-BN (bottom)

## 5.5 Differential Scanning Calorimeter Test

The thermal properties of nanocomposite coatings were measured by the DSC Q1000 thermal analyzer (TA instrument) with a DSC module, purged with nitrogen gas, and quenched with nitrogen liquid. The specimens were scanned from  $-50^{\circ}\text{C}$  to  $250^{\circ}\text{C}$  by heating rate of  $10^{\circ}\text{C}/\text{min}$ . The cell was calibrated using an indium standard. The weight of sample was 5-10 mg.

### 5.5.1 DSC Analysis

Figure 62 shows a DSC analysis of 6.3 mg polyurethane floor finish. As the sample passed through the  $T_g$  region the molecules gain sufficient mobility to affect the crosslinking reaction, which then appears as an exothermic peak. The  $T_g$  in this region is generally responsible for cured material above room temperature. This would indicate that the polymer matrix has hardened to the touch. As the sample is further heated, the cure is advanced with the exothermic peak indicating further crosslinking.  $T_g$  has shifted to a higher temperature ( $36.15^{\circ}\text{C}$ ) which is not much different with the glass transition temperature from manufacturing of polyurethane ( $T_g=35.46^{\circ}\text{C}$ ) [64], indicating that the material has achieved greater mechanical strength.

Below are the DSC graphs of polyurethane with silanized graphene, and silanized h-BN with various amount of graphene and BN in coating.

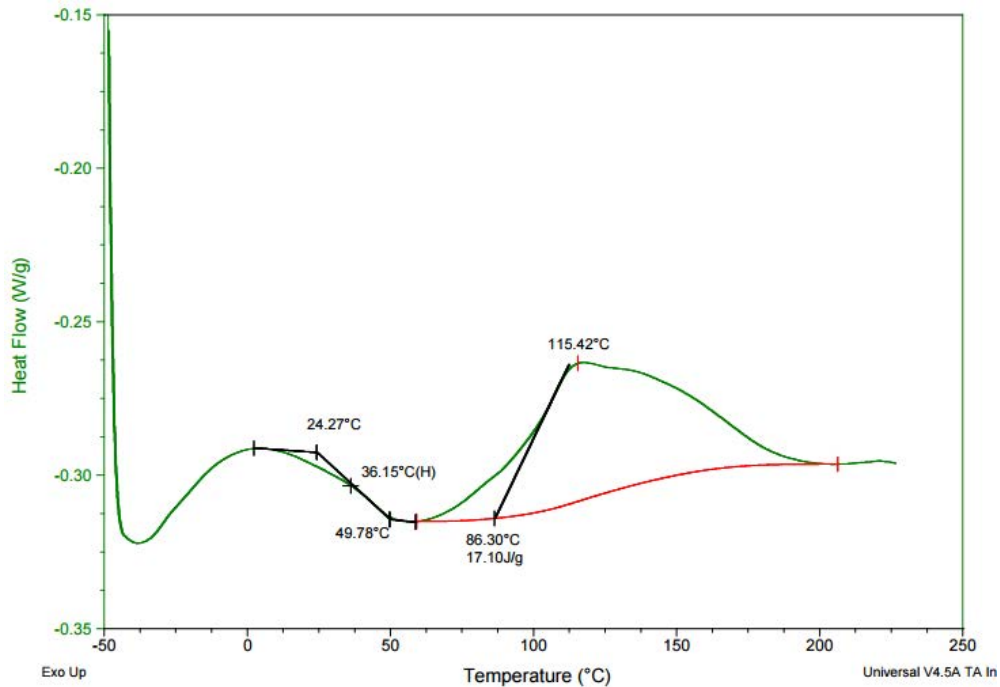


Figure 62: DSC of polyurethane Floor finish Dried after Application for 48 hours

Figure 63 is the DSC analysis of the nanocomposite coating with 0.1wt% silanized h-BN. The sample size is 8.7 mg. the transition temperature  $T_g = 35.53^\circ\text{C}$ . The  $T_g$  of 0.1wt% of h-BN is smaller than the  $T_g$  of the PU coating itself. Figure 64 is the DSC graph of the 0.1wt% unsilanized h-BN with the sample size is 9.2 mg. It shows the  $T_g$  of this sample is  $32.63^\circ\text{C}$ . Figure 65 is the DSC of the 0.4wt% silanized h-BN with the sample size is 8.5 mg and the  $T_g = 33.99^\circ\text{C}$ . Figure 66 is the DSC analysis of the 0.4wt% unsilanized h-BN with the sample size is 9.3 mg and the  $T_g = 33.09^\circ\text{C}$ . Figure 67 is the DSC graph of the 0.1wt% silanized graphene with the sample size is 8.5 mg and  $T_g = 35.14^\circ\text{C}$ . Figure 68 is the DSC graphene of the 0.1wt% of unsilanized graphene with the sample size is 7.3 mg and the  $T_g = 38.34^\circ\text{C}$ . Figure 69 is the DSC graph of 0.4wt% silanized graphene with the sample size is 5.7 mg and the  $T_g = 23.21^\circ\text{C}$ . Figure 70 is the DSC of the 0.4wt% unsilanized graphene with the sample size is 7.0 mg and the

T<sub>g</sub> = 17.22°C. Finally, Figure 71 is the DSC graph of 0.4wt% of silanized graphene & BN with the sample size is 5.6 mg and T<sub>g</sub> = 31.03°C.

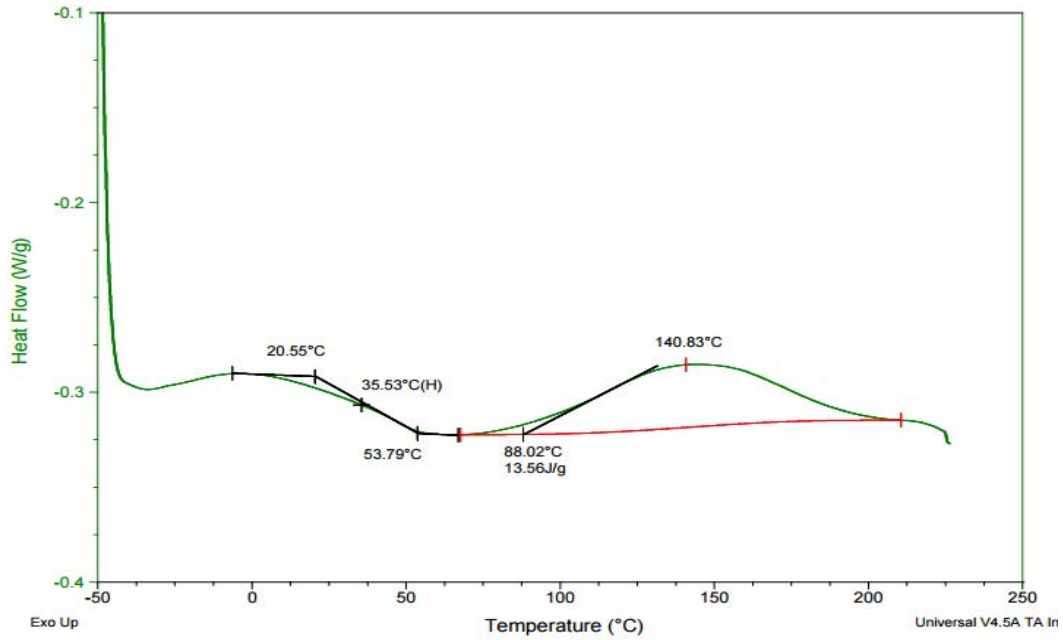


Figure 63: DSC of Polyurethane and 0.1wt% Silanized h-BN with T<sub>g</sub> = 35.53°C

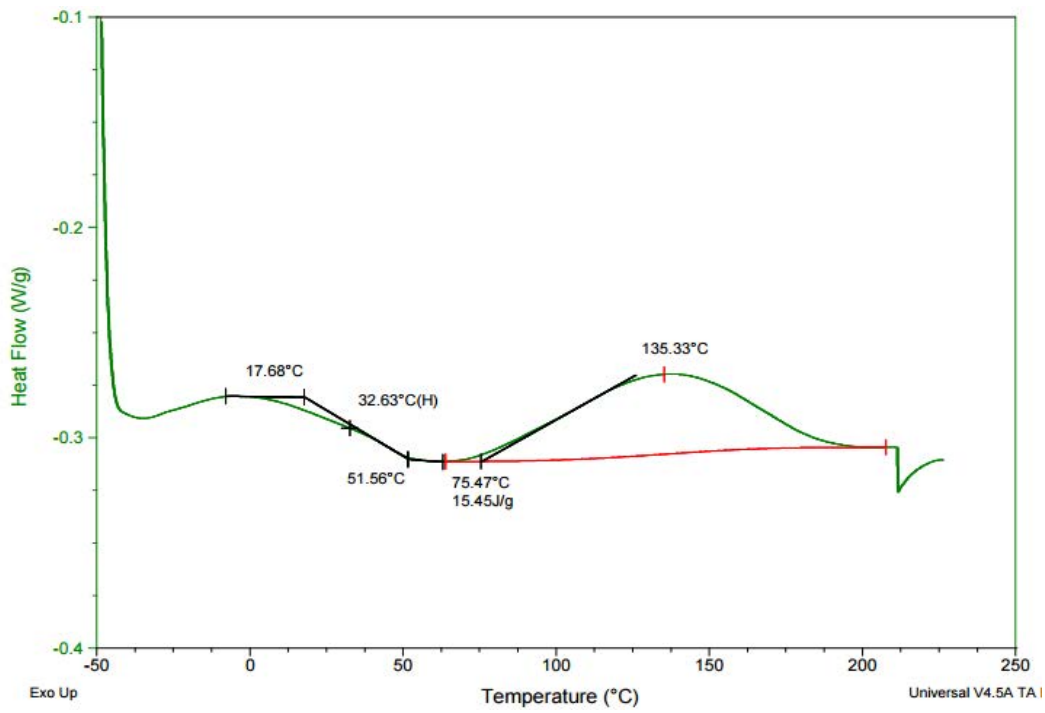


Figure 64: DSC of Polyurethane with 0.1 wt % Unsilanized h-BN with Tg = 32.63°C

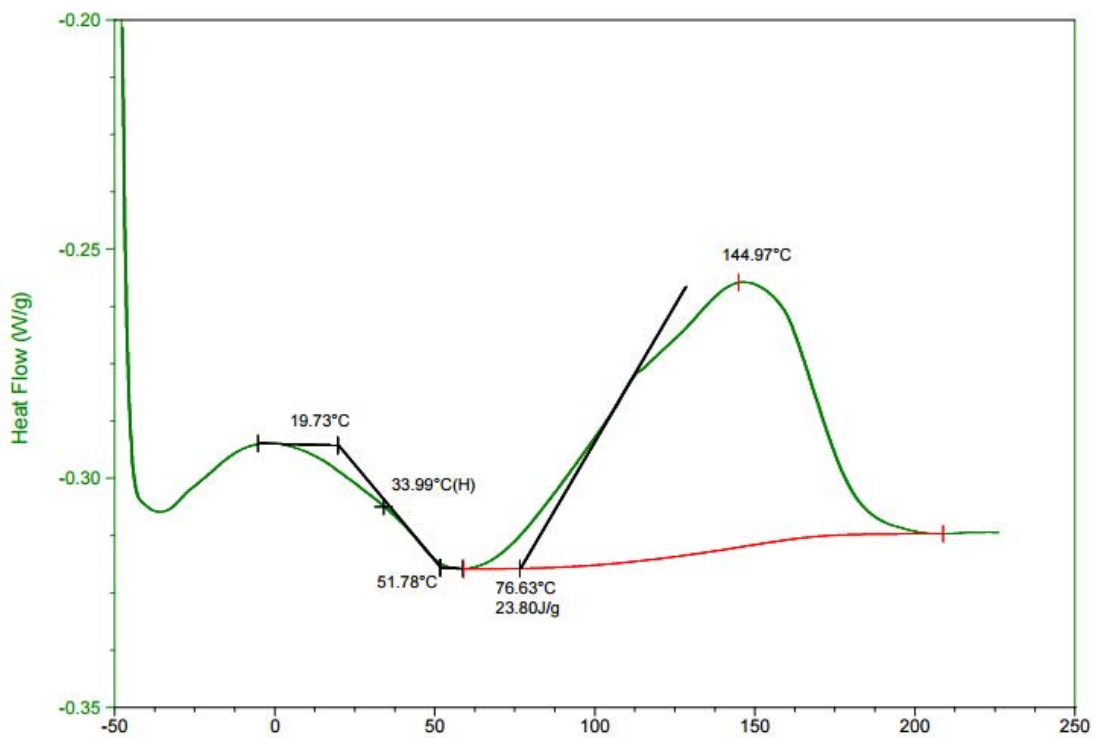


Figure 65: DSC of Polyurethane with 0.4 wt % Silanized h-BN with Tg = 33.99°C

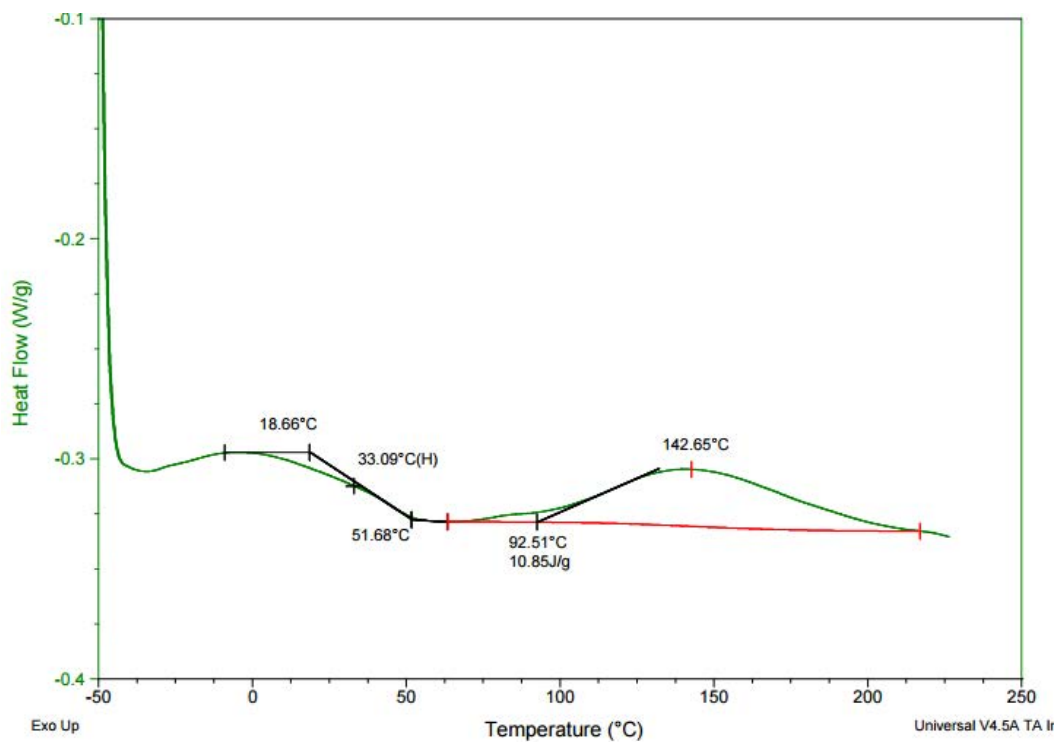


Figure 66: DSC of Polyurethane and 0.4wt% Unsilanized h-BN with  $T_g = 33.09^\circ\text{C}$

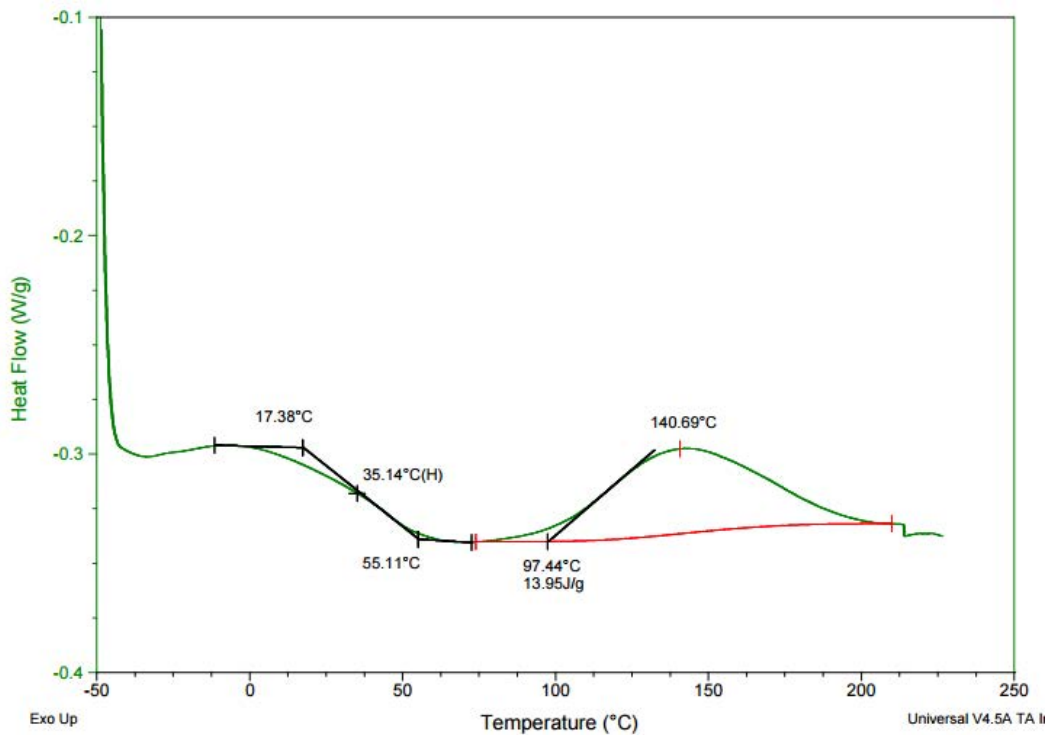


Figure 67: DSC of Polyurethane and 0.1wt% Silanized Graphene with  $T_g = 35.14^\circ\text{C}$

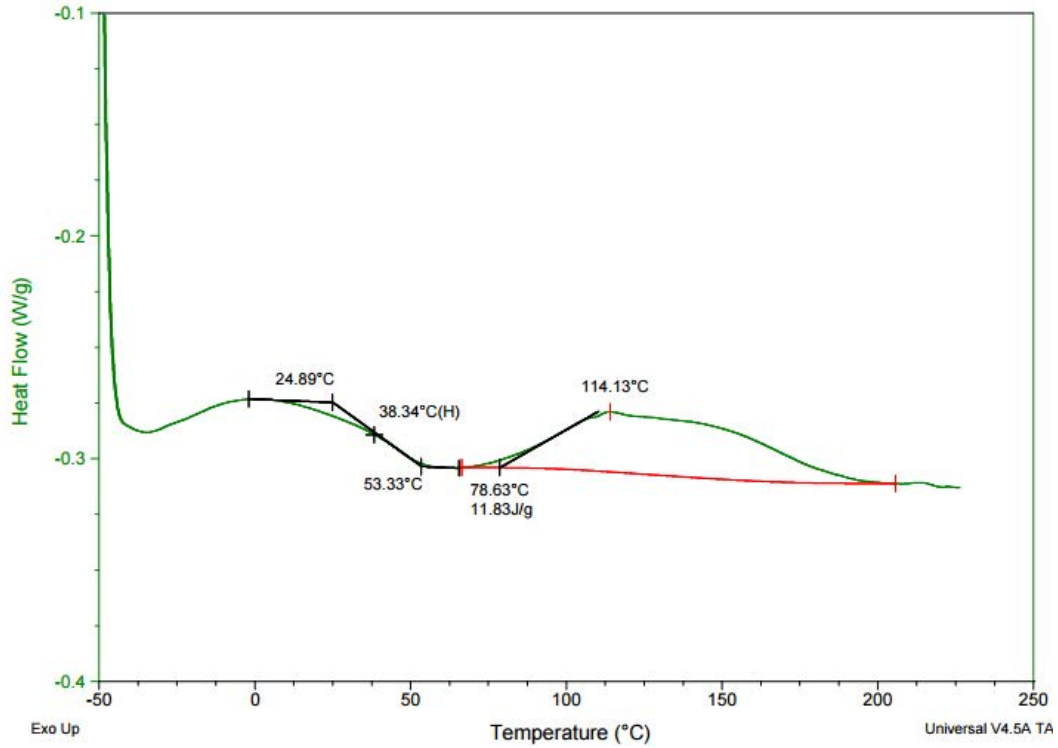


Figure 68: DSC of Polyurethane and 0.1 wt% Unsilanized Graphene with  $T_g = 38.34^\circ\text{C}$

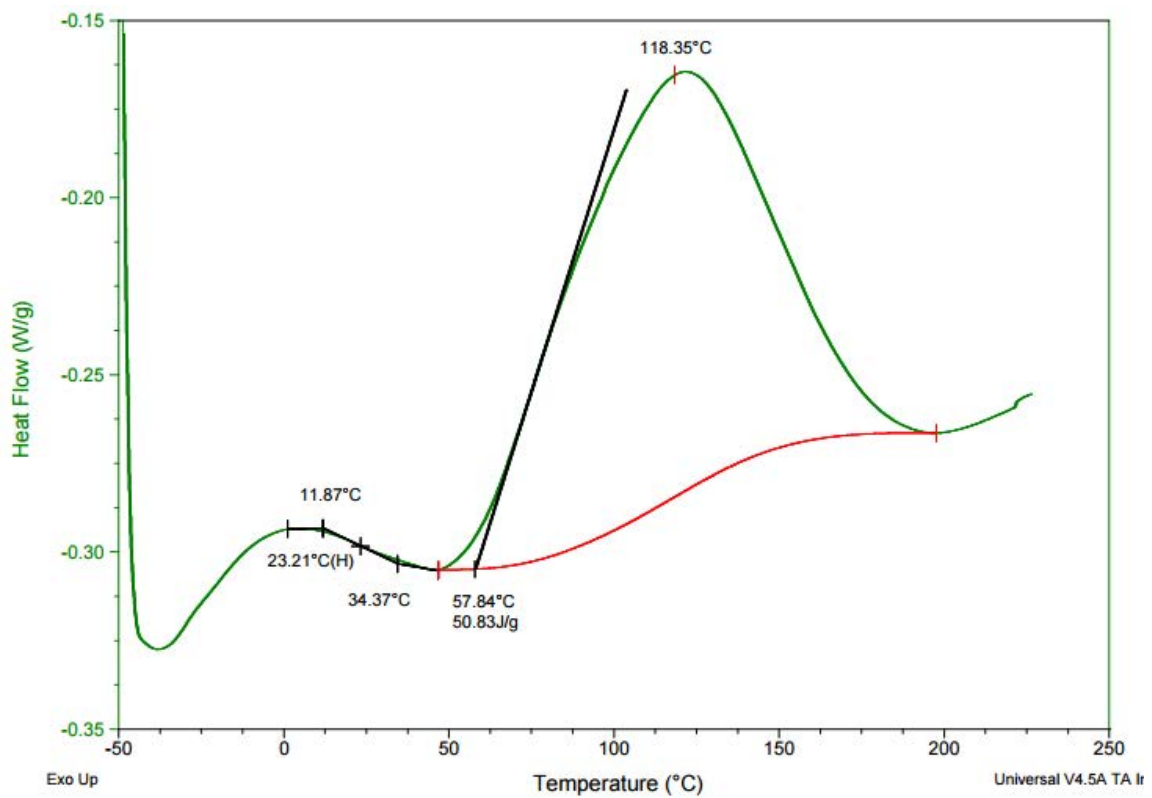


Figure 69: DSC of Polyurethane and 0.4 wt% Silanized Graphene and  $T_g = 34.37^\circ\text{C}$

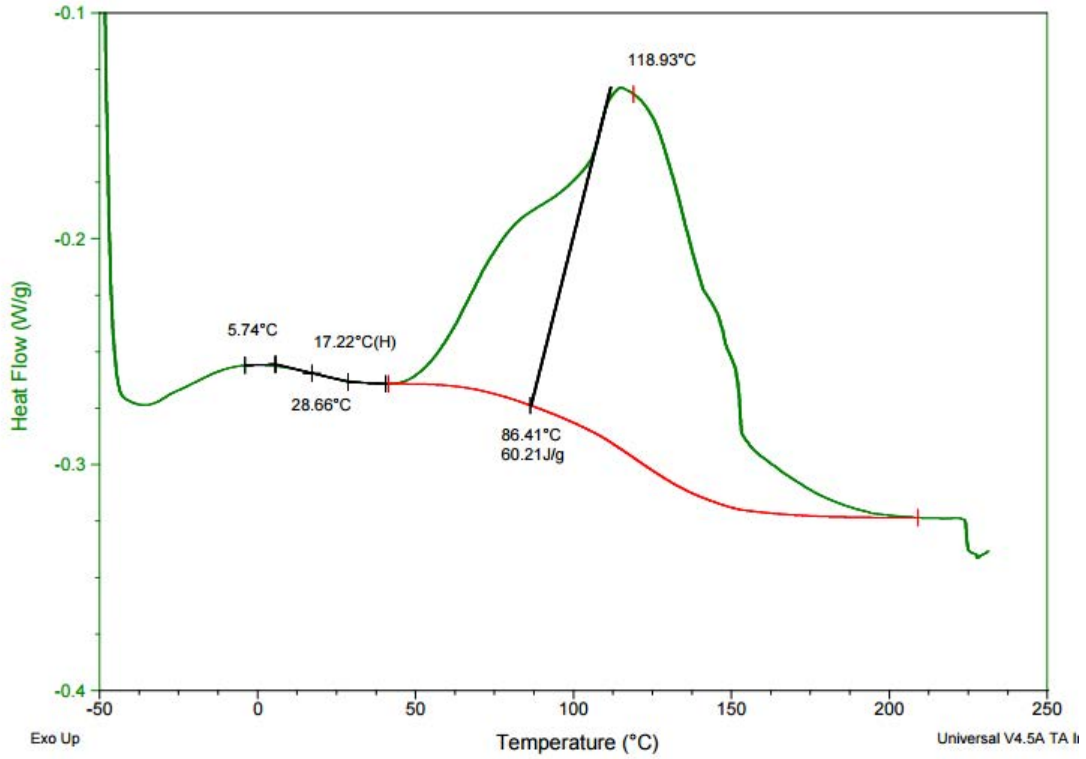


Figure 70: DSC of polyurethane and 0.4wt% Unsilanized Graphene with  $T_g = 17.22^\circ\text{C}$

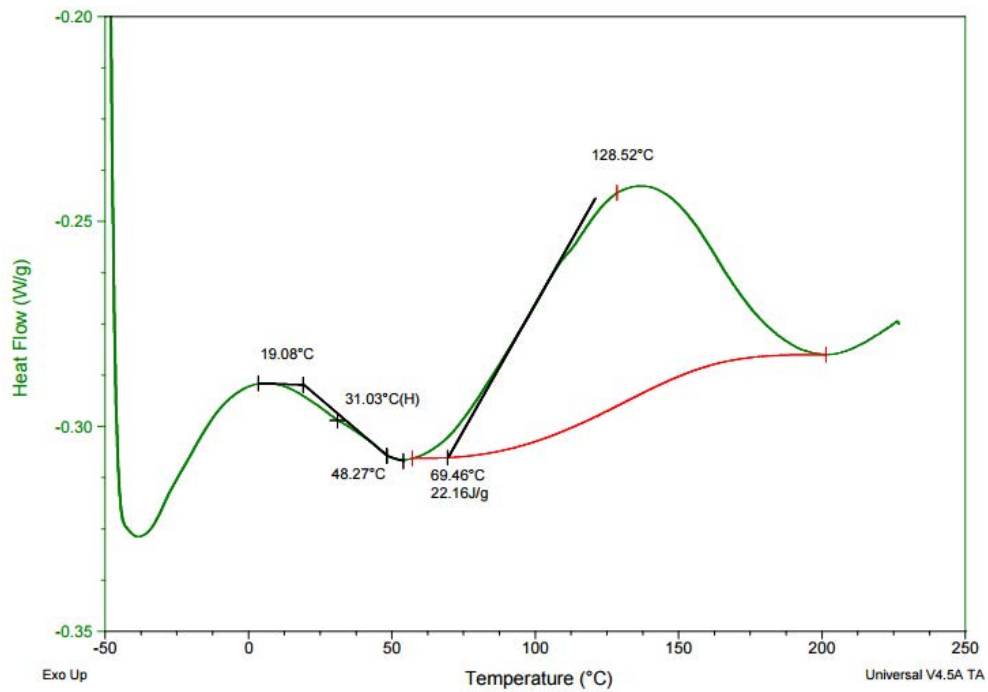


Figure 71: DSC of polyurethane and 0.4wt% of silanized graphene & h-BN with  $T_g = 31.03^\circ\text{C}$

### 5.5.2 Glass Transition Temperature Comparisons

The effect of silanized graphene and h-BN in nanocomposite coatings on the  $T_g$ ,  $T_m$ , and enthalpy was studied by DSC (Figure 72). The higher amount of silanized graphene or h-BN added to the paint, the lower the glass transition temperature. Especially, with 0.4wt% silanized graphene nanocoating, the  $T_g$  had the lower value compared with  $T_g$  of silanized h-BN (Table 4). The same method was used to compare the  $T_g$ ,  $T_m$ , and enthalpy of unsilanized graphene and BN in nanocomposite coatings (Table 5). The effect of unsilanized graphene & h-BN in the  $T_g$  of nanocomposite coatings is shown in the Figure 73.

TABLE 5

THE GLASS TRANSITION TEMPARTURE OF COATINGS WITH DIFFERENT PERCENTAGES OF SILANIZED GRAPHENE & h-BN

Coatings	$T_g$	$T_m$	$\Delta H$ (J/g)	Crystallinity (%)
PU	36.15	11542	17.10	26.89
.1wt% S-G	35.14	140.69	13.95	21.94
.1wt% S-BN	35.53	140.83	13.56	21.32
.4wt% S-G	23.21	118.35	50.83	79.93
.4wt% S-BN	33.99	144.97	23.80	37.42

TABLE 6

THE GLASS TRANSITION TEMPARTURE OF COATINGS WITH DIFFERENT PERCENTAGES OF UNSILANIZED GRAPHENE & h-BN

Coatings	$T_g$	$T_m$	$\Delta H$ (J/g)	Crystallinity (%)
PU	36.15	115.42	17.10	26.89
.1wt% US-G	38.34	114.13	11.83	18.60
.1wt% US-BN	32.63	135.33	15.45	24.30
.4wt% US-G	17.22	118.93	60.21	94.68
.4wt% US-BN	31.03	128.52	22.16	34.85

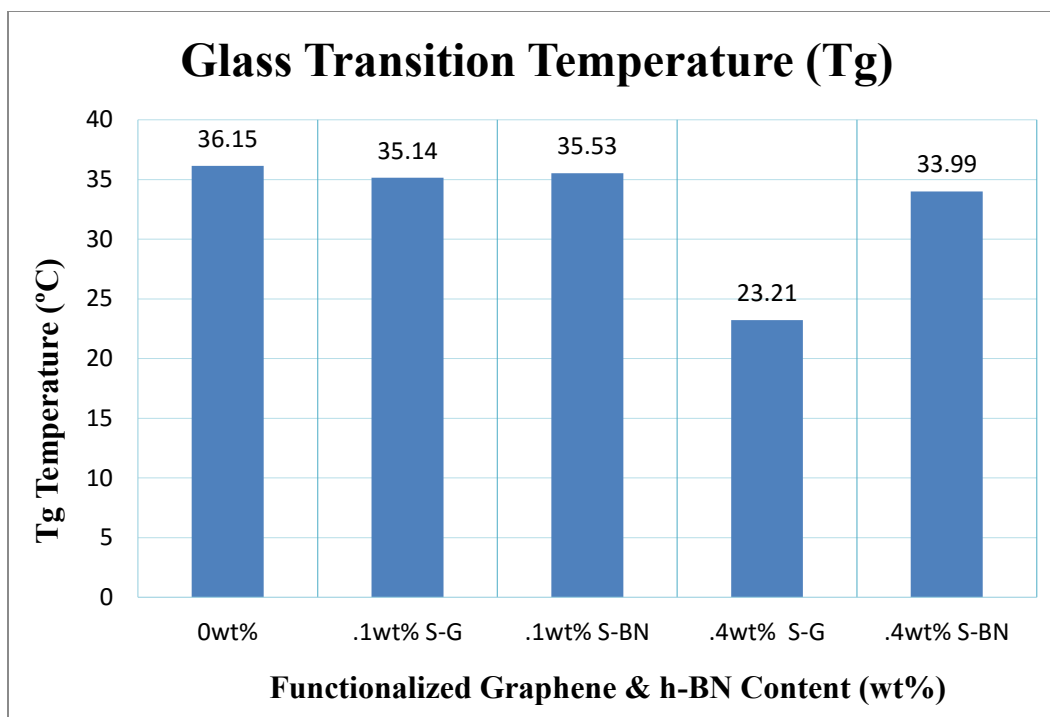


Figure 72: Glass Transition Temperature of PU and Functionalized Nanocomposite Coatings

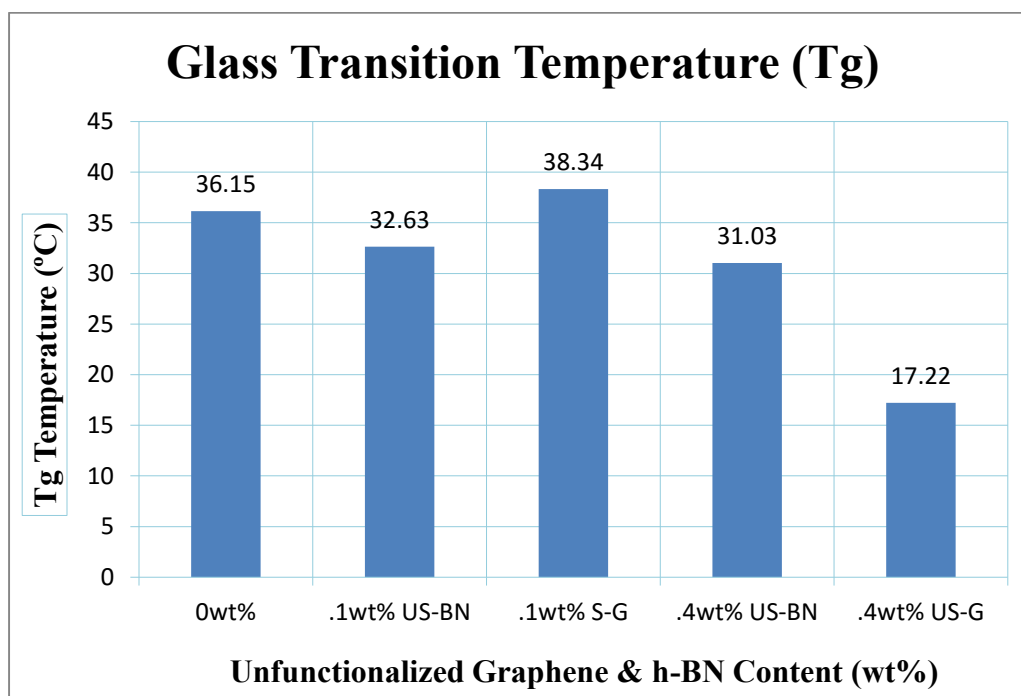


Figure 73: Glass Transition Temperature of PU and Unfunctionalized Nanocomposite Coatings

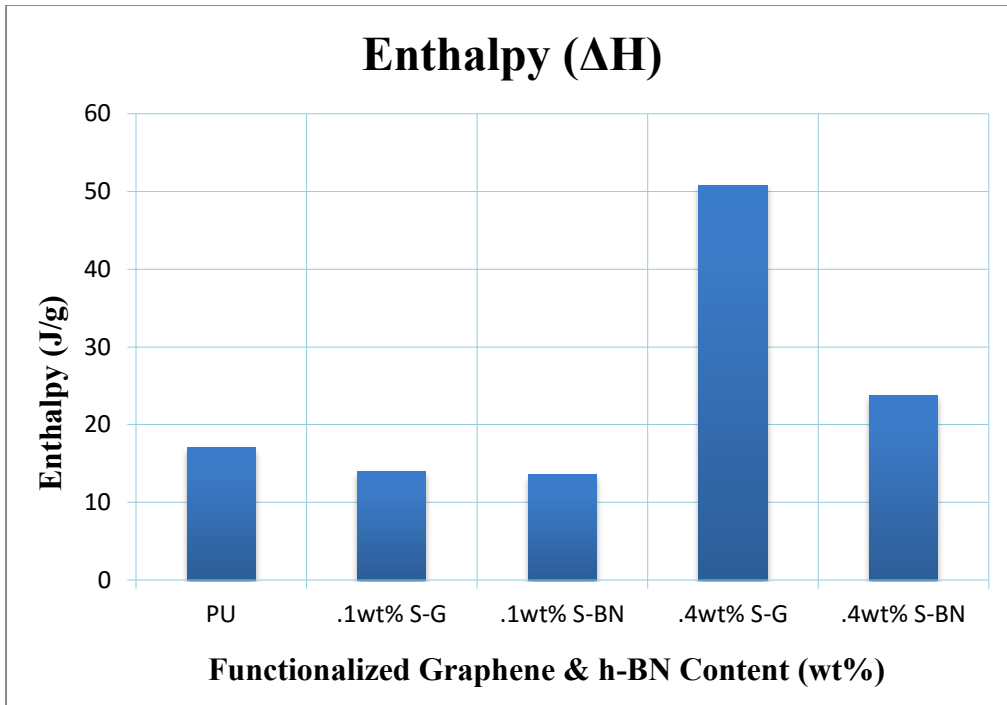


Figure 74: Enthalpy of Nanocomposite Coatings with Silanized Graphene and BN

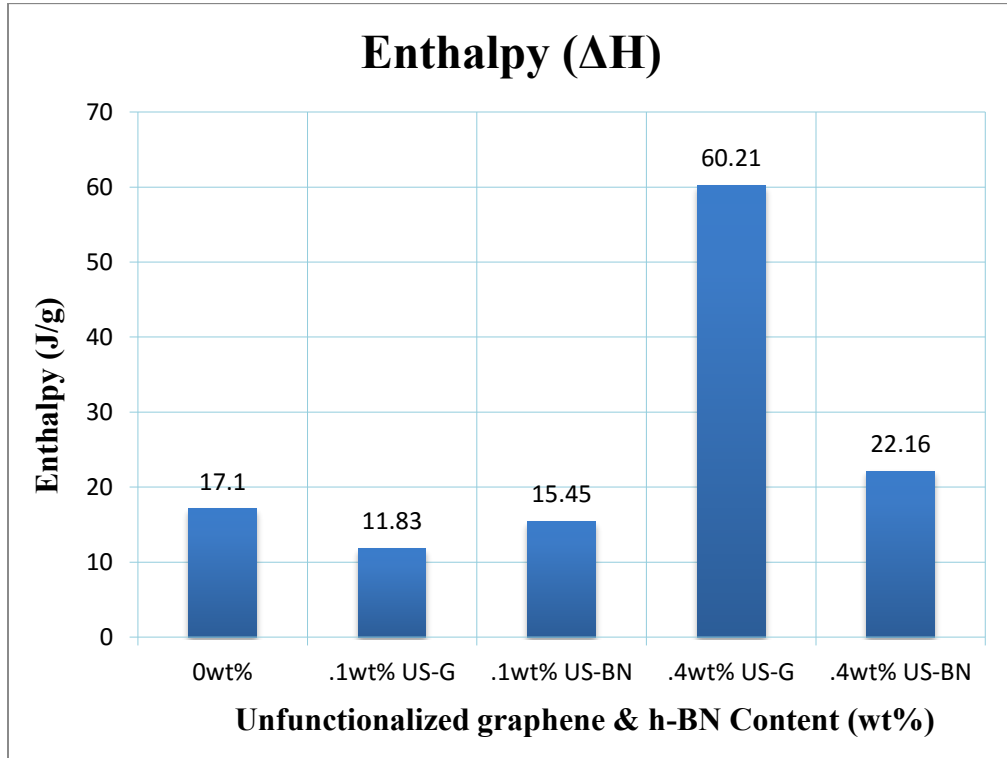


Figure 75: Enthalpy of Nanocomposite Coatings with Unsilanized Graphene and BN

The enthalpy of nanocomposite coatings with silanized graphene and h-BN is shown in Figure 74. With higher percentage of silanized graphene in the coating, the enthalpy was increased dramatically when compared with the silanized BN coating. The enthalpy of the nanocomposite of unsilanized graphene coating was also higher than unsilanized BN coating (Figure 75).

### 5.5.3 Crystallinity of Silanized & Unsilanized Nanocomposite Coatings

Crystallization affects optical, mechanical, thermal and chemical properties of the polymer. The fraction of the ordered molecules in polymer is characterized by the degree of crystallinity, which typically ranges between 10% and 80% [65]. Higher values are only achieved in materials that have small molecules, which are usually brittle, or in samples stored for long time at temperatures just under the melting point. The latter procedure is costly and is applied only in special cases. In this research, this evaluation was carried out by using the endothermic peak related to the crystalline melting. A higher quantity of heat is absorbed during the melting when the sample chains present arranged (more crystalline regions or higher degree of crystallinity). So, the crystallinity percentage can be reached by the equation below [66]:

$$\% \text{ Crystallinity} = \frac{\Delta H_{\text{sample-melting}}}{\Delta H_{\text{reference}}} \times 100\% \quad (5)$$

$\Delta H_{\text{sample melting}}$  is the sample melting enthalpy with unknown crystallinity percentage and  $\Delta H_{\text{reference}}$  is the sample melting enthalpy with the known crystallinity percentage. The unique properties of polyurethanes result from both their chemical structure and the extent of microphase separation between hard and soft segments [67]. The  $\Delta H_{\text{reference}}$  in this study is 63.59J/g [68]. Crystallinity of silanized & unsilanized graphene and BN showed on table 5 & 6. All silanized and unsilanized BN and 0.1wt% of graphene coatings had a very good degree of crystallinity. Except for the silanized and unsilanized graphene of 0.4wt%, this showed very

high percentages of crystallinity. It means that these coatings are very brittle, easy to damage and degrade with the fast rate during UV exposure. Figure 76 is the crystallinity graph of the PU and silanized graphene & h-BN nanocomposite coatings. The 0.4wt% silanized graphene coating had the highest percentage of crystallinity (79.93%). Figure 77 showed the crystallinity graph of the PU and unfunctionalized graphene & h-BN nanocomposite coatings. The 0.4wt% unfunctionalized graphene had the highest percentages of crystallinity (94.68%).

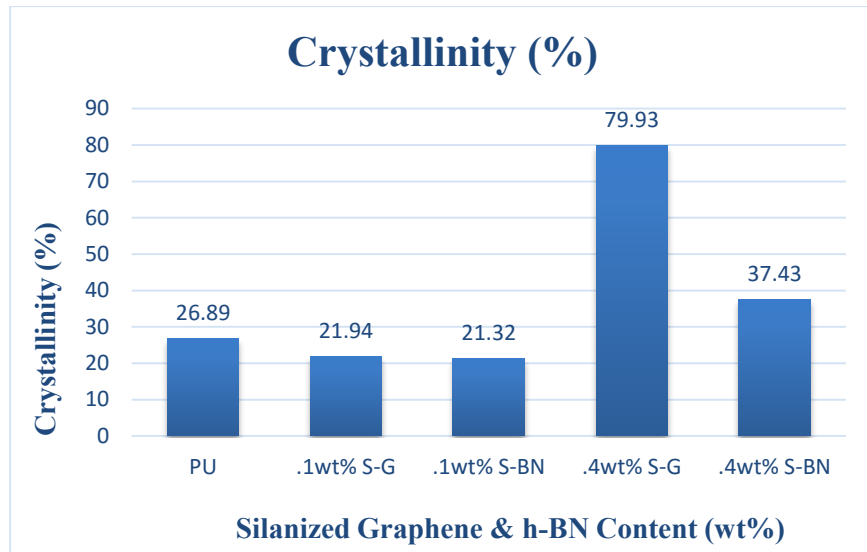


Figure 76: Crystallinity (%) of the Nanocomposite Coatings with PU Silanized Graphene & BN

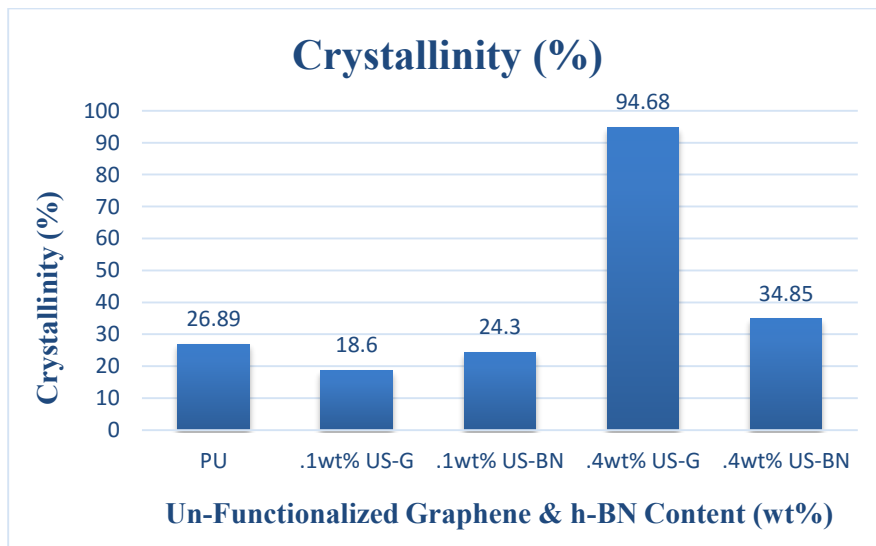


Figure 77: Crystallinity (%) of the Nanocoatings of PU and Unfunctionalized Graphene &h-BN.

Nowadays, safety is one of the major concerns for the nanotechnology related studies in many institutions worldwide. The nanomaterials utilized in these studies are considered safe for producing different coating nanomaterials for many industrial applications, such as aircraft, wind energy, automobile, infrastructures, etc. [69-72].

## CHAPTER 6

### CONCLUSIONS

The purpose of this study was to develop multifunctional nanocomposite coatings with silanized graphene, h-BN, and a mixture of graphene & h-BN. These coatings will improve the UV degradation resistance, absorption of UV harmful light, self-cleaning surface ability, and corrosion resistance. They will also reduce the intensity of laser illumination incidents, and impact of environment factors due to the natural color of graphene. Corrosion and weathering cause trillions of dollars in loss every year to the world economy. The development of a more efficient protective coating is an efficient way to decrease these losses. It has been documented that by adding a certain percentage of graphene nanoparticles or silanized graphene by weight percent into the polymeric coating or paints, it will dramatically increase the resistance of the coating to UV radiation and corrosion.

With the results for the water contact angle test, the coating with different amount of silanized h-BN gave the largest angles of water contact between the surfaces and the coatings ( $\approx 90^\circ$ ). The result of the coatings with silanized graphene showed the water contact angles had a small change after UV chamber around 4 degrees. In the coatings with the mixture of two nanomaterials such as graphene and h-BN, it still showed better contact angle (81.56 degrees) compared with the pure polyurethane coating itself (78.62 degree). In a comparison of the thickness of the coatings before and after UV chamber, the coatings with higher percentages of silanized h-BN and graphene showed significant improvement over the coatings of PU after UV chamber such as lower degradation and delamination rate.

After FTIR testing was done using pure PU, silanized graphene, silanized h-BN, and silanized graphene & h-BN without the UV chamber. There was a high percentage of unstable and sharply stretching free O-H and N-H bonds of alcohol and phenols. These are the main components of the polyurethane paint. A broad stretching of the N-H bond of asymmetry stretching and the symmetric stretching CH of Alkanes groups was also seen as well. These results are expected because polyurethane paint consists of 53.8% hydrogen carbon solvent in its ingredients. They continued vibrating at  $1714\text{ cm}^{-1}$  and  $1685\text{ cm}^{-1}$  of amide group. The four coatings started degrading earlier at the wavelength  $1700\text{ cm}^{-1}$  with carbonyl C=O bonds.

The FTIR results with these same four coatings after they were in the UV chamber, shows a significant improvement on the graphs. There was no longer a sharply stretching of the O-H bonds at the wavelength  $4000\text{-}3000\text{ cm}^{-1}$ , but they still had the vibrations of the  $\text{CH}_3$ ,  $\text{CH}_2$ , and CH bonds. However, they were less intense than the vibrations before UV chamber. They experienced degradation later than the PU coating due to the silicone functional groups such as Si-O-Si and Si- $\text{CH}_3$ . These functional groups should be agents that will help the coatings last longer.

The UV-Vis test results showed that the coating with silanized graphene absorbed more of the visible light spectrum and UV harmful light in comparison with the coating with unsilanized graphene. In contrast, the coating with unsilanized h-BN absorbed more visible light than the coating with silanized h-BN. However, the silanized h-BN coating absorbed more UV light than the coating with unsilanized h-BN. When we compare the three graphs together with different silanized materials such as silanized graphene, silanized h-BN, and silanized graphene & h-BN, the silanized graphene coating let the most visible lights pass through it. The silanized graphene & h-BN coating absorbed the maximum UV harmful light.

The glass transition temperature of the nanocomposite coatings with silanized and unsilanized nanomaterials (0.1wt% S-G, 0.1wt% S-BN, and 0.4wt % S-BN) were lower than the Tg of the PU coating due to the fact that their purpose is to make the coatings more durable and also due to their bundling tendency. The coating with 0.4wt% and 0.8wt% of silanized and unsilanized graphene had a very high concentration of Tg which caused the coatings to be thicker and created high crosslink chains and interfacial forces with the polyurethane paint components. The Tg results affect the degree of crystallinity and the crystallinity of the nanocomposite coatings with unsilanized and silanized nanomaterials (0.1 wt% S-G, 0.1wt% S-BN, and 0.4Wt % US-BN). These were lower than the crystallinity of silanized and unsilanized graphene (0.4wt% S-G and 0.4wt% US-G). The same results indicated that adding functionalized graphene or h-BN to paints will provide a promising approach to fabricate nanocomposite coatings. These same coatings will excel in protecting against UV light, UV degradation and photo responsiveness because of the natural color of graphene. Specifically, the coatings with h-BN will make better corrosion and UV degradation resistance. The study was successful in creating nanocomposite coatings on the transparent plastics with silanized graphene and h-BN. By adding h-BN nanoparticles into the coating, it will help to create excellent corrosion and degradation protection on the substrates. In addition, silanized graphene coatings absorbed more UV light and visible light to slow down the UV degradation process.

## CHAPTER 7

### FUTURE DEVELOPMENT

New generations of self-repairing coatings are being developed to further enhance UV absorption properties of transparent plastic substrates and degradation of polymeric materials. In today's technology, the barrier property of the coating is the main mechanism for material protection against corrosion and degradation. The barrier performance of this coating will help protect against damage, corrosive electrolytes, or weathering environment that come into contact with the materials' substrate with conventional coatings. Nanomaterials greatly improved the qualities of coatings and paints by making them have increased flexibility, higher scratch & wear resistance, and are better self-cleaning. They also have the benefits of lasting much longer in between applications. Nanocoatings improve barrier properties of organic electro coatings against corrosive electrolyte penetration. The protection of the surfaces from environmental conditions includes less weathering due to biological attack, energy savings, and lower maintenance. The economic benefits of these coatings are an added bonus.

Hexagonal boron nitride is an excellent material to use in the coating. It slows the degradation process by the UV light and gives a better water contact angle after 20 days in the UV chamber. These show that it is a very good agent to protect the surface substrates from corrosion. The silanized h-BN didn't completely dissolve in the PU paint however it solutes in the polyacrylic paint (water-based). There are further studies needed to see if there is a better method to modify the h-BN nanoparticles, create a homogeneous solution between h-BN and coatings for corrosion purposes.

The challenge is to get the most benefits from the nanomaterials and generate them into the coating. Graphene and h-BN have excellent physical and chemical properties. Another way

should be developed to modify graphene or h-BN. For example, graphene is a semiconductor but the coating with 0.8wt% graphene was not conductive. The question remains, how do we create a graphene coating that will be conductive? In many journals and articles, it has been stated that they can make electronic devices flexible and transparent. Through the test results in this study, it was observed that graphene coatings were not able to be transparent. It progressively became darker as a higher percentage of graphene was added into the coating. The present need is to develop a better method to modify graphene in order to make a transparent coating. This would allow a new coating with good conductivity for aircraft windshields for the purposes of anti-ice, anti-fogging, and defrosting. This coating would have the additional benefit of being able to apply on the leading edge of the airplane's wings for the anti-icing.

## REFERENCES

## REFERENCES

1. R. Lambourne, Ed.; Ellis Horwood. "Paint and Surface Coatings: Theory and Practice." Chichester, England, 1987.
2. Clive H. Hare, "The Degradation of Coatings by Ultraviolet Light and Electromagnetic Radiation." *Anatomy of Paint*. Materials Technology Section, May 1992.
3. Gail L. Persily, "Campus Perspective on the National Institutes of Health Public Access Policy: University of California, San Francisco, library experience." 2010 Jul; 98 (3): 256-259.
4. D. Golberg, Y. Bando, Y. Huang, T. Terao, M. Mitome, C. Tang, and C. Zhi. "ACS Nano." 4(6), 2979 (2010).
5. R. Seizer and K. Friedrich. "Mechanical Properties and Failure Behavior of carbon Fiber-Reinforced Polymer Composites under the Influence of Moisture." Vol. 28, Issue 6, 1997, Pg. 595-604.
6. Edinger C., Grimaudo V., and Broekmann P., Waldvogel S. R.: "Stabilizing Lead Cathodes with Ammonium salt Additives in the Deoxygenation of Aromatic Amides." *Chem Electro Chem*, 1, 1018–1022 (2014).
7. Wang S, Jiang L (2007). "Definition of super hydrophobic states". *Advanced Materials* **19** (21): 3423– 3424.
8. Extrand C. W.: Model for Contact Angles and Hysteresis on Rough and Ultra phobic Surfaces. *Langmuir*, 18, 7991– 7999 (2002).
9. Chen L., Yang G., Wang S.: Air-grid surface patterning provided by super hydrophobic Surfaces. *Small*, 8, 962– 965 (2012).
10. Oliveira N. M., Reis R. L., Mano J. F.: "Super hydrophobic surfaces engineered using Diatomaceous earth." *ACS Applied Materials and Interfaces*, 5, 4202–4208 (2013).
11. Sun M., Luo C., Xu L., Ji H., Oujang Q., Yu D., Chen Y.: "Artificial Lotus Leaf by Nano Casting." *Langmuir*, 21, 8978–8981 (2005).
12. Zang D., Li F., Geng X., and Lin K., Clegg P. S.: "Turning the Wet Ability of an Aluminum Surface via a Chemically Deposited Fractal Dendrite Structure." *The European Physical Journal E*, 36, 59/1–59/8 (2013).

13. Twardowski, T.E., "Introduction to Nanocomposite Materials: Properties, Processing, Characterization." 2007: Destech Publications, Incorporated.
14. Mahadik S. A., Fernando P. D., Hegade N. D., Wagh P. B., Gupta S. C.: "Durability and Restoring of Superhydrophobic Properties in Silica-based Coatings." *Journal of Colloid and Interface Science*, 405, 262–268 (2013).
15. Wang J., Song X., Rui L., Shen J., Yang G., Huang H.: "Fluorocarbon Thin Film with Super hydrophobic Property Prepared by Pyrolysis of Hexafluoropropylene Oxide." *Applied Surface Science*, 258, 9782–9785 (2012).
16. Ou J., Hu W., Xue M., Wang F., Li W.: "Super hydrophobic surfaces on light alloy Substrates fabricated by a versatile process and their corrosion protection." *ACS Applied Materials and Interfaces*, 5, 3101–3107 (2013).
17. Gu H. Y., Qi Z. Y., Wu W., and Zeng Y., Song L. X.: "Super Hydrophobic Polyimide Films with High Thermal Endurance via UV Photo-oxidation." *Express Polymer Letters*, 8, 588–595. (2014).
18. Asmatulu, R., Mahmud, G.A., Hille, C., and Misak, E.H. "Effects of UV Degradation on Surface Hydrophobicity, Crack and Thickness of MWCNT-based Nanocomposite Coatings," *Progress in Organic Coatings*, 2011, Vol. 72, pp. 553-561.
19. R. V. Lapshin, A. P. Alekhin, A. G. Kirilenko, S. L. Odintsov, V. A. Krotkov (2010). "Vacuum Ultraviolet Smoothing of nanometer-scale asperities of poly (methyl Methacrylate) Surface".
20. Burrows, H. D.; Canle L, M.; Santaballa, J. A.; Steenken, S., "Reaction Pathways and Mechanisms of Photo Degradation of Pesticides", *J. Photochem. Photobiology. B* 2002, 67, 71-108.
21. Oldak, D.; Kaczmarek, H.; Buffeteau, T. & Sourisseau, C. - J. "Mater. Sci.," **40**, p.4189 (2005).
22. Emas Yousif and Raghad Haddad. "Photodegradation and Photostabilization of Polymers, Especially Polystyrene: review". Springer plus, 2013.
23. Galdi A., Foltis P., Shah A., "UV Protecting Composition and Methods of Use." Application: US Patent 20120015016. Jan 19, 2012.
24. Geuskens G, David C (1979b) Polymer Photo Degradation: "Mechanisms and Experimental Methods." *Pure Appl. Chem* 51:233-240.
25. Ryan S. Phillip, et al. "Measuring the Effectiveness of Photo Responsive Nanocomposite Coatings on Aircraft Windshields to Mitigate Laser Intensity." *JATE (Journal of Aviation Technology and Engineering)* 4:2. 2015. 49-54.

26. Wenshi Ma, Li Wu, Donqiao Zhang, Shuangfeng Wang. "Preparation and Properties of 3-Aminopropyltriethoxysilane Functionalized Grapheme/Polyurethane Nanocomposite Coatings." Springer-Verlag Berlin Heidelberg. 17 Jul 2013.
27. Naffakh M, Diez-pascual AM, Gomez-Fatou MA (2011). "New hybrid Nanocomposites Containing Carbon Nanotubes, Inorganic Fullerene like WS<sub>2</sub> Nanoparticles and Poly (Ether ketone) (PEEK)." *J master Chem* 21: 7425-7433.
28. Arai S, Sato T, Endo M (2011) "Fabrication of Various Electrodes Ni-P Alloy/Multiwall Carbon Nanotubes Composite Films on an Acrylo-Nitrile Butadiene Styrene resin." *Surf Coat Tech* 205: 3175-3181.
29. Abyzov AM, Kidalov SV, Shakhov FM (2012) "High Thermal Conductivity Composite of Diamond Particles with Tungsten Coating in a Copper Matrix for Heat Sink Application." *Appl. Thermal Eng.* 48: 72-80.
30. Novoselov KS, Geim AK, Morozov SV et al. (2004) "Electric Field Effect in Atomically Thin Carbon Films." *Science* 306: 666-669.
31. Min Yi, Zhigang Shen, Xiaohu Zhao, et al. "Boron Nitride Nanosheets as Oxygen-atom Corrosion Protective Coatings." *Applied physic Letters* 104, 143101. 7 April 2014.
32. J. S. Bunch, S. S. Verbridge, J. S. Alden, J. M. Parpia, H. G. Craighead, and P. L. Mc Euen. "Nano Lett." 8(8), 5458 (2008).
33. Asmatulu, R., Claus, R.O., Mecham, J.B., and Corcoran, S.G. "Nanotechnology-Associated Coatings for Aircrafts," *Materials Science*, 2007, Vol. 43, pp. 415-422.
34. E. Husain, T. N. Narayanan, J. J. Taha-Tijerina, S. Vinod, R. Vajtai, and P. M., Ajayan, *ACS Appl. "Matters, Interfaces 5."* (10), 4129 (2013).
35. Traditional Oil Painting. Watson-Guptill Publications. 2007.
36. Acrylic Paint Common Questions. "Technical Summary of Acrylic Paint accessed." December 06, 2010 Archived January 1, 2011 at the Wayback Machine.
37. Liao, L.; Lin, Y.-C.; Bao, M.; Cheng, R.; Bai, J.; Liu, Y.; Qu, Y.; Wang, K. L.; Huang, Y.; Duan, X. "Nature." **2010**, 467, 305-8.
38. Lin, Y.-M.; Jenkins, K. A.; Valdes-Garcia, A.; Small, J. P.; Farmer, D. B.; Avouris, P. "Nano Letters." **2009**, 9, 422-6.
39. Kim, K. S.; Zhao, Y.; Jang, H.; Lee, S. Y.; Kim, J. M.; Kim, K. S.; Ahn, J.-H.; Kim, P.; Choi, J.-Y.; Hong, B. H. "Nature." **2009**, 457, 706-10.

40. Li, X.; Cai, W.; An, J.; Kim, S.; Nah, J.; Yang, D.; Piner, R.; Velamakanni, A.; Jung, I.; Tutuc, E.; Banerjee, S. K.; Colombo, L.; Ruoff, R. S. "Science." **2009**, 324, 1312–4.
41. Asmatulu, R., Khan, I.S., and Jenkinson, M.L. "Improving the Corrosion Resistances via Graphene Nanocomposites," in *Graphene Science Handbook: Size-Dependent Properties*, CRC Press / Taylor and Francis Group, LLC., Editor M. Aliofkhazaei, N. Ali, W.I. Milne, C.S. Ozkan, S. Mitura, and J. Gervasoni, 2015, pp. 465-476..
42. Denis, P. A.; Iribarne, F. (2013). "Comparative Study of Defect Reactivity in Graphene." *Journal of Physical Chemistry C* **117**(37): 19048–19055.
43. Kuzmenko, A. B.; Van Heumen, E.; Carbone, F.; Van Der Marel, D. (2008). "Universal Infrared Conductance of Graphite". *Physical Review Letters* **100** (11): 0712.0835.
44. Zhang, Y.; Tang, Tsung-Ta; Girit, Caglar; Hao, Zhao; Martin, Michael C.; Zettl, Alex; Crommie, Michael F.; Shen, Y. Ron; Wang, Feng (11 June 2009). "Direct Observation of a Widely Turnable Bandgap in Bilayer Graphene." *Nature* **459** (7248): 820–823.
45. Heyrovska, Raji (2008). "Atomic Structures of Graphene, Benzene and Methane with Bond Lengths as Sums of the Single, Double and Resonance Bond Radii of Carbon."
46. Asmatulu, R., Nguyen, O., and Asmatulu, E. "Nanotechnology Safety in Automotive Industry," in *Nanotechnology Safety*, Elsevier, Editor R. Asmatulu, 2013, pp. 57-72.
47. Huang XY, Jiang PK, Tanaka T. A. Review of dielectric polymer composites with high Thermal conductivity. *IEEE Electr Insult Mag.* 2011; 27: 8-16.
48. K. Watanabe, T. Taniguchi, and H. Kanda. "Natural Matter." 3, 404-409 (2004).
49. S. Cho and M. S. Foer, "Phys. Rev B." 77, 081402 (2008).
50. Jabbarnia, A., Ghazinezami, A., and Asmatulu, R. "Nanostructured Coatings and Their Recent Applications," in *Comprehensive Guide for Nanocoatings Technology*, Nova Science Publishers, Inc., Editor M. Aliofkhazaei, 2015, Vol. 4, pp. 131-155.
51. Li, B., et al., "Simultaneous Enhancements in Damping and Static Dissipation Capability of Polyetherimide Composites with Organosilane Surface Modified Graphene Nano platelets." *Polymer*, 2011. **52**(24): p. 5606-5614.
52. Asthana, R., A. Kumar, and N.B. Dahotre, "*Materials Processing and Manufacturing Science*." 2006: Elsevier Science.
53. Valentine, C; Craig, T.A.; Hager, S.L (1993). "Inhibition of the Discoloration of Polyurethane Foam Caused by Ultraviolet Light". *J. Cellular Plastics* **29** (6): 569–590.

54. Blair, G. Ron; Bob Dawe; Jim McEvoy; Roy Pask; Marcela Rusan de Priamus; Carol Wright. "The Effect of Visible Light on the Variability of Flexible Foam Compression Sets (PDF)." Orlando, Florida: Center for the Polyurethane Industry. Retrieved 2008-01-26.
55. Newman, C.R.; Forciniti, D. (2001). "Modeling the Ultraviolet Photodegradation of Rigid Polyurethane Foams". *Ind. Eng. Chem. Res.* **40** (15): 3336–3352.
56. Grillo, D.J.; Housel, T.L. (1992). "Physical Properties of Polyurethanes from Polyesters and Other Polyols". Polyurethanes '92 Conference Proceedings. New Orleans, LA: The Society of the Plastics Industry, Inc.
57. Delebecq E, Pascault JP, Boutevin B, Ganachaud F (2013). "On the Versatility of Urethane/Urea Bonds: Reversibility, Blocked Isocyanate, and Non-Isocyanate."
58. Hyunwoo Kim, et al. "Graphene/Polyurethane Nanocomposites for Improved Gas Barrier and Electrical Conductivity." Department of Chemical Engineering and Materials Science, University of Minnesota, Minneapolis. Feb 15, 2010.
59. Kim, K. S.; Zhao, Y.; Jang, H.; Lee, S. Y.; Kim, J. M.; Kim, K. S.; Ahn, J.-H.; Kim, P.; Choi, J.-Y.; Hong, B. H. "Nature" 2009, 457, 706–710.
60. Ganesh Rahul Bhimanapati, et al. "Large-Scale Synthesis and Fictionalization of Hexagonal Boron Nitride Nanosheets." *Nanoscale*, 2014, 6, 11671-11675.
61. A. Dravniece, L. Gerca1, K. Kundzins, K. Teivena, V. Kampars, M. Rutkis. "Optimized Deposition of Graphene Oxide Langmuir-Blodgett Thin Films." *Latvian Journal of Physics and Technical Science*. 2014 N. 4
62. Dmitri Golberg, et al. "Recent Advances in Boron Nitride Nanotubes and Nanosheets." *Israel Journal of Chemistry*. Vol. 50, Issue 4, Pg. 405-416. Oct 2010.
63. Paula, Peter Atkins, Julio de (2009). "*Elements of physical chemistry* (5th Ed.)." Oxford: Oxford U.P. p. 459. ISBN 978-0-19-922672-6
64. PCI- Paint & Coatings Industry. "DSC Technology: An Enhanced Tool for Coatings Analysis." Feb 28, 2002.
65. G. W. Ehrenstein, Richard P. Theriault (2001). "Polymeric Materials: Structure, Properties, Applications." Hanser Verlag. pp. 67–78. ISBN 1-56990-310-7.
66. Liliana B. Nohara; Evandro L. Nohara; Andreza Moura; Joseane M. R. P. Gonçalves; Michelle L. Costa; Mirabel C. Rezende. "Study of Crystallization Behavior of Poly (phenylene sulfide)." *Polymers* vol. 16no. 2 Sao Carlos Abr. / June 2006.

67. K. Kojio, Y. Mitsui, M. Furukawa, "Polymer 50," 3693, (2009).
68. Matthew A. Hood, et al. "Morphology Control of Segmented Polyurethanes by Crystallization of Hard and Soft Segments." Vol.51, Issue 10, May 4, 2010. Pg. 2191-2198.
69. Asmatulu, R. "Nanocoatings for Corrosion Protection of Aerospace Alloys," (Part 2), in *Corrosion Protection and Control using Nanomaterials*, Woodhead Publishing, Editors V.S. Saji and R. Cook, 2012, pp. 357-375.
70. Asmatulu, R., Khan, I.S., and Jenkinson, M.L. "Improving the Corrosion Resistances via Graphene Nanocomposites," in *Graphene Science Handbook: Size-Dependent Properties*, CRC Press / Taylor and Francis Group, LLC., Editor M. Aliofkhazaei, N. Ali, W.I. Milne, C.S. Ozkan, S. Mitura, and J. Gervasoni, 2015, pp. 465-476.
71. Nuraje, N., Khan, S.I., Misak, H.E., and Asmatulu, R. "The Addition of Graphene to Polymer Coatings for Improved Weathering," *ISRN Polymer Science*, 2013, Vol. 2013, 8 pages.
72. Asmatulu, R., *Nanotechnology Safety*, Elsevier, Amsterdam, the Nederland, August, 2013, (ISBN-10: 0444594388).